

**JAERI-Review  
2002-029**



JP0250576



**JAERI TANDEM ANNUAL REPORT 2001  
APRIL 1, 2001 – MARCH 31, 2002**

**November 2002**

**Department of Materials Science**

**日本原子力研究所  
Japan Atomic Energy Research Institute**

本レポートは、日本原子力研究所が不定期に公刊している研究報告書です。

入手の問い合わせは、日本原子力研究所研究情報部研究情報課（〒319-1195 茨城県那珂郡東海村）あて、お申し越し下さい。なお、このほかに財団法人原子力弘済会資料センター（〒319-1195 茨城県那珂郡東海村日本原子力研究所内）で複写による実費頒布を行っております。

This report is issued irregularly.

Inquiries about availability of the reports should be addressed to Research Information Division, Department of Intellectual Resources, Japan Atomic Energy Research Institute, Tokai-mura, Naka-gun, Ibaraki-ken 〒319-1195, Japan.

© Japan Atomic Energy Research Institute, 2002

編集兼発行 日本原子力研究所

**JAERI TANDEM Annual Report 2001**  
**April 1, 2001 – March 31, 2002**

**Department of Materials Science\***

Tokai Research Establishment  
Japan Atomic Energy Research Institute  
Tokai-mura, Naka-gun, Ibaraki-ken

(Received September 13, 2002)

This annual report describes research activities which have been performed with the JAERI tandem accelerator and the Van de Graaff accelerator from April 1, 2001 to March 31, 2002. Summary reports of 48 papers, and lists of publication, personnel and cooperative research with universities are contained.

Keywords: JAERI Tandem, Nuclear Structure, Nuclear Reactions, Nuclear Chemistry,  
Nuclear Theory, Atomic Physics, Solid State Physics,  
Radiation Effects in Materials, Progress Report.

---

Editors: Suehiro TAKEUCHI, Hiroshi IKEZOE, Satoshi CHIBA,  
Yuichiro NAGAME, Masao SATAKA and Akira IWAMOTO

原研タンDEM加速器  
2001年度年次報告

日本原子力研究所東海研究所  
物質科学研究部\*

(2002年9月13日受理)

本年次報告書は、東海研究所の原研タンDEM及びバンデグラフ加速器で、2001年4月1日から2002年3月31日までの間に行われた研究活動を取りまとめたものである。

(1) 加速器の運転状況および開発 (2)原子核構造 (3)原子核反応 (4)核化学 (5)原子核理論 (6)原子分子物理及び固体物理 (7)材料の照射効果の7部門にまたがる48編の研究報告、公表された文献、関与した職員及び大学等との協力研究のリストを収録している。

---

東海研究所：〒319-1195 茨城県那珂郡東海村白方白根2-4

※(編集者) 竹内末広・池添 博・千葉 敏・永目諭一郎・左高正雄  
岩本 昭

## Preface

This report covers research and development activities using the tandem accelerator and its superconducting booster at JAERI, Tokai, for the period of April 1, 2001 to March 31, 2002. During this period, the tandem accelerator was operated over 4,776 hours or 202 days to deliver ion beams to the experiments in the fields of nuclear structure, nuclear reactions, atomic physics, solid state physics and radiation effects in materials. The super-conducting booster was utilized over 56 days for 16 experimental subjects. Twenty-five research programs have been carried out in collaboration with about a hundred researchers from universities and research institutes. The fruits of studies and special topics in FY2001 are the following:

The bench work for the up-grade plan of the in-terminal ECR ion injector introducing a high performance 14.5 GHz permanent magnet ECRIS has been proceeding in expectation of mounting it within a few years.

JAERI-Tokai and KEK-IPNS(Institute of Particle and Nuclear Studies) signed up for a joint project of developing an ISOL-based radioactive-nuclear-beam(RNB) facility in the tandem accelerator laboratory starting from 2001. The RNB facility will be built in an old target room, where an existing KEK's 1 MeV/u RNB linac system will be installed in 2003. Neutron-rich RNB will be extracted from proton induced fission products of a uranium target. In FY2001, the building plans were drawn and a utility building for the linac system was built near the room for the RNB linac.

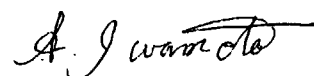
In Coulomb excitation experiments utilizing the gamma-ray detector array, GEMINI, shape coexistence has been widely observed for  $^{68}\text{Zn}$ ,  $^{70,74,76}\text{Ge}$  and  $^{98}\text{Mo}$  nuclei. The experimental technique was demonstrated to be useful for the study of neutron-rich nuclei by applying it to the radioactive nuclear beam in the JAERI-KEK project.

The sub-barrier fusion of reactions  $^{82}\text{Se} + ^{134,138}\text{Ba}$  was investigated and the importance of the shell structure was demonstrated in the fusion process. The recoil mass separator JAERI-RMS was successfully used for the production of a radioactive  $^{16}\text{N}$  nuclear beam for the research of nuclear astrophysics.

In the study of heavy element nuclear chemistry, the transactinide nuclei,  $^{261}\text{Rf}$  and  $^{262}\text{Db}$ , have been successfully produced via the reactions of  $^{248}\text{Cm}(^{18}\text{O},5\text{n})$  and  $^{248}\text{Cm}(^{19}\text{F},5\text{n})$ , respectively, and the excitation functions for each reaction have been measured. On-line ion-exchange experiments of Rf together with the lighter homologues Zr and Hf in the HCl and  $\text{HNO}_3$  solutions have been conducted, and the results clearly show that the behavior of Rf is typical of the group-4 element.

In the field of nuclear theory, the structure of neutron-rich nuclei, in particular the disappearance of the magic number and its relation to the effective interaction, was studied by the Monte Carlo shell model. Furthermore, hyperon pairing in nuclear matter, formation and decay of super-heavy elements and structure of low-density nuclear matter were investigated.

Through the measurements of AC susceptibility in 200 MeV Xe ion irradiated FeNi invar alloys, it has been found that the high density electron excitation induced by the reaction causes a large increase of Curie temperature. From the point of view of the processing of magnetic materials, a further study is under way.



Akira Iwamoto

Director

Department of Materials Science

## Contents

1. Accelerator Operation and Development.....	1
1.1 Tandem Accelerator and Booster Operation.....	3
1.2 Utilization of Tandem Accelerator and Booster.....	6
1.3 JAERI-KEK Joint RNB Project.....	7
1.4 Ion Source Development for On-line Mass Separation of Light Radioactive Nuclear Beam.....	9
1.5 A 14.5GHz in-terminal ECR Ion Source.....	11
2. Nuclear Structure.....	13
2.1 Preliminary Experiment to Study K-isomers Based on the Intruder Configurations around $^{124}\text{Sn}$ .....	15
2.2 Shape Coexistence in $^{98}\text{Mo}$ .....	16
2.3 Excited States in $^{187}\text{Re}$ Populated by Inelastic Scattering.....	18
2.4 Rotational Bands and Signature Inversion in Odd-odd $^{176}\text{Ir}$ .....	20
2.5 Hyperfine Structure and Isotope Shift Measurements of $^{135}\text{La}$ by Collinear Laser Spectroscopy.....	22
2.6 Nanosecond Isomers in $^{32,33}\text{Si}$ and $^{34}\text{P}$ .....	23
2.7 Nano-second Isomer in $^{68}\text{Cu}$ .....	25
2.8 $Q_\beta$ Measurements of $^{158}\text{Pm}$ , $^{159}\text{Sm}$ , and New Isotope $^{166}\text{Tb}$ using the JAERI-ISOL.....	26
3. Nuclear Reactions.....	29
3.1 Effect of Shell Structure in the Fusion Reactions $^{82}\text{Se}+^{134}\text{Ba}$ and $^{82}\text{Se}+^{138}\text{Ba}$ .....	31
3.2 Mass Division of $^{240}\text{Pu}$ Following $\beta$ -vibrational Resonance.....	34
3.3 Measurement of the $^{16}\text{N}(\alpha, n)$ Cross Section.....	36
3.4 Anomalous Excitation Energy Dependence of Shell Effects in Asymmetric Fission Mode.....	38
3.5 Sub-barrier Fusion of $^{82}\text{Se}+^{176}\text{Yb}$ .....	40
3.6 Monitoring and Rejection of Background Particles using a PPAC Installed in the JAERI-recoil Mass Separator in the Measurement of Fusion Evaporation Residues.....	41
4. Nuclear Chemistry.....	43

4.1	Search for "Missing" $\alpha$ -Emitters for the Mass Mapping of Superheavy Elements.....	45
4.2	Anion Exchange Behavior of Rf in HCl and HNO <sub>3</sub> .....	47
4.3	Development of Automated Liquid Chromatography Apparatus Coupled with an On-line Alpha-particle Detection System.....	49
4.4	New Technique for Determination of Trace Elements Using Multiparameter Coincidence Spectrometry -Ultra Sensitive Measurement of Ir -.....	51
4.5	Synthesis of Plutonium Metallofullerene.....	53
4.6	Determination of Disintegration Rate and Gamma-ray Emission Probabilities for <sup>66</sup> Ga Source.....	55
5.	Nuclear Theory.....	57
5.1	Extreme Location of the Fluorine Drip Line and the N=20 Shell Gap.....	59
5.2	Possibility of $\Lambda\Lambda$ Pairing in NA Matter.....	61
5.3	Formation and Decay of Super Heavy Systems .....	63
5.4	First Order Phase Transition of Expanding Matter.....	65
5.5	Ratio of the r- and s-process in the Solar System.....	67
5.6	Clustering Properties in Neutron-rich Nuclear Matter in Low Density Region.....	68
6.	Atomic Physics and Solid State Physics.....	71
6.1	High-resolution Zero-degree Electron Spectroscopy of Highly Charged Argon Ion.....	73
6.2	Studies on the Diffusion Processes in Solid Materials by Radioactive Nuclear Beams.....	75
6.3	A Comparison between B- and n-irradiation on MgB <sub>2</sub> Bulk Samples.....	77
6.4	Electronic Excitation Effects on Secondary Ions Emission from Conductive Materials Bombarded by Heavy Ions.....	79
7.	Radiation Effects in Materials.....	81
7.1	Electronic Sputtering of Non-conductive Oxides by High Energy Heavy Ions.....	83
7.2	Structural Change by High-energy Irradiation and Post-annealing in EuBa <sub>2</sub> Cu <sub>3</sub> O <sub>y</sub> .....	85
7.3	Structure of Beam Tracks Induced by Swift Heavy Ion in Bi-2212.....	87



7.4	Defect Production Induced by High-density Electronic Excitation in Iron.....	90
7.5	Anomalous Shift of Curie Temperature in Iron-nickel Invar Alloys by High-energy Heavy Ion Irradiation.....	92
7.6	Surface Damages in MgO Irradiated with Energetic Iodine Ions.....	93
7.7	Study of Radiation Damage Mechanisms in Steels Using High Energy Ion Irradiation.....	95
7.8	Radiation Effects of High Energy Fission Products in Light Water Reactor Fuels.....	97
7.9	Study on Disorder in $\text{Li}_2\text{TiO}_3$ Irradiated with High Energy Ions.....	99
7.10	Effects of Zr Ion Irradiation on Some Properties of Superplastic Ceramic 3Y-TZP.....	101
7.11	Radiation Defects in Nanocrystalline Materials.....	103
7.12	Ion Irradiation Effects of New Carbon Composite Materials and Carbon Fibers having High Thermal Conductivity.....	104
7.13	The Study about the Structure of Power MOSFETs with High Radiation Tolerance.....	106
8.	Publication in Journal and Proceedings, and Contribution to Scientific Meetings.....	109
9.	Personnel and Committees .....	139
10.	Cooperative Researches .....	147

## 目次

1. 加速器の運転状況および開発.....	1
1.1 タンデム加速器とブースターの運転.....	3
1.2 タンデム加速器とブースターの利用.....	6
1.3 原研-KEK共同RNB計画.....	7
1.4 軽放射性核ビームのオンライン質量分離用イオン源開発.....	9
1.5 14.5GHzターミナルECRイオン源.....	11
2. 原子核構造.....	13
2.1 $^{124}\text{Sn}$ 近傍における励起変形配位に基づくKアイソマーを 研究するための予備実験.....	15
2.2 $^{98}\text{Mo}$ における変形共存.....	16
2.3 非弾性散乱により生成された $^{187}\text{Re}$ の励起状態.....	18
2.4 $^{176}\text{Ir}$ における回転バンドと指標逆転.....	20
2.5 コリニアー・レーザー分光による $^{135}\text{La}$ の超微細構造と 同位体シフトの測定.....	22
2.6 $^{32,33}\text{Si}$ , $^{34}\text{P}$ のナノ秒アイソマー.....	23
2.7 $^{68}\text{Cu}$ のナノ秒アイソマー.....	25
2.8 JAERI-ISOLを用いた $^{158}\text{Pm}$ , $^{159}\text{Sm}$ および新核種 $^{166}\text{Tb}$ の $Q_\beta$ 測定.....	26
3. 原子核反応.....	29
3.1 $^{82}\text{Se}+^{134}\text{Ba}$ , $^{82}\text{Se}+^{138}\text{Ba}$ 核融合反応におけるShellの効果について.....	31
3.2 $\beta$ 振動状態を経由する $^{240}\text{Pu}$ の核分裂片質量数分布.....	34
3.3 $^{16}\text{N}(\alpha, n)$ 反応断面積の直接測定.....	36
3.4 非対称核分裂モードにおける殻効果の特異な励起エネルギー変化.....	38
3.5 クーロン障壁近傍の融合核反応 $^{82}\text{Se}+^{176}\text{Yb}$ の研究.....	40
3.6 反跳生成核分離装置に設置したPPACによる融合蒸発残留核の 生成実験におけるバックグラウンドの観測と低減.....	41
4. 核化学.....	43
4.1 超重元素質量決定のための未知 $\alpha$ 放射性核種の探索.....	45
4.2 塩酸ならびに硝酸溶液系におけるRfの陰イオン交換挙動.....	47
4.3 オンライン $\alpha$ 線測定装置と結合した自動液体クロマトグラフィー の開発.....	49

4.4	多重ガンマ線分析を利用した微量元素分析の新技术 ーイリジウムの超高感度分析ー	51
4.5	プルトニウム金属フラーレンの合成	53
4.6	$^{66}\text{Ga}$ 線源の崩壊率測定と $\gamma$ 線放出率決定	55
5.	原子核理論	57
5.1	フッ素ドリップ線の極端な位置と $N=20$ 殻ギャップ	59
5.2	核子- $\Lambda$ ハイペロン物質における $\Lambda\Lambda$ 対相関の可能性	61
5.3	巨大複合核の生成と崩壊	63
5.4	膨張物質の1次相転移	65
5.5	太陽系における $r$ 過程と $s$ 過程の存在比	67
5.6	低密度中性子過剰核物質におけるクラスターの性質	68
6.	原子分子物理及び固体物理	71
6.1	高電離アルゴンイオンの高分解能0度電子分光	73
6.2	短寿命核を用いた固体内の拡散過程の研究	75
6.3	$\text{MgB}_2$ バルク試料への $B$ -照射と $n$ -照射の比較	77
6.4	高エネルギー重イオン衝突による伝導材料からの 二次イオン放出における電子励起効果	79
7.	材料の照射効果	81
7.1	高エネルギー重イオンによる非導電性酸化物の 電子励起スパッタリング	83
7.2	高エネルギーイオン照射とポストアニーリングによる $\text{EuBa}_2\text{Cu}_3\text{O}_y$ の構造変化	85
7.3	高エネルギー重イオン照射による $\text{Bi-2212}$ の飛跡構造	87
7.4	鉄の高密度電子励起による欠陥生成	90
7.5	高エネルギーイオン照射による鉄ニッケルインバー合金の キュリー温度上昇	92
7.6	高エネルギー酸素イオン照射した $\text{MgO}$ における表面損傷	93
7.7	高エネルギーイオン照射を利用した鉄鋼材料等の 照射損傷機構の研究	95
7.8	軽水炉燃料体での核分裂生成物照射効果に関する基礎研究	97
7.9	高エネルギーイオン照射した $\text{Li}_2\text{TiO}_3$ の無秩序化に関する研究	99
7.10	超塑性セラミックス $3\text{Y-TZP}$ の特性に及ぼす $\text{Zr}$ イオン照射の影響	101

7.11 ナノクリスタルにおける照射欠陥の研究.....	103
7.12 高熱伝導性炭素繊維及び新炭素系複合材料のイオン照射効果.....	104
7.13 放射線耐性を有するパワーMOSFETの構造に関する研究.....	106
8. 雑誌及び国際会議等の刊行物、学会報告-----	109
9. 関連課室、職員及び委員会-----	139
10. 共同・協力研究-----	147

## **1. Accelerator Operation and Development**

This is a blank page.

## 1.1 TANDEM ACCELERATOR AND BOOSTER OPERATION

### TANDEM ACCELERATOR GROUP

Tandem Accelerator and Booster : There were two scheduled machine times in this fiscal year and the operations of the tandem accelerator and booster for experiments were performed as scheduled. The operation time of the tandem accelerator was 4746 hours in 202 days. The superconducting energy booster was operated steadily for 56 days for 16 experimental subjects. During these times, the helium refrigeration systems for the tandem booster were in operation for 108 days from March 15 in 2001, 111 days from September 10 in 2001. Both of the scheduled machine times prepared preliminary days continuously on the end of scheduled machine time, and these days utilized to relieving the canceled schedule by unexpected maintenance's of the accelerator. The summary of the operation from April 1, 2001 to March 31, 2002 is as follows.

#### 1) Time distribution in terms of terminal voltages (Tandem accelerator)

>16 MV	0 days	0 %
15-16	112	55.4
14-15	28	13.9
13-14	7	3.
12-13	0	0
11-12	9	4.4
10-11	15	7.4
9-10	18	8.9
8-9	3	1.5
<8	10	5.0

#### 2) Booster operation for research programs

<sup>70</sup> Zn	~585 MeV	9 days
<sup>76</sup> Ge	~635	8
<sup>76,78,82</sup> Se	~490	9
<sup>84</sup> Kr	~610	19
<sup>90</sup> Zr	~276	4
<sup>136</sup> Xe	~655	7

Maintenances and Improvements : The yearly maintenances of the SF<sub>6</sub> gas handling system and the helium refrigeration system were performed, and the governmental inspection passed in September and the end of 2001 respectively. We carried out three principal maintenances as follows in the second scheduled maintenance period.

#### 1) Replacement of the acceleration tube

The tandem accelerator group tried test to improving characteristic of high voltage by replacing

with the acceleration tubes. The performance of the accelerator is greatly depends on the performance of the acceleration tube. So, we tried some inspection of the acceleration tube itself before installing to the accelerator. At first, we measured amounts of micro particles using particle counter at the original condition of the tube with blowing the gas. As the results, a lot of micro particles were measured. The micro particles cause of small sparks inside the tube, and the small sparks will cause of radial spark in the accelerator. We, therefore, tried cleaning up process inside of the new tubes by high-purity water which was the resistivity of  $15 \times 10^6 \text{ ohm} \cdot \text{cm}$  with pressurized gas. After this process by 0.1Mpa, 10 minutes blow the gas with water, the amounts of micro particles decreased to 0.5~2%. In the test operation on the tandem accelerator, the washed acceleration tube module and the present using tubes( un-washed ) module were tested independently. The tests showed that the washing process causes very good results. That is, on the module with the washed tubes, the voltage could increase to 1MV in short time without small sparks inside the tubes. On the other hand, on the modules with the un-washed tubes, many small sparks inside the tubes were observed. Figure 1 shows the test results of voltage, vacuum and x-ray behavior.

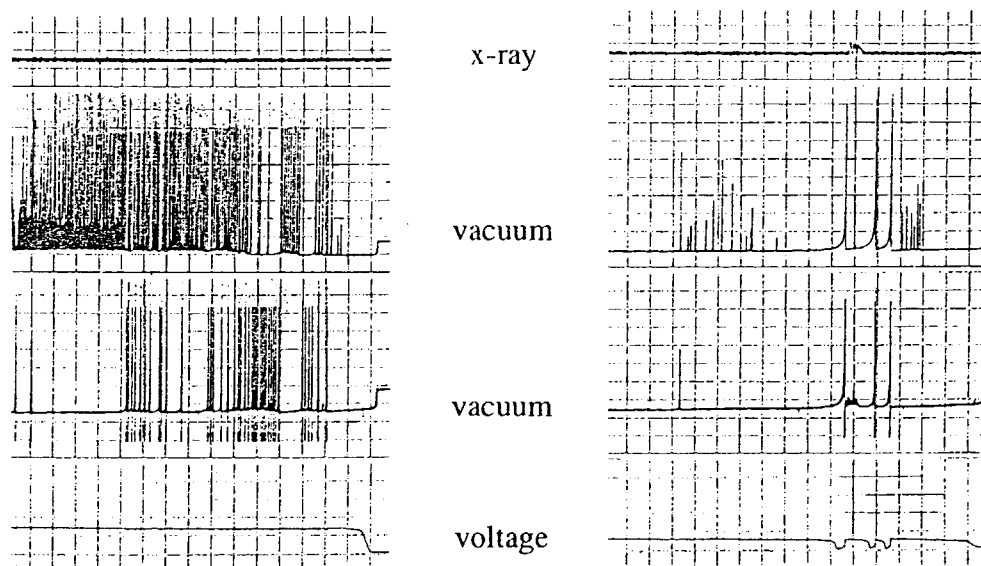


Figure 1 Test results. Right is the washed tube section and left is un-washed present using 3 sections.

## 2) Change of the voltage dividing system

JAERI tandem accelerator introduced resistor network system instead of corona dividing system. The corona dividing systems for the acceleration tube and the equipotential column supply the voltage uniformly to each electrode. But, these systems often appear the distinctive character of instability by shortage of corona current at low voltage operation. The resistor sets were installed with special fittings for tubes and column with 1.2Gohm and 4Gohm respectively between every electrode. On the operation of the accelerator at the low voltage operation, the instability by the electron loading of the acceleration tube were greatly improved. Figure 2 and 3 show the installed resistor network.



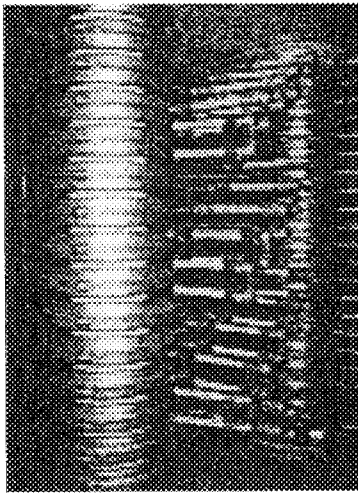


Figure 2 Column resistors.  
2 Gohm serial for every section.

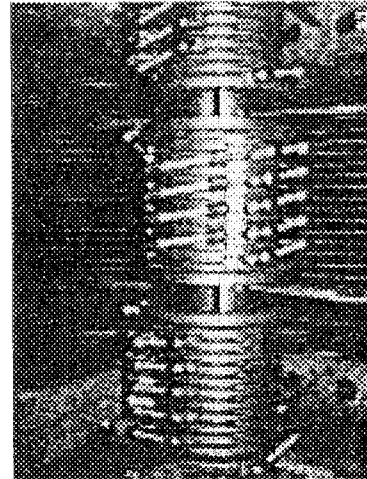


Figure 3 Acceleration tube resistor.  
1.2Gohm for each section (top and bottom  
end installed resistor to parallel)

### 3) Maintenance of the superconducting booster

There were a few troubles in FY2001. A small helium leak happened to a cryo-module, which was fixed by replacing all the indium gaskets between the flanges used to connect the resonators. Such a leak was clearly attributed to too many(20-30) thermal cycles repeated over 8 years, from the fact that the bolts for the gaskets were very loose. The time had come to re-tighten the bolts for all the gaskets. An RF input coupler drive mechanism in another cryo-module was out of order. As a result, maintenance was done for three cryo-modules in FY 2001, which included frequency re-tuning at the room temperature as well as bolt tightening.

## 1.2 UTILIZATION OF TANDEM ACCELERATOR AND BOOSTER

T. YOSHIDA and S. KANDA

The utilization of the tandem accelerator facility was carried out for 202 days for various experiments in two scheduled machine time periods in the FY 2001. Collaboration research proposals for the FY 2001 were examined at late November in 2000, and 24 subjects were accepted by the program advisory committee. The middle of 2001, one collaboration research program and two JAERI programs were proposed. These programs were accepted at the program advisory committee. The collaboration programs accounted for approximately 76% of the whole machine time. Twenty-five ion species were utilized in the two experimental periods as follows. Inert gas ions like Ar, Kr, Xe were accelerated steadily from a terminal ECR ion source for various experiments.

### 1) Time distribution in terms of projectiles

$^1\text{H}$	23 days	$^{40}\text{Ar}$	4 days
$6,7\text{Li}$	9	$^{58,60}\text{Ni}$	12
$^{11}\text{B}$	1	$^{64}\text{Zn}$	9
$^{12,13}\text{C}$	11	$^{74}\text{Ge}$	9
$^{14}\text{N}$	7	$^{86}\text{Kr}$	14
$^{16,18}\text{O}$	34	$^{82}\text{Se}$	15
$^{19}\text{F}$	2	$^{90}\text{Zr}$	4
$^{28}\text{Si}$	4	$^{127}\text{I}$	4
$^{31}\text{P}$	4	$^{136}\text{Xe}$	13
$^{32,33}\text{S}$	14	$^{197}\text{Au}$	9

The experimental terms allotted in the two periods were 108 days in March 15 to July 10, 111 days in September 10 to January 24 in 2002. The first term period contained 17 days in the term of FY 2000, so the data excluded from this report. The summary of allotted days to various experimental subjects is as follows.

<u>Research field</u>	<u>allotted days</u>	<u>total number of subjects</u>
Nuclear physics	94	28
Atomic and Solidstate physics	51	42
Nuclear chemistry	48	26
Material research	8	7
Accelerator development	1	1

### 1.3 JAERI-KEK JOINT RNB PROJECT

S.TAKEUCHI and H. MIYATAKE<sup>1</sup>

JAERI-Tokai and KEK-IPNS(Institute of Particle and Nuclear Studies) signed up for a joint project of developing a radioactive-nuclear-beam(RNB) facility in the tandem accelerator laboratory starting from 2001. The RNB facility will have a linac system which has been developed at KEK-Tanashi for acceleration of RNB. For producing RNB, proton beams from the tandem accelerator are to be used as the drive beams. A prospective RNB production target is a uranium-carbide which emits a number of neutron-rich fission products(FP). An existing ISOL system will be utilized for isotope separation. A charge breeder is under development at KEK at Tsukuba, which will be used to strip many electrons from the RNB primary ions in order to inject high charge state ions to the RNB linac. An ECR ion source is also planned to be implemented as an injector for intense SNB(stable ion beams). The first acceleration unit is a split-coaxial RFQ linac of 26MHz with acceleration energy of 0.17 MeV/u and the second unit is an IH(interdigital-H type) linac of 52 MHz with exit beam energy of 1 MeV/u[1,2]. Another linac with exit beam energy of 2 MeV/u needs to be built in future to inject the beams into the booster(of which frequency is 130 MHz) in order to get the beam energy beyond the Coulomb barrier energy for most of the beam and target species.

We expect that the RNB will be obtained with an intensity of  $10^5$  to  $10^7$  particle/s and will develop innovations in the studies on nuclear structures of unstable nuclei, formation processes of nuclear species in astro-physics, material science with RNB implantation and so on. For SNB from the ECR ion source and accelerated by linacs, there is a big prospect to multiply the present intensities from the tandem or booster by orders of 10 to 1000, or to the order of 1  $\mu$ A. Such an increase of SNB is useful for the studies of the synthesis of super heavy nuclei and chemical structures of actinoids from the point of relativistic effect on orbital electrons or for the experiments which need a high beam fluence.

From a few years ago, layout plans, building expansion plans and various practical problems have been studied by working groups which involved users and staff members of the tandem accelerator lab and KEK staff members of nuclear physics and accelerator physics. The layout plan settled in FY 2000 is shown in Fig. 1. The existing linacs and experimental apparatus will be installed in an old neutron target room with some expansion. In FY2001, the building plans were drawn by architects and a utility building for accelerator power supplies and cooling systems was built near the neutron-target room. A series of safety studies against generating FP with protons and uranium-carbide and accelerations of radioactive isotopes have been carried out and made it ready to take steps to get this RNB plan authorized by the government. R&D for RNB ion sources were carried on by nuclear chemists and physicists. KEK built an 18GHz ECR type charge breeder and started experiments with it. In FY2002, the old target room will be expanded and changed to the RNB acceleration room with a ventilation system capable of handling non-enclosed radioactive isotopes. The linacs will be installed in the room in FY2003 after some modifications are given to them in FY 2002. The first beam is expected in FY 2004.

<sup>1</sup> Institute of Particle and Nuclear Studies, KEK

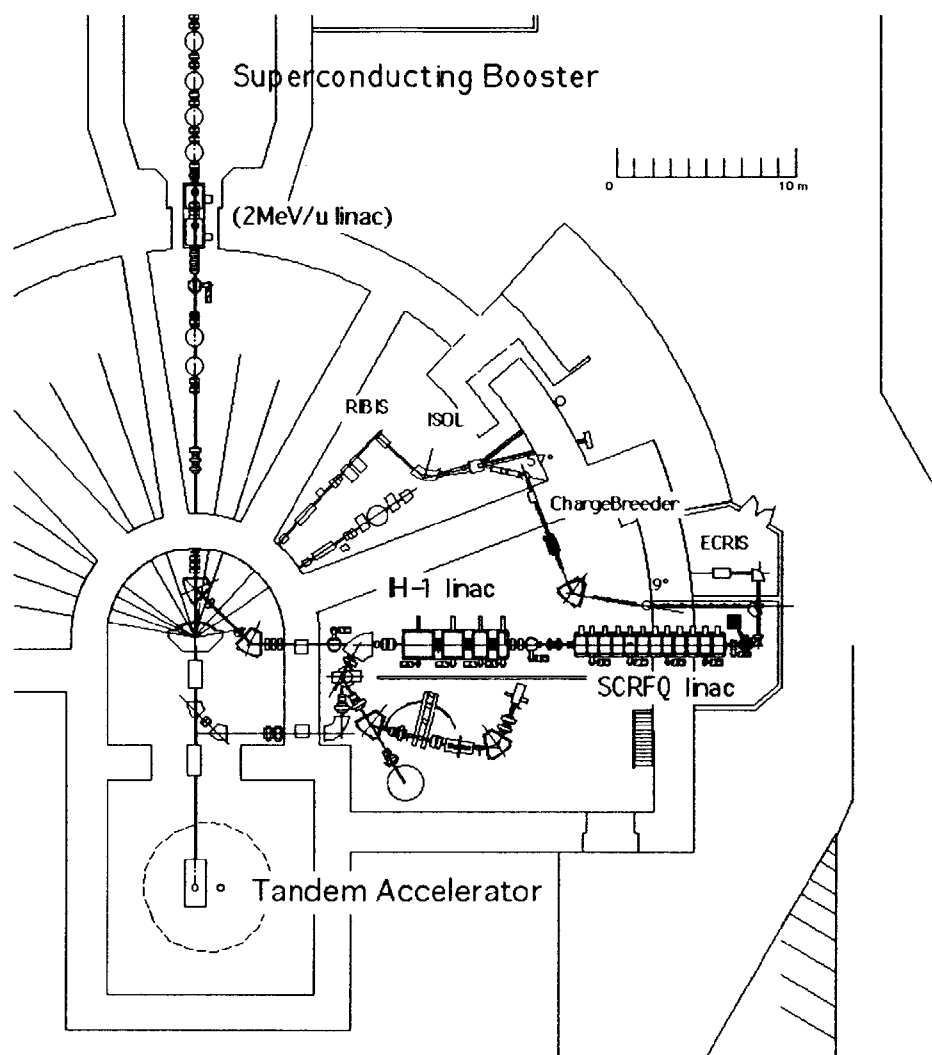


Fig. 1. Layout plan of the JAERI-KEK's RNB project.  
(The first three year plan does not include the transport line and additional injector linac to the superconducting booster.)

### References

- [1] S. Arai et al, Nucl. Instr. and Methods **A390**(1997)9-24.
- [2] M. Tomizawa et al, Proc. of the Heavy Ion Accelerator Technology: Eighth International Conference, AIP 1-56396-806-1/99, pp451-465

## 1.4 ION SOURCE DEVELOPMENT FOR ON-LINE MASS SEPARATION OF LIGHT RADIOACTIVE NUCLEAR BEAM

A.OSA, M.MATSUDA, K.TSUKADA, S.ICHIKAWA,  
S.C.JEONG<sup>1</sup> and I. KATAYAMA<sup>1</sup>

An ISOL-based radioactive nuclear beam (RNB) facility is under construction to provide RNBs having energy up to 1 MeV/u. The RNBs will be produced by nuclear fusion and nucleon transfer reactions, and particle-induced fission with proton and various heavy ion beams. The produced RNBs will be used for researches in the fields of nuclear physics, nuclear astrophysics and in material sciences. The RNB,  $^8\text{Li}$ ,  $^{18}\text{F}$  and  $^{20}\text{F}$  nuclei, will be used to study thermal diffusion processes in materials at the very early stage of the RNB facility. We have investigated the release time of Li atom and separation yield of  $^8\text{Li}$  produced in the neutron transfer reaction with  $^7\text{Li}$  beam, and molecular-ion formation of F atom to produce the RNBs of  $^8\text{Li}$ ,  $^{18}\text{F}$  and  $^{20}\text{F}$ .

Release time of  $^7\text{Li}$  from the target-catcher-ion-source system was measured using the heavy ion implantation technique given by Kirchner [1] with a cavity type thermal ion source. In this method, the stable isotopes accelerated by the tandem accelerator were implanted at a constant beam current  $I_{in}$  into the target/catcher inside the ion source. During the irradiation, the mass-separated beam intensity of the same isotope was monitored. After the mass-separated intensity  $I_{out}$  was saturated, time dependence of the mass-separated beam intensity after switching off the primary beam directly corresponds to the release behavior. Also, the intensity ratio  $I_{out}/I_{in}$  is directly given as the separation yield. Target units of four 0.1-mm thick graphite sheets, four 25- $\mu\text{m}$  thick tantalum foils and 1-mm thick BN (Boron Nitride), were respectively bombarded with 60 MeV  $^7\text{Li}$  beams with intensity of about 150 pA. The mass-separated ions were collected by a Faraday cup and the  $^7\text{Li}$  ion currents were measured with a Pico-ammeter controlled by a personal computer. The release profiles of Li atom from the target units measured at target/ion - source temperature of 2500 K are shown in Fig. 1. The release times and fractional yields of the first component deduced from the two and/or three exponential fit to the data were; 1.1 s and 67 % for graphite, 1.1 s and 60 % for BN, 1.3 s and 1.4 % for Ta target.

For the separation yield measurements of  $^8\text{Li}$  produced in the transfer reaction, the

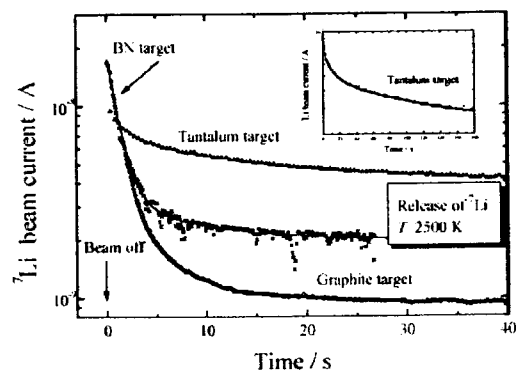


Fig.1. Release profiles of  $^7\text{Li}$ .

<sup>1</sup>High Energy Accelerator Research Organization

Table 1. Separation yield of  $^8\text{Li}$  and overall efficiency.

Target/catcher	Yield of $^8\text{Li}$ (/atoms/s/ 100 pA)	Overall efficiency (%)
Ta	$1.3 \times 10^4$	5~7
Graphite	$3.0 \times 10^4$	5~6
BN	$7.5 \times 10^4$	6

mass-separated products were collected on an aluminized Mylar tape and  $\beta$ -ray measurements were performed with an HPGe detector. In Table 1, we summarized the overall efficiencies measured by  $^7\text{Li}$  atoms together with the separation yields of  $^8\text{Li}$  produced in the transfer reactions using the same target units.

Taking account of the release time, fractional yield and formation cross section [2] and assuming that the  $^{13}\text{C}$  graphite target is bombarded with  $^7\text{Li}$  beams of 300 pA, the separation yield of  $^8\text{Li}$  is expected to be  $1 \times 10^7$  atoms/s.

For mass separation of fluorine atom, we studied molecular ion formation,  $\text{AlF}^+$  and  $\text{HF}^+$ , using a FEBIAD ion source. To form  $\text{AlF}^+$  molecular ions, natural  $\text{Al}_2\text{O}_3$  powder pressed together with natural graphite powder was used as a target. The target was directly attached to the anode of the FEBIAD ion source with a small tantalum target holder. With this arrangement, the ionization efficiency of Xe atoms was 10-12 %. The experiments were carried out using the heavy ion implantation technique and 124 MeV  $^{19}\text{F}$  beams with intensity of about 100 pA. The overall efficiency was 7% for  $^{27}\text{Al}^{19}\text{F}^+$ .  $\text{HF}^+$  molecular ion formation was observed when using thin rhodium and tantalum foils as the target materials. The thickness of these targets was 3  $\mu\text{m}$  and 4  $\mu\text{m}$ , respectively: most of the primary beam hit the tantalum cathode of the ion source. The fluorine atoms were combined with the residual hydrogen in the vacuum. Though, the overall efficiency achieved 12% for  $\text{H}^{19}\text{F}^+$ . As a result, the  $\text{HF}^+$  ion formation gave better overall efficiency than the  $\text{AlF}^+$  ion formation. If we could control the formation of the HF in the ion source, it becomes a useful method to separate the radioactive fluorine atoms. In the present study, the separation yields were observed to be  $1 \times 10^4$  atoms/s for  $\text{H}^{18}\text{F}$  and  $5 \times 10^2$  atoms/s for  $\text{H}^{20}\text{F}$  at incident beam currents of 300 pA, respectively. This result indicates that the release time of F or HF atoms from the target/ion-source was somewhat too long for the mass separation of a fluorine isotope  $^{20}\text{F}$  of  $T_{1/2}=11\text{s}$ .

## References

- [1] R. Kirchner, Nucl. Instrum. Methods. B70,(1992) 186.
- [2] L. Trache *et al.*, Cyclotron Progress Report, 1999-2000, Texas A&M Univ.

## 1.5 A 14.5GHz IN-TERMINAL ECR ION SOURCE

M. MATSUDA, Y.FUJII<sup>1</sup>, S. TAKEUCHI

In-terminal ECR ion source (TECRIS) is stably working to mainly accelerate proton, oxygen and noble gas ions. The operation time of TECRIS was 37days which were 18% of the whole machine time scheduled in FY2001. The trouble of TECRIS system was only occurred in the high voltage power supplies for an electrostatic steerer.

Present TECRIS is composed of the small permanent magnet ECR ion source which works at 10 GHz and RF power up to 200 W. Accelerated beam current is increased as compared with a conventional negative ion source, but it is not sufficient yet. In addition, the beam energy is inadequate for the post super conducting booster linac which optimum velocity is 10% of the light velocity. That is because, the field strength and the analyzing power of the 45° injection magnet of present TECRIS are insufficient. For that reason, in Kr and Xe ions, the pre-accelerating voltage is restricted to lower than 80kV. And enriched isotope gases are used for the source gases.

In order to solve these problems, we are planning to the next project which is to install higher performance ECRIS at the optimum position in the high voltage terminal. Space, electric power and cooling for ion source system are taken into accounts. It was chosen that an all permanent magnet ECR ion source, called SuperNanogan, which works at 14.5GHz and RF power up to 200 W. The SuperNanogan works without the mirror coil which needs more space, DC power supplies and powerful cooling system. Accordingly, it is possible to use about the same condition like the present TECRIS system.

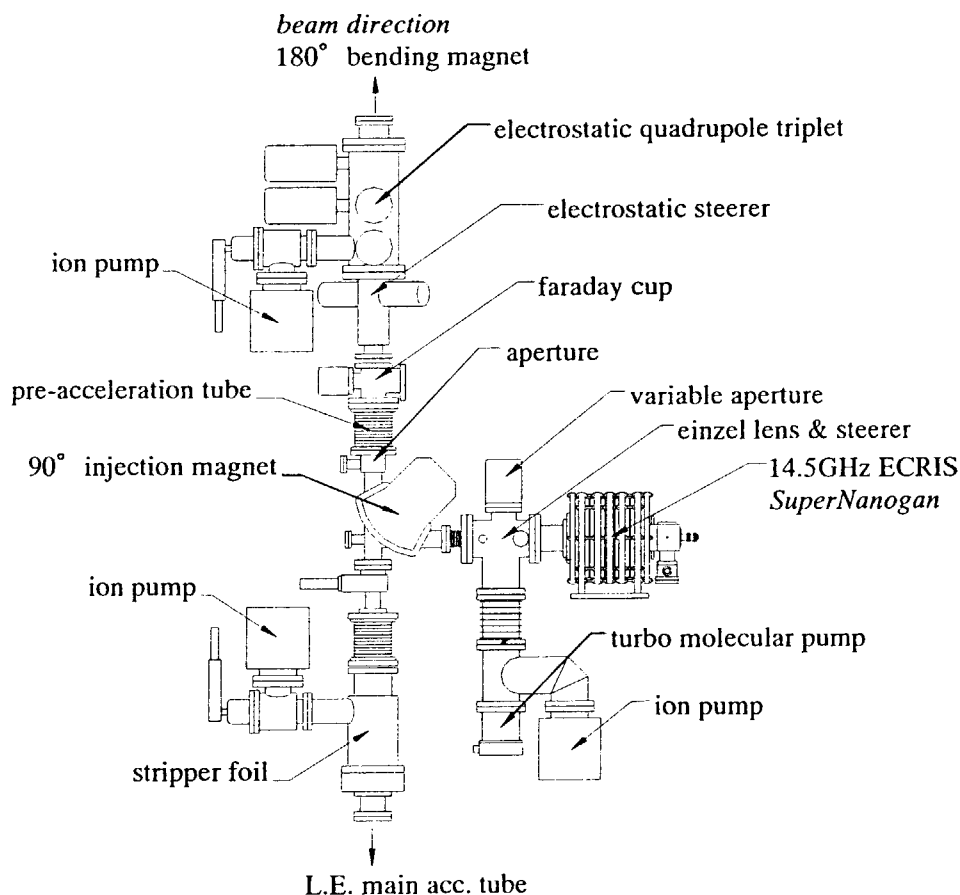


Figure 1. Installation arrangement of 14.5GHz in-terminal ECR ion source

<sup>1</sup> Nihon Advanced Technology. Co.

The arrangement of the new TECRIS system is designed as shown in Fig.1. It is impossible to install the same place that was set present TECRIS, because the size of the SuperNanogan are 40cm diameter, 40cm length and its weight is about 150kg. So that, the position of the new TECRIS system is intended to attach the low energy beam line at the terminal. The  $90^\circ$  injection magnet will be set the position of existing gas stripper. The ECR ion source, extraction system and the  $90^\circ$  injection magnet are placed at the 80kV Deck. Acceleration tube is set to the downstream of the  $90^\circ$  injection magnet for pre-acceleration. The ion beams are extracted by a 30kV(maximum) potential gap from the ion source, focused by an Einzel lens, and then the mass and charge of them are roughly selected by the  $90^\circ$  injection magnet. The horizontal beam direction is corrected by an electrostatic steerer placed just before the injection magnet. After acceleration by a 80kV pre-acceleration tube, desired ions are selected by the  $180^\circ$  bending magnet. The field strength and an analyzing power of the  $180^\circ$  bending magnet are sufficient to select the ion beams. Finally, ion beams are focused by an electrostatic quadrupole triplet lens, and injected into the main acceleration tube of high energy side. In order to take this layout, existing gas stripper canal which is used to obtain low energy beams for atomic and solid state physics have to remove. Fortunately, new TECRIS system will be able to generate such low energy beams by accelerating of low charge state ions. Comparison of expected beam energies between both TECRIS and the conventional negative ion source with foil stripping process is shown in Fig.2.

In this project, the gas flow is intended to adjust in order to generate highly charged ions. And a variable aperture which placed just after the einzel lens is going to control the beam current without adjusting operational parameter of ion source. That is because, especially proton ions, beam current control is too difficult only adjusting ion source parameter.

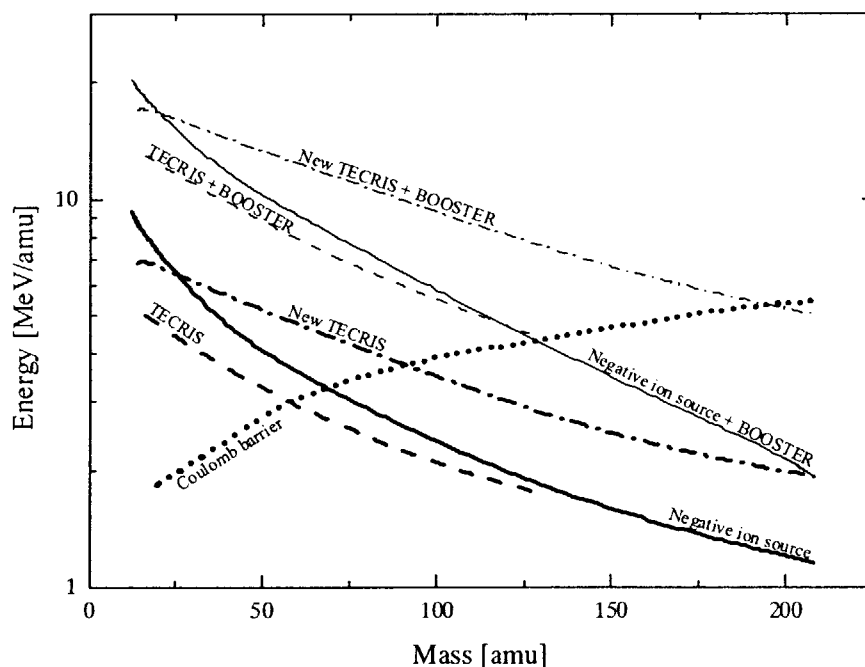


Figure 2. Comparison of expected beam energies between both TECRIS and the conventional negative ion source with foil stripping process.

## References

- [1] M. Matsuda et al., JAERI TANDEM & V.d.G Annual Report 1997 p.10.
- [2] M. Matsuda et al., JAERI TANDEM & V.d.G Annual Report 2000 p.7.
- [3] P. Sortais et al., Rev. of Sci. Instrum. (1998) p.656.



## **2. Nuclear Structure**

This is a blank page.

## 2.1 PRELIMINARY EXPERIMENT TO STUDY K-ISOMERS BASED ON THE INTRUDER CONFIGURATIONS AROUND $^{124}\text{Sn}$

M. SUGAWARA<sup>1</sup>, T. SHIZUMA, T. HAYAKAWA, Y. TOH, M. OSHIMA,  
M. KOIZUMI, A. OSA, Y. H. ZHANG<sup>2</sup> and Z. LIU<sup>2</sup>

In the  $N=74$  even- $Z$  isotones from Xe to Gd,  $K^\pi=8^-$  isomers are systematically observed, whose configuration is the combination of  $\nu[514]9/2$  and  $\nu[404]7/2$  which is the neutron counterpart to the proton configuration forming the similar K isomers in  $A\approx 180$  Ta, Hf, and W region. On the other hand, the deformed intruder bands are systematically known in the Sn isotopes up to  $^{118}\text{Sn}$  which are of spherical shapes in their ground states. Therefore we can naturally expect to observe the K isomers based on the deformed intruder configurations around  $^{124}\text{Sn}$  which is the crossing point of the  $N=74$  and  $Z=50$  lines on the nuclear chart.

Since  $^{124}\text{Sn}$  lies in the neutron rich side of the  $\beta$ -stability line, the deep inelastic collision(DIC) is suitable for producing its neighboring nuclei. To check whether the DIC can populate the intruder states around  $^{124}\text{Sn}$ , a preliminary experiment was performed as a short run of 6 hours by the bombardment of 430MeV  $^{82}\text{Se}$  beam on a  $^{nat}\text{In}$  foil of 11 mg/cm<sup>2</sup> thickness. The beam energy was chosen so as to exceed the Coulomb barrier of  $^{82}\text{Se} + ^{115}\text{In}$  system by 16%. Emitted  $\gamma$ -rays were detected with an array of 12 HPGe detectors with BGO Compton suppressors(GEMINI)[1]. In Fig. 1, an example of gated spectra was shown, in which the transitions both within the intruder band and between the intruder and ground bands in  $^{116}\text{Sn}$  were seen. Encouraged by these results, we are planning to make a long run experiment using the combination of  $^{82}\text{Se}$  beam and  $^{nat}\text{Sb}$  foil.

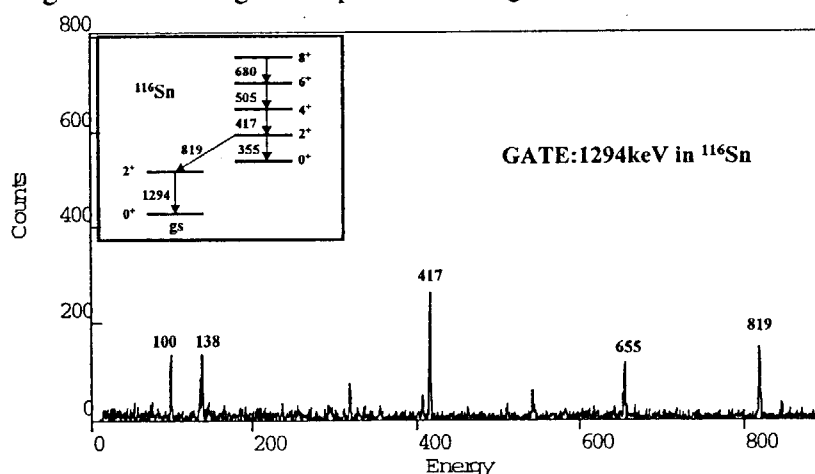


Fig.1. An example of gated spectra for  $^{116}\text{Sn}$ .

### References

- [1] K. Furuno et al., Nucl. Instrum. Methods A **421**(1999)211.

<sup>1</sup>Chiba Institute of Technology

<sup>2</sup>Institute of Modern Physics, P. R. China

## 2.2 SHAPE COEXISTENCE IN $^{98}\text{Mo}$

Y. TOH, M. ZIELINSKA<sup>1</sup>, T. CZOSNYKA<sup>1</sup>, J. CHOINSKI<sup>1</sup>, J. IWANICKI<sup>1</sup>,  
P. NAPIORKOWSKI<sup>1</sup>, M. OSHIMA, A. OSA, M. KOIZUMI,  
Y. HATSUKAWA, Y. UTSUNO, J. KATAKURA, M. MATSUDA, N. SHINOHARA,  
H. KUSAKARI<sup>2</sup>, M. SUGAWARA<sup>3</sup> and T. MORIKAWA<sup>4</sup>

The low energy structure of the even-even Mo isotopes undergoes a change from spherical at  $^{92}\text{Mo}$  to rotational at  $^{104}\text{Mo}$ . In these isotopes,  $^{98}\text{Mo}$  has a first excited  $0^+$  state. Only four even-even stable nuclei with  $Z > 20$ , namely  $^{72}\text{Ge}$ ,  $^{90}\text{Zr}$ ,  $^{96}\text{Zr}$  and  $^{98}\text{Mo}$  have a  $0^+$  first excited state. These  $0^+$  states would be interpreted the band-heads of the  $\beta$  vibrational bands within the framework of the collective model. However, Coulomb excitation studies of  $^{72}\text{Ge}$ [1] and  $^{96}\text{Zr}$ [2] proved that the ground  $0^+$  states are deformed, while the first excited  $0^+$  states have a spherical shape and can be interpreted as an intruder state.  $^{98}\text{Mo}$  is the best candidate for further investigation of the nature of the shape coexistence in this mass region.

The  $^{84}\text{Kr}$  and  $^{136}\text{Xe}$  beams of 1pnA from the tandem accelerator in JAERI bombarded on a self-supporting  $^{98}\text{Mo}$  target. The experimental setup, whose details are described elsewhere, consists of a gamma-ray detector array of 12 Ge detectors with BGO anti-Compton suppressors, GEMINI [3], and a newly developed position-sensitive particle detector system with 4 photomultiplier tubes in combination with 2 plastic and 2 Yap Ce scintillators[4]. Preliminary data were obtained in a simple experiment with a  $^{20}\text{Ne}$  beam, performed at the Heavy Ion Laboratory in Wawsaw with the use of the CUDAC set-up[5]. The least-squares analysis code GOSIA [6] was used to extract the E2 matrix elements and the Q moments from the experimental data. A resulting set of reduced matrix elements was rich and precise enough to perform further analysis of the nucleus shape. For example, the crucial matrix elements connecting  $0^+$  states with all observed  $2^+$  states were determined with accuracy better than 15%.

Figure 1 and 2 show the quadrupole deformation parameters, calculated for both  $0^+$  states in  $^{98}\text{Mo}$ , in comparison with available data from selected Ge isotopes[1,7,8] which also have a low-lying excited  $0^+$  state. In case of Ge isotopes the ground state is deformed, while the second  $0^+$  state tends to be spherical. For  $^{98}\text{Mo}$  overall deformation is the same for both  $0^+$  states. The triaxiality remains the same for each of Ge isotopes. On the contrary, the ground  $0^+$  state of  $^{98}\text{Mo}$  is triaxial, while the first excited  $0^+$  state has a prolate shape.

---

<sup>1</sup>SLCJ, University of Warsaw

<sup>2</sup>Chiba University

<sup>3</sup>Chiba Institute of Technology

<sup>4</sup>Kushu University

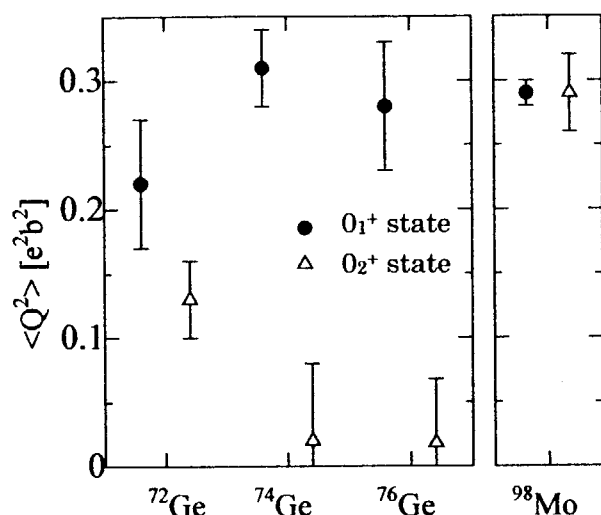


Fig. 1. Mean values of  $Q^2$  parameter found for the two first  $0^+$  states in  $^{98}\text{Mo}$  and  $^{72,74,76}\text{Ge}$  isotopes.

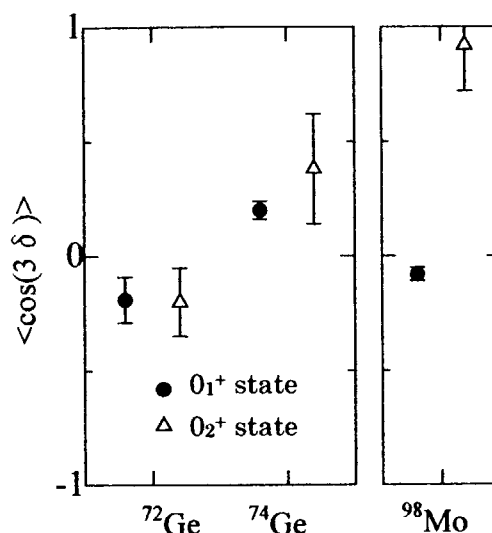


Fig. 2. Mean values of  $\cos(3\delta)$  parameter found for the two first  $0^+$  states in  $^{98}\text{Mo}$  and  $^{72,74}\text{Ge}$ .

## References

- [1] B. Kotlinski, T. Czosnyka, D. Cline, J. Srebrny, C.Y. Wu, A. Backlin, L. Hasselgren, L. Westerberg, C. Baktash, S.G. Steadman, Nucl. Phys. A **519**(1990) 646.
- [2] D. Cline, Acta Phys.Pol. **B30**(1999) 1291.
- [3] K. Furuno, M. Oshima, T. Komatsubara, K. Furutaka, T. Hayakawa, M. Kidera, Y. Hatsukawa, M. Matsuda, S. Mitarai, T. Shizuma, T. Saitoh, N. Hashimoto, H. Kusakari, M. Sugawara, T. Morikawa, Nucl. Instrum. Methods Phys. Res. A **421**(1999) 211.
- [4] Y. Toh, M. Oshima, T. Hayakawa, Y. Hatsukawa, J. Katakura, M. Matsuda, H. Iimura, H. Kusakari, D. Nishimiya, M. Sugawara, Y.H. Zhang, Rev. Sci. Instrum. **73**(2002) 47.
- [5] J. Iwanicki, J. Choinski, T. Czosnyka, J. Kownacki, M. Kisielinski, P. Napiorkowski, L. Zemlo, J. Srebrny, J.de Boer, M. Loewe, M. Wurfner, Acta Phys. Pol. **B28**(1997)153.
- [6] T. Czosnyka, D. Cline, L. Hasselgren, C.Y. Wu, R.M. Diamond, H. Kluge, C. Roulet, E.K. Hulet, R.W. Loughheed, C. Baktash, Nucl. Phys. A **458**(1986) 123.
- [7] Y. Toh, T. Czosnyka, M. Oshima, T. Hayakawa, H. Kusakari, M. Sugawara, Y. Hatsukawa, J. Katakura, N. Shinohara, M. Matsuda, Eur. Phys. J. A **9**(2000) 353.
- [8] Y. Toh, T. Czosnyka, M. Oshima, T. Hayakawa, H. Kusakari, M. Sugawara, Y. Hatsukawa, J. Katakura, N. Shinohara, M. Matsuda, J. Phys. G **27**(2001) 1475.

## 2.3 EXCITED STATES IN $^{187}\text{Re}$ POPULATED BY INELASTIC SCATTERING

T. SHIZUMA, M. SUGAWARA<sup>1</sup>, T. HAYAKAWA, Y. TOH, M. OSHIMA,  
M. KOIZUMI, A. OSA, Y.H. ZHANG<sup>2</sup> and Z. LIU<sup>2</sup>

The nucleus  $^{187}\text{Re}$  lies in a region where many high- $j$  and high- $\Omega$  orbitals are close to both the proton and neutron Fermi surfaces. High- $K$  ( $= \sum_i \Omega_i$ ) multi-quasiparticle states, therefore, can exist at low excitation energy, competing with collective excited states forming a yrast line. For the axially deformed nuclei, the projection of the total angular momentum onto the nuclear symmetry axis,  $K$ , is approximately conserved. Consequently, the  $K$  selection rule governs the decay of high- $K$  states, so that transitions from high- $K$  to low- $K$  bands are hindered. These transitions, however, can proceed by admixture of  $K$  values. The Coriolis interaction changes the spin orientation which leads to a  $\Delta K = \pm 1$  mixing, while shape fluctuations towards  $\gamma$  deformation can couple states with  $K$  quantum numbers differing by two units ( $\Delta K = \pm 2$  mixing). In the high- $K$  isomeric decay, surprisingly low hindrance factors have been observed in spite of the very large  $K$  changes of the transitions [1]. So far, different mechanisms including Fermi-aligned Coriolis  $K$  mixing [2],  $\gamma$ -tunneling through the potential barrier [3], and the statistical  $K$  mixing due to high level density [4] have been proposed.

High-spin studies of  $^{187}\text{Re}$  have been limited due to inaccessibility using the fusion-evaporation reaction with stable isotopes for both the projectile and the target. By employing an inelastic scattering reaction on  $^{187}\text{Re}$ , the present study has revealed near-yrast excited levels up to high spins. The experiment was carried out by use of the JAERI tandem and booster accelerator. A natural rhenium foil with a thickness of 26 mg/cm<sup>2</sup> was bombarded by a 500 MeV  $^{82}\text{Se}$  beam. The beam energy was selected as 15 % higher than the Coulomb barrier for the  $^{82}\text{Se} + ^{187}\text{Re}$  system. Emitted  $\gamma$  rays were detected by the GEMINI Ge-detector array consisting of twelve Compton-suppressed HP-Ge detectors, positioned at 32° (2 detectors), 58° (2), 90° (4), 122° (2) and 148° (2) with respect to the beam axis. Events were recorded on magnetic tapes when two or more Ge detectors were fired in coincidence.

Figure 1 shows a  $\gamma$ -ray spectrum gated on the 134 keV transition in the ground state band assigned as the  $\pi 5/2^+[402]$  configuration. We have extended the  $\pi 5/2^+[402]$  band to  $I^\pi = 21/2^+$ , and the  $\pi 9/2^-[514]$  band to  $I^\pi = 19/2^-$ . The intensity ratios of  $\Delta I = 1$  and  $\Delta I = 2$  transitions in the bands have been used to extract the  $g_K$  factors for conforming the quasiparticle configurations. Above the  $\pi 9/2^-[514]$  band, we have observed a new isomer with  $I = 21/2$  or  $23/2$ . Following configurations can be coupled with the low-lying  $I = 21/2$  or  $23/2$  states;

$$\begin{aligned} K^\pi &= 21/2^+ \pi 9/2^-[514] \otimes \nu\{1/2^-[510] 11/2^+[615]\} \\ K^\pi &= 23/2^- \pi 5/2^+[402] \otimes \nu\{7/2^-[503] 11/2^+[615]\} \end{aligned}$$

<sup>1</sup>Chiba Institute of Technology

<sup>2</sup>Institute of Modern Physics, Chinese Academy of Sciences

Both the configurations would be energetically favoured because of the residual spin-spin interaction, known as the Gallagher-Moszkowski rule. Further analysis is in progress.

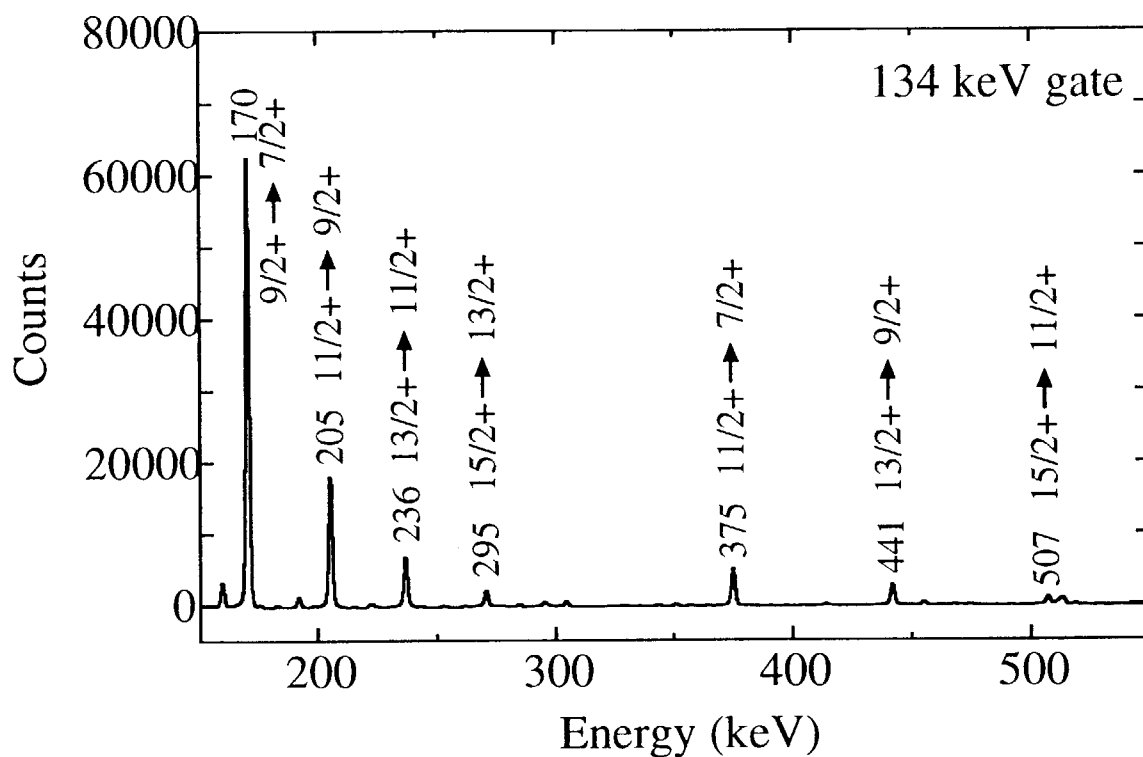


Fig. 1. A  $\gamma$ -ray spectrum gated on the 134 keV transition.

## References

- [1] P. Chowdhury *et al.*, Nucl. Phys. **A485**, 136 (1988); P.M. Walker *et al.*, Phys. Rev. Lett. **65** 416 (1990); B. Crowell *et al.*, Phys. Rev. Lett. **72** 1164 (1994).
- [2] P.M. Walker *et al.*, Phys. Rev. Lett. **67**, 433 (1991); P.M. Walker *et al.*, Phys. Lett. B **309**, 17 (1993).
- [3] K. Narimatsu, Y.R. Shimizu and T. Shizuma, Nucl. Phys. **A601**, 69 (1996).
- [4] P.M. Walker *et al.*, Phys. Lett. B **408**, 42 (1997).

## 2.4 ROTATIONAL BANDS AND SIGNATURE INVERSION IN ODD-ODD $^{176}\text{Ir}$

Y. H. ZHANG<sup>1</sup>, T. MORIKAWA<sup>2</sup>, M. OSHIMA, Y. TOH,  
M. KOIZUMI, A. OSA, T. SHIZUMA, T. HAYAKAWA,  
H. KUSAKARI<sup>3</sup>, M. SUGAWARA<sup>4</sup>, S.X. WEN<sup>5</sup> and L.H. ZHU<sup>5</sup>

Signature inversion [1] is one of interesting phenomena observed in a number of deformed odd-odd nuclei. In the nuclear mass regions of  $A \sim 80, 130$  and  $160$ , the signature inversion has been systematically observed for the rotational bands having configurations such as  $\pi g_{9/2} \otimes \nu g_{9/2}$ ,  $\pi h_{11/2} \otimes \nu h_{11/2}$ ,  $\pi h_{11/2} \otimes \nu i_{13/2}$  or  $\pi h_{9/2} \otimes \nu i_{13/2}$ . Since the phenomenon has been observed in the band involving high- $j$  orbitals, it is natural to expect the similar inversion for the band having configurations such as  $\pi i_{13/2} \otimes \nu i_{13/2}$ ; the  $\pi i_{13/2} - 1/2^+ [660]$  orbital is involved instead of  $\pi h_{9/2} - 1/2^- [541]$  in the  $\pi h_{9/2} \otimes \nu i_{13/2}$  structure [2]. A number of efforts have been devoted recently to reveal the feature of signature inversion of such bands in  $^{178}\text{Ir}$  [3, 4, 5] and  $^{182}\text{Au}$  [6]. To extend the systematics and investigate the phenomenon in this mass region, we undertook an experiment on  $^{176}\text{Ir}$ . The full paper of present study has been published in [7].

The experiment was made at the Japan Atomic Energy Research Institute (JAERI). A target of  $2.1 \text{ mg/cm}^2$   $^{149}\text{Sm}$  foil with a  $5.5 \text{ mg/cm}^2$  Pb backing was bombarded by a  $^{31}\text{P}$  beam delivered from the JAERI tandem accelerator. A BGO-Ge array GEMINI [8] was used to detect the  $\gamma$ -rays. The array consisted of 11 HP-Ge's and one LOAX with BGO anti-Compton shields. Figure 1 shows a partial level scheme of  $^{176}\text{Ir}$  proposed in the present work. The uncertainty of  $\gamma$ -ray energies in the level scheme are within 0.5 keV. The ordering of  $\gamma$ -rays in the level scheme was determined on the basis of coincidence relations, energy sums and relative intensities. The spin and parity assignment was made by using measured DCO ratios and/or interband transitions involving the levels of known spin/parity.

The signature splitting in the  $\pi h_{9/2} \otimes \nu i_{13/2}$  (band 1) and  $\pi i_{13/2} \otimes \nu i_{13/2}$  (band 4) configurations is presented in Fig. 2, where the level staggering curves of these bands are plotted together with those of  $^{178}\text{Ir}$ . For both nuclei, the favored branch lies higher than the unfavored one showing the so-called low-spin signature inversion [1]. The signature splitting reverts to normal at the critical spin  $I_c = (18) \hbar$  for the  $\pi h_{9/2} \otimes \nu i_{13/2}$  band in  $^{176}\text{Ir}$ . The  $I_c$  for  $^{176}\text{Ir}$  is  $3 \hbar$  smaller than that for  $^{178}\text{Ir}$ , which is consistent with an expectation from the systematic trend [4], and could probably be interpreted qualitatively due to the lowering of neutron Fermi surface and the reduced deformation of the core [9]. On the other hand, the critical spin  $I_c$  for the  $\pi i_{13/2} \otimes \nu i_{13/2}$  band in  $^{176}\text{Ir}$  was not reached in the present work, which indicates that the  $I_c$  may be larger than  $25 \hbar$ . A retardation of  $I_c$  for  $\pi i_{13/2} \otimes \nu i_{13/2}$  band with respect to that of  $\pi h_{9/2} \otimes \nu i_{13/2}$  band would be expected by considering the following points; 1) Both quasi-proton and quasi-neutron occupy the same high- $j$  orbitals in the  $\pi i_{13/2} \otimes \nu i_{13/2}$  configuration; this may lead to a stronger p-n interaction which tends to keep the inverted splitting, as compared to the  $\pi h_{9/2} \otimes \nu i_{13/2}$  configuration. 2) The  $i_{13/2} - 1/2^+ [660]$  proton drives the nucleus towards larger deformation, which will reduce the amplitude of normal signature splitting caused by Coriolis force. However, we could not understand so far the non-observation of  $I_c$  in the  $\pi i_{13/2} \otimes \nu i_{13/2}$  band of  $^{176}\text{Ir}$  up to  $I^\pi = (25^+) \hbar$ .

<sup>1</sup> Institute of Modern Physics, Chinese Academy of Science, Lanzhou, PRC.

<sup>2</sup> Faculty of Sciences, Kyushu University.

<sup>3</sup> Faculty of Education, Chiba University.

<sup>4</sup> Chiba Institute of Technology.

<sup>5</sup> China Institute of Atomic Energy, Beijing, PRC.



The authors wish to thank the JAERI tandem accelerator crew for providing  $^{31}\text{P}$  beam and their hospitality during the beam time. This work is supported in part by the National Natural Sciences Foundation of China (grant No. 10025525) and the Major State Basic Research Development Program of China (Contract No. G2000077400).

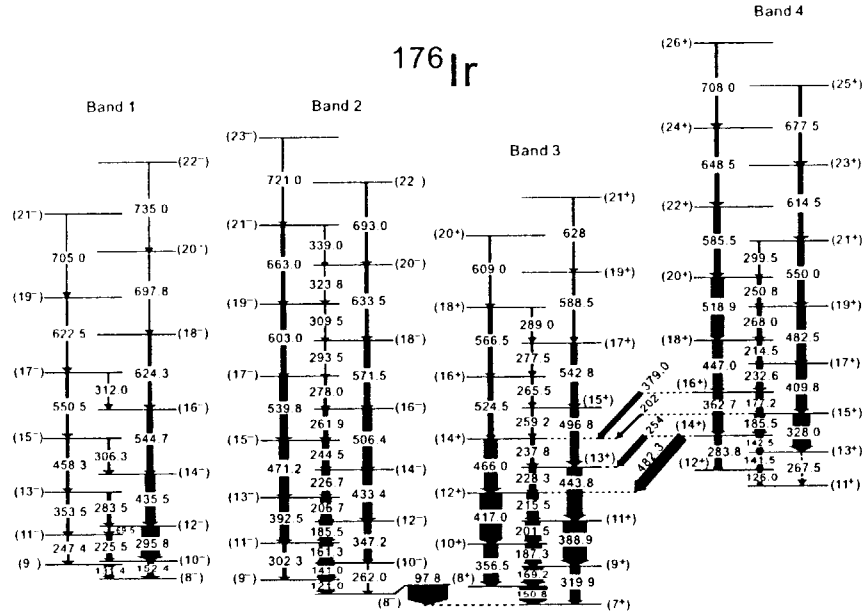


Figure 1: Partial level scheme of  $^{176}\text{Ir}$  proposed in the present work.

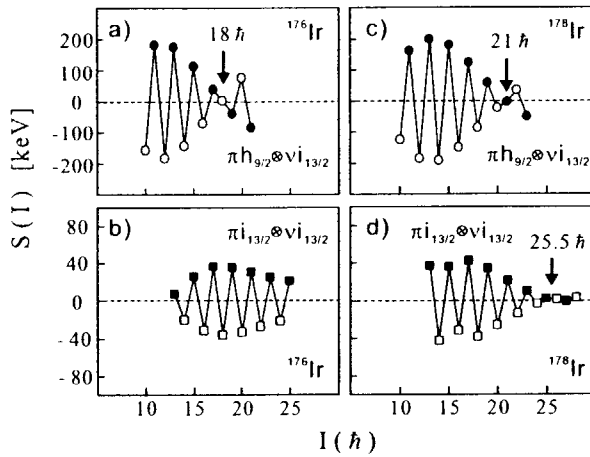


Figure 2: Plot of signature splitting vs  $I$  for the  $\pi h_{9/2} \otimes \nu i_{13/2}$  (upper panel) and  $\pi i_{13/2} \otimes \nu i_{13/2}$  (lower panel) bands in both  $^{176}\text{Ir}$  and  $^{178}\text{Ir}$  [3, 5]. The arrow indicates the critical spin  $I_c$ .

## References

- [1] R. Bengtsson et al., Nucl. Phys. **A415** (1984) 189.
- [2] R.A. Bark et al., Phys. Lett. **B 406** (1997) 193.
- [3] D. Hojman et al., Eur. Phys. J. **A 10** (2001) 245.
- [4] Y.H. Zhang et al., Eur. Phys. J. **A 8** (2000) 439.
- [5] Y.H. Zhang et al., Chin. Phys. Lett. **18** (2001) 1323.
- [6] Y.H. Zhang et al., Proc. of 8<sup>th</sup> National Conf. on Nucl. Structure, 24-31 Mar. 2000, Hakou, China; High Energy Phys. & Nucl. Phys. **24**, Suppl. 21 (2000) (in Chinese).
- [7] Y.H. Zhang et al., Eur. Phys. J. **A 13** (2002) 429.
- [8] K. Furuno et al., Nucl. Instrum. Methods Phys. Res. **A421** (1999) 211.
- [9] R. Bengtsson, Proc. of Int'l Conf. on High Spin Physics and Gamma-Soft Nuclei, Pittsburgh, USA, 1990, ed. J.X. Saladin, R.A. Sorensen, C.M. Vincent (World Scientific, Singapore, 1990) p. 289.

## 2.5 HYPERFINE STRUCTURE AND ISOTOPE SHIFT MEASUREMENTS OF $^{135}\text{La}$ BY COLLINEAR LASER SPECTROSCOPY

H. IIMURA, Y. ISHIDA<sup>1</sup>, M. KOIZUMI, N. SHINOHARA, M. OBA, M. MASABUMI, T. HORIGUCHI<sup>2</sup> and H.A. SCHUESSLER<sup>3</sup>

The La isotopes ( $Z=57$ ) are in a region of rapid transition from nuclei with nearly spherical shape (the singly magic  $^{139}\text{La}$ ) to nuclei that are soft towards deformation, presenting a good opportunity to test various nuclear models. So far we measured the hyperfine structure (HFS) and the isotope shift (IS) of accelerator-produced long-lived nuclide  $^{137}\text{La}$  ( $T_{1/2}=6\times 10^4$  y), and naturally occurring nuclides  $^{139}\text{La}$  (stable) and  $^{138}\text{La}$  ( $1.05\times 10^{11}$  y). Recently we have extended the measurement to short-lived  $^{135}\text{La}$  (19.5 h). There is no other previous measurement of HFS and IS of this nuclide.

The measurement of  $^{135}\text{La}$  was made by collinear laser ion-beam spectroscopy as those of other La isotopes. The nuclide  $^{135}\text{La}$  was produced by (p,3n) reaction. After the irradiation, La was chemically separated from the enriched  $^{137}\text{Ba}$  targets by an ion exchange technique. The sample of  $^{135}\text{La}$  was then deposited in the surface ionization ion source of a mass separator. The La ions were accelerated to 40 keV and mass-separated by a magnet. The intensity of the beam was less than 30 pA. The ions were excited by a counter propagating laser beam. Optical resonance was observed by detecting the fluorescence light by a photomultiplier tube. The signal from the photomultiplier tube was counted during the laser frequency scanning. An obtained hyperfine spectrum for  $^{135}\text{La}$  ion from the metastable  $6s^2\ ^1S_0$  level to the  $5d6p\ ^3D_1$  level ( $\lambda=538.2$  nm) is shown in Fig. 1. The line width is approximately 120 MHz (FWHM). Two of three hyperfine components are appeared in this spectrum. The other component,  $5/2-7/2$ , is out of this frequency range, and was observed at other scans made at higher frequency region.

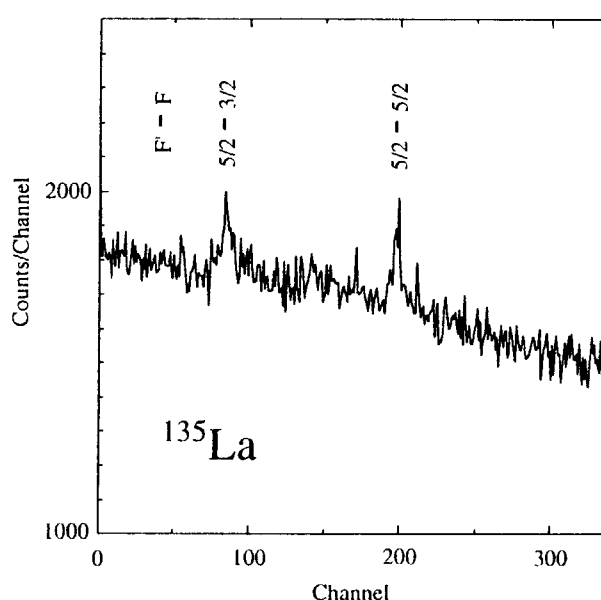


Fig. 1. Part of hyperfine spectrum of the 538.2-nm transition of  $^{135}\text{La}$ .

From preliminary analysis of these spectra, tentative values of the nuclear moments of the  $5/2^+$  ground state of  $^{135}\text{La}$  were obtained. Since the ground state of  $^{137,139}\text{La}$  is  $7/2^+$ , there is little experimental data of the nuclear moments of  $5/2^+$  levels in these nuclides, which can be compared with present results. However, obtained values of the nuclear moments of  $^{135}\text{La}$  are consistent with those of  $d_{5/2}$  states in Cs isotopes ( $Z=55$ ). The IS of 538.2-nm transition in  $^{135}\text{La}$  was also obtained. The change in mean-square nuclear charge radius was determined from the IS, and it was found that the deformation of this nucleus is larger than theoretical predictions based on the FRDM [1], ETFSI [2] and HFBCS [3]. Further analysis is now in progress.

### References

- [1] P. Möller *et al.*, At. Data and Nucl. Data Tables **59** (1995) 185.
- [2] Y. Aboussir *et al.*, At. Data and Nucl. Data Tables **61** (1995) 127.
- [3] S. Goriely *et al.*, At. Data and Nucl. Data Tables **77** (2001) 311.

<sup>1</sup>Institute of Physical and Chemical Research (RIKEN)

<sup>2</sup>Hiroshima International University

<sup>3</sup>Texas A&M University

## 2.6 NANOSECOND ISOMERS IN $^{32,33}\text{Si}$ and $^{34}\text{P}$

M. ASAI, T. ISHII, A. MAKISHIMA<sup>1</sup>, M. OGAWA<sup>2</sup>, and M. MATSUDA

The  $N=20$  closed shell is formed by a large energy spacing between the  $sd$ -shell orbitals and the next  $f_{7/2}$  orbital. However, recent experimental and theoretical investigations revealed that the closed shell properties of  $N=20$  vanish in the neutron-rich region around  $^{32}\text{Mg}$  [1,2]. Neutron excitations across the  $N=20$  shell gap play an important role in this phenomenon. The energies and the order of the neutron single-particle states in  $N\approx 20$  nuclei are expected to become a direct measure of this gap energy.

The  $\nu f_{7/2}$  states have been established in  $^{37}\text{Ar}$  and  $^{35}\text{S}$ , the neutron-rich  $N=19$  nuclei, at 1611 and 1991 keV, respectively. In  $^{36}\text{Cl}$  the  $(\pi d_{3/2}\nu f_{7/2})5^-$  state is known at 2518 keV. These levels are depopulated by M2 transitions between  $\nu f_{7/2}$  and  $\nu d_{3/2}$  with nanosecond lifetimes. Fornal *et al.* [3] reported the 1435 keV level in  $^{33}\text{Si}$  and the 2305 keV level in  $^{34}\text{P}$  whose spin-parities were suggested tentatively as  $(7/2^-)$  and  $(3^-, 4^-)$ , respectively, although there was no experimental evidence for their spin-parity assignments. An isomer-scope [4] can observe nanosecond isomers in neutron-rich nuclei produced in heavy-ion deep-inelastic collisions. Using the isomer-scope, we have observed nanosecond isomers in neutron-rich  $N\approx 20$  nuclei and established the  $\nu f_{7/2}$  excitations in  $^{32,33}\text{Si}$  and  $^{34}\text{P}$  through spin-parity assignments.

The neutron-rich  $N\approx 20$  nuclei were produced in the heavy-ion deep-inelastic collisions of  $^{198}\text{Pt} + ^{37}\text{Cl}$  (9 MeV/nucleon). Projectile-like fragments (PLF's) were stopped in an annular Si detector placed 55 mm downstream from the target, and  $\gamma$  rays emitted from the stopped PLF's were measured with four Ge detectors by PLF- $\gamma$ (- $\gamma$ ) coincidences. The atomic number of the PLF was identified using Si  $\Delta E$  detectors. Lifetimes of isomers were deduced from PLF- $\gamma$  time spectra. Multipolarities of  $\gamma$  transitions were determined through an in-plane to out-of-plane  $\gamma$ -ray anisotropy analysis [5].

Figure 1 shows decay curves of  $\gamma$  rays associated with the isomers in  $^{32,33}\text{Si}$  and  $^{34}\text{P}$  obtained from the PLF- $\gamma$  coincidence data. The half-lives of the isomers were determined to be 33.1(5) ns, 10.2(3) ns, and  $0.3 < t_{1/2} < 2.5$  ns for  $^{32,33}\text{Si}$  and  $^{34}\text{P}$ , respectively. The lower limit for  $^{34}\text{P}$  was estimated from the detection limit of the isomer-scope. Figure 2 shows the decay schemes of the isomers established through the  $\gamma$ - $\gamma$  coincidence analysis. The  $\gamma$ -ray anisotropy analysis revealed that the 1435 and 1876 keV transitions in  $^{33}\text{Si}$  and  $^{34}\text{P}$  are stretched quadrupole transitions. Combined with their lifetimes, the M2 multipolarity was assigned to these transitions. The spin-parity of the ground state of  $^{33}\text{Si}$  is  $3/2^+$ , and that of the 429 keV level in  $^{34}\text{P}$  is  $2^+$ . (The anisotropy of the 429 keV transition was also consistent with the known M1 multipolarity.) Therefore, the spin-parities of  $7/2^-$  and  $4^-$  were assigned to the 1435 and 2305 keV isomers in  $^{33}\text{Si}$  and  $^{34}\text{P}$ , respectively. The in-plane to out-of-plane ratio of the 3562 keV transition in  $^{32}\text{Si}$  was consistent with that of the stretched octupole transition although the stretched quadrupole assignment could not be excluded. Fornal *et al.* [6] reported the 79 keV transition above the 5504 keV level in  $^{32}\text{Si}$  and assigned this transition as the isomeric E1 transition of  $5^- \rightarrow 4^+$  with  $t_{1/2} = 27(2)$  ns. However, we could not observe the 79 keV  $\gamma$  rays in coincidence with the 3562 and 1942 keV ones. Therefore, we conclude that the 5504 keV level is the isomeric  $5^-$  state with  $t_{1/2} = 33.1(5)$  ns depopulated by the 3562 keV E3 transition to the 1942 keV first  $2^+$  state.

The  $\nu f_{7/2}$  excitations decrease in energy from  $^{36}\text{Cl}$ ,  $^{35}\text{S}$  to  $^{34}\text{P}$ ,  $^{33}\text{Si}$  but it is still high at  $^{33}\text{Si}$ .

<sup>1</sup>Department of Liberal Arts and Sciences, National Defense Medical College

<sup>2</sup>Research Laboratory for Nuclear Reactors, Tokyo Institute of Technology

Although there is lack of experimental data for more neutron-rich  $N=19$  nuclei, especially for spin-parity assignments, level structures in  $^{32}\text{Al}$  and  $^{31}\text{Mg}$  seem to be significantly different from those in  $^{33}\text{Si}$  and  $^{34}\text{P}$ . This fact indicates that the shell structure of  $N\approx 20$  drastically changes just below the  $Z=14$ , which is consistent with the investigation with the Monte Carlo shell model calculations [2]. The 5504 keV  $5^-$  state in  $^{32}\text{Si}$  is considered as the  $(\nu f_{7/2}\nu d_{3/2})5^-$  state. The first  $4^+$  state in  $^{32}\text{Si}$  is also expected around this energy region [2]. Since the previous  $4^+$  assignment was excluded by the present result, the location of the first  $4^+$  state in  $^{32}\text{Si}$  is still unknown. However, if the  $4^+$  state were located below the  $5^-$  state, the  $5^- \rightarrow 4^+$  transition should be observed. Thus the present result defines a lower boundary of the first  $4^+$  state in  $^{32}\text{Si}$ .

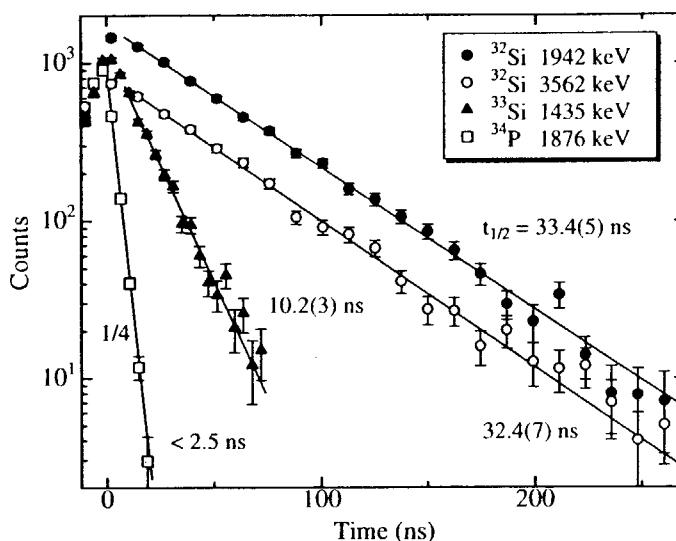


Fig. 1. Decay curves of  $\gamma$  rays associated with the isomers in  $^{32,33}\text{Si}$  and  $^{34}\text{P}$ .

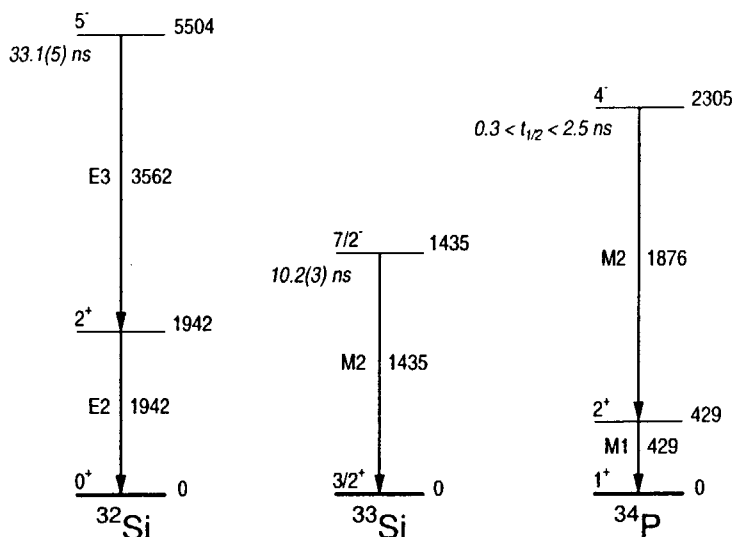


Fig. 2. Decay schemes of the isomers in  $^{32,33}\text{Si}$  and  $^{34}\text{P}$ .

## References

- [1] T. Motobayashi *et al.*, Phys. Lett. B **346** (1995) 9.
- [2] Y. Utsuno *et al.*, Phys. Rev. C **60** (1999) 054315.
- [3] B. Fornal *et al.*, Phys. Rev. C **49** (1994) 2413.
- [4] T. Ishii *et al.*, Phys. Rev. Lett. **84** (2000) 39.
- [5] M. Asai *et al.*, Phys. Rev. C **62** (2000) 054313.
- [6] B. Fornal *et al.*, Phys. Rev. C **55** (1997) 762.

2.7 NANO-SECOND ISOMER IN  $^{68}\text{Cu}$ 

T. ISHII, M. ASAI, P. KLEINHEINZ, M. MATSUDA, A. MAKISHIMA<sup>1</sup>, T. KOHNO<sup>2</sup>,  
and M. OGAWA<sup>3</sup>

We have found an isomer in  $^{68}\text{Cu}$  in the  $^{76}\text{Ge}$  (635 MeV) +  $^{198}\text{Pt}$  reaction using an isomer-scope consisting of  $\Delta E - E$  Si detectors, a tungsten  $\gamma$ -ray shield and Ge detectors [1]. This isomer locates at 777 keV in excitation energy and its decay scheme is shown in Fig. 1. The lifetime of this isomer is shorter than 4 ns but longer than 0.7 ns. The lower limit of this half-life was estimated from the yield of this isomer and the flight time ( $\sim 1.5$  ns) between the target and the Si detector. The 777 keV isomer is considered to be correspondent to the 772 keV level which was identified as one of the  $(\pi p_{3/2} \nu g_{9/2}) 3^-, 4^-, 5^-, 6^-$  multiplet members by the  $(t, ^3\text{He})$  reaction experiment [2]. The lifetime of this isomer and its decay to the  $2^+$  state indicates that the spin of this isomer is  $3^-$ . We have also found the 179 keV  $\gamma$  ray between the  $(\pi p_{3/2} \nu g_{9/2})$  multiplet states, although the intensity of this transition is much weaker than that of the 693 keV transition. The observation of the 179 keV  $\gamma$  ray suggests that the 956 keV level or a higher lying state feeding the 956 keV level has a half-life of  $> 0.1$  ns.

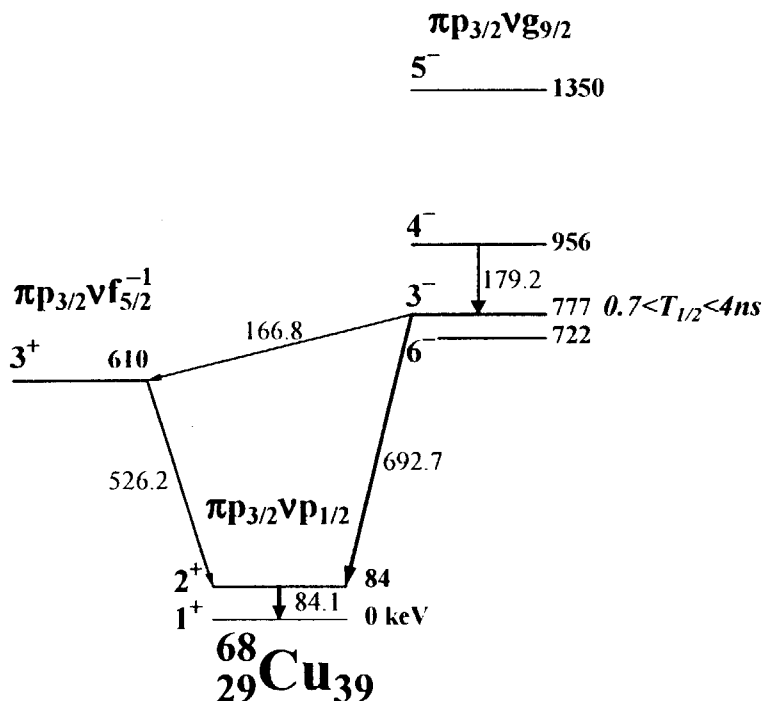


Fig. 1. Level scheme of  $^{68}_{29}\text{Cu}_{39}$

## References

- [1] T. Ishii *et al.*, Nucl. Instrum. Methods Phys. Res. **A395** (1997) 210.
- [2] J.D. Sherman *et al.*, Phys. Lett. **67B** (1977) 275.

<sup>1</sup>Department of Liberal Arts and Sciences, National Defense Medical College

<sup>2</sup>Department of Energy Sciences, Tokyo Institute of Technology

<sup>3</sup>Research Laboratory for Nuclear Reactors, Tokyo Institute of Technology

## 2.8 $Q_{\beta}$ MEASUREMENTS OF $^{158}\text{Pm}$ , $^{159}\text{Sm}$ , AND NEW ISOTOPE $^{166}\text{Tb}$ USING THE JAERI-ISOL

M. SHIBATA<sup>1</sup>, T. SHINDOU<sup>2</sup>, Y. KOJIMA<sup>3</sup>, M. ASAI, K. TSUKADA,  
S. ICHIKAWA, H. HABA, Y. NAGAME and K. KAWADE<sup>2</sup>

Both atomic masses and half-lives are essential constants in nuclear physics related to the stability of nuclei and nuclear structure. However, concerning new isotopes, only the half-lives were measured and the atomic masses were not reported owing to their low yields. The  $\beta$ -decay energy ( $Q_{\beta}$ ) measurement is one of the precise methods for atomic mass determination. In the radioactivity measurements, if all radiation from the source can be completely absorbed, the highest energy point of the spectrum indicates the  $Q_{\beta}$ . Recently, we successfully identified some new isotopes using the gas-jet coupled on-line mass separator JAERI-ISOL at the tandem accelerator [1-3]. In order to determine their atomic masses within the precision of 0.3 MeV, we developed a total absorption detector having a high efficiency. The  $Q_{\beta}$  of short-lived neutron rich isotopes  $^{158}\text{Pm}$ ,  $^{159}\text{Sm}$  and new isotope  $^{166}\text{Tb}$  have been measured for the first time.

The total absorption detector was developed for the purpose of  $Q_{\beta}$  measurements of rare nuclei like new isotopes without precise information of the decay scheme [4,5]. The detector is composed of twin BGO scintillation detectors ( $12\text{cm}^{\phi}\times 10\text{cm}^l$ ) that are arranged at  $180^{\circ}$  geometry and the distance of 3 mm. It can absorb almost all  $\gamma$ -rays and  $\beta$ -rays including their backscattering and bremsstrahlung by high-energy  $\beta$  particles from the sandwiched radioactivities. As the results, the end-points of the measured spectra are expected to give the  $Q_{\beta}$ s. The unstable nuclei were produced with the  $^{238}\text{U}(p,f)$  reaction with a 20 MeV proton beam ( $\sim 1\mu\text{A}$ ) generated by the tandem accelerator. The target was composed of eight aluminum foils on which uranium was electrodeposited and a total amount of  $^{238}\text{U}$  was  $43\text{mg}/\text{cm}^2$ . The fission products were transported into a thermal ion source by the He gas-jet system containing  $\text{PbI}_2$  aerosols. The mass-separated beam was implanted in a computer-controlled aluminized Mylar tape, which was moved to a counting position periodically. The overall efficiency of the ISOL is smaller than 1% for rare earth elements, approximately. It resulted in the source intensity in the order of 10 decays per second at  $A\sim 160$ . The experimental detector setup was described in elsewhere [4,5].

Ten fission products (see Fig.1), which have well-determined  $Q_{\beta}$ , were measured for the on-line energy calibration of the detector. The counting rate of the background was 30 cps, approximately, and counting rates of the mass-separated activities were always kept below 1.5 kcps in order to suppress pulse pile-up. The origin of the background was mainly the  $\gamma$ -rays from the  $^{207}\text{Bi}$  in the BGO crystals and the neutron capture  $\gamma$ -rays by the fission of  $^{238}\text{U}$ . The collecting, cooling and counting times were predetermined properly for each isotope to reduce daughter activities. The measurement times for  $^{158}\text{Pm}$ ,  $^{159}\text{Sm}$  and  $^{166}\text{Tb}$  were 13 hours, 12 hours and 22 hours, respectively.

The end-points were determined by means of the conventional square root plot analysis [4,5] after subtracting the background spectrum. The energy calibration line, which was obtained with the least square fitting between the obtained end-points and the evaluated  $Q_{\beta}$  [6] by Audi *et al.* for the ten nuclei, is shown in Fig.1. It shows good linearity between 3 MeV and 9 MeV. The preliminary results  $Q_{\beta}$  of  $^{158}\text{Pm}$ ,  $^{159}\text{Sm}$  and  $^{166}\text{Tb}$  (Fig.2) following the on-line energy calibration are listed in Table 1 together with the systematics [6] and three theoretical values [7,8]. The uncertainties were evaluated to be 0.1 MeV, approximately, from the

<sup>1</sup> School of Engineering, Nagoya University

<sup>2</sup> Graduate School of Engineering, Nagoya University

<sup>3</sup> Graduate School of Engineering, Hiroshima University

accuracy of the energy calibration line ( $\sim 50$  keV) and from the statistics of each spectrum. The statistics of the  $^{166}\text{Tb}$  is poorer than those of the others, so that the uncertainty is relatively larger. The present results are in good agreement with the systematics [6]. The systematics gives better prediction than the theoretical values do in this region. Precise analysis is in progress.

In conclusion, the  $Q_\beta$  of the short-lived neutron-rich nuclei including a new isotope were determined using the total absorption detector installed with the JAERI-ISOL. The measurements for other new isotopes in the region of  $A \geq 160$  will be continued systematically.

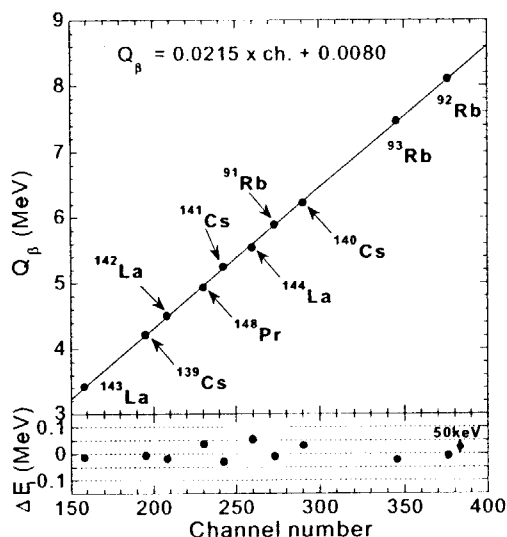


Fig.1 On-line energy calibration obtained from ten nuclei.

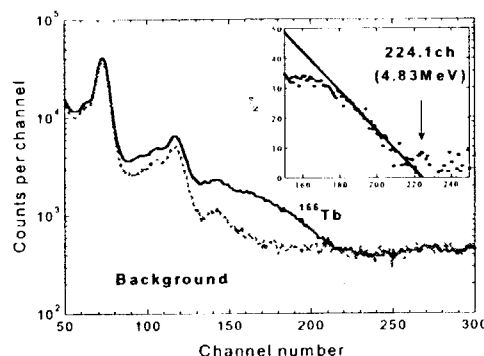


Fig.2 Total absorption spectrum of  $^{166}\text{Tb}$  and its square root plot (inset).

TABLE 1 Determined  $Q_\beta$  and comparisons with the systematics and the theoretical values.

Nuclei	Half-life	$Q_\beta$ -value (MeV)				
		Present	Systematics Audi et al. <sup>(6)</sup>	KUTY <sup>(7)</sup>	Theoretical	
					FRDM <sup>(8)</sup>	FRLDM <sup>(8)</sup>
$^{166}\text{Tb}$	25.6(22) s	4.83( $\sim 10$ )	4.887(298)	4.86	4.96	4.97
$^{159}\text{Sm}$	11.37(15) s	3.84( $\sim 10$ )	3.834(298)	3.45	3.53	3.62
$^{158}\text{Pm}$	4.8(5) s	6.12( $\sim 10$ )	6.243(408)	6.27	6.58	6.63

## References

- [1] M. Asai, K. Tsukada, S. Ichikawa, A. Osa, Y. Kojima, M. Shibata, H. Yamamoto, K. Kawade, N. Shinohara, Y. Nagame, H. Iimura, Y. Hatsukawa and I. Nishinaka, J. Phys. Soc. Jpn. **65** (1996) 1135.
- [2] S. Ichikawa, K. Tsukada, I. Nishinaka, Y. Hatsukawa, H. Iimura, K. Hata, Y. Nagame, A. Osa, M. Asai, Y. Kojima, T. Hirose, M. Shibata, K. Kawade and Y. Oura, Phys. Rev. C **58** (1998) 1329.
- [3] M. Asai, S. Ichikawa, K. Tsukada, M. Sakama, M. Shibata, Y. Kojima, A. Osa, I. Nishinaka, Y. Nagame, K. Kawade and T. Tachibana, Phys. Rev. C **59** (1999) 3060.
- [4] M. Shibata, Y. Kojima, H. Uno, K. Kawade, A. Taniguchi, Y. Kawase, S. Ichikawa, F. Maekawa and Y. Ikeda, Nucl. Instrum. Methods Phys. Res. A **450** (2001) 581.
- [5] M. Shibata, T. Shindou, A. Taniguchi, Y. Kojima, K. Kawade, S. Ichikawa and Y. Kawase, J. Phys. Soc. Jpn. **71** (2002) 1401.
- [6] G. Audi and A. H. Wapstra, Nucl. Phys. A **595** (1995) 409.
- [7] H. Koura, M. Uno, T. Tachibana and M. Yamada, RIKEN-AF-NP-394, ISSN 1345-244X.
- [8] P. Möller, J.R. Nix and W.J. Swiatecki, At. Data Nucl. Data Tables **59** (1995) 185.

This is a blank page.



### **3. Nuclear Reactions**

This is a blank page.

### 3.1 EFFECT OF SHELL STRUCTURE IN THE FUSION REACTIONS $^{82}\text{Se} + ^{134}\text{Ba}$ AND $^{82}\text{Se} + ^{138}\text{Ba}$

K.SATOU<sup>1</sup>, H.IKEZOE, S.MITSUOKA, K.NISHIO and S. C. JEONG<sup>2</sup>

Fusion process between massive nuclei has been extensively studied so far, where the fusion probability is strongly affected by the charge product of projectile and target nuclei ( $Z_p Z_t$ ). When the charge product is less than 1800, the fusion cross section is well reproduced by the theoretical calculation taking into account the one dimensional barrier penetration and the coupled channel effect of excited states of both projectile and target nuclei. On the other hand, when the charge product comes to over 1800, the fusion cross section becomes considerably small. In order to fuse a colliding system completely, the system needs not only to surmount the fusion barrier but also to get over the fission saddle point of the compound nucleus. In the heavy system with  $Z_p Z_t > 1800$ , the saddle point locates usually inside the contact point of the colliding system, so that the system after contact needs an additional energy to go inside the saddle point against friction. The additional energy is called as the extra-extra push energy. This energy makes the fusion probability small considerably.

In this experiment, we measured the evaporation residue (ER) cross sections for the fusion reactions  $^{82}\text{Se} + ^{134}\text{Ba}$  and  $^{82}\text{Se} + ^{138}\text{Ba}$  to investigate the dependence of fusion on the nuclear structure. The nucleus  $^{138}\text{Ba}$  has a closed neutron shell  $N = 82$  while the nucleus  $^{134}\text{Ba}$  has a neutron number  $N = 78$ , four neutron less than the closed shell. The charge product for these reaction systems is 1904.  $^{82}\text{Se}$  beams from JAERI tandem booster accelerator irradiated the barium carbonate targets. The ERs emitted in the beam direction were separated in flight from the primary beam by the JAERI recoil mass separator. The details of the experimental procedure are described in [1].

The obtained ER cross sections are shown together with the calculated results in Fig. 1 and Fig. 2 as a function of c.m. energy determined in the middle of the target layer. In the present theoretical calculation, first, the fusion cross section was estimated by the coupled channel calculation using the code CCDEF [2] including the coupling with the first  $2^+$  and  $3^-$  excited states for both projectile and target nuclei. Second the survival probability of each ER was calculated by using the statistical calculation code HIVAP [3]. The details of the theoretical calculation are described elsewhere [1]. As shown in Fig. 1, the experimental data for the fusion reaction  $^{82}\text{Se} + ^{138}\text{Ba}$  have an excellent

<sup>1</sup>Department of Physics and Tandem Accelerator Center, Tsukuba University

<sup>2</sup>Institute of Particle and Nuclear Studies, KEK

agreement with the present theoretical calculation. On the other hand, as shown in Fig. 2, the measured ER cross sections for the fusion reaction  $^{82}\text{Se} + ^{134}\text{Ba}$  show clear deviations from the calculated ones mainly in the low excitation energy region  $E_{\text{ex}} = 20 - 30$  MeV. There is a large deficit of the  $2n + 3n$  cross section in the reaction  $^{82}\text{Se} + ^{134}\text{Ba}$ , which is two orders of magnitude smaller than that of the reaction  $^{82}\text{Se} + ^{138}\text{Ba}$ .

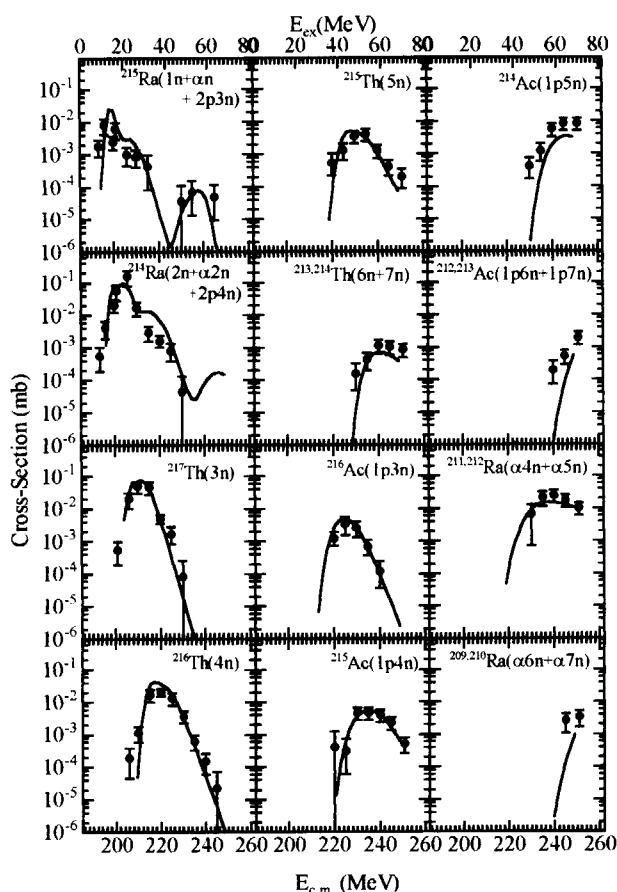


Fig. 1. Evaporation residue cross sections for the reaction  $^{82}\text{Se} + ^{138}\text{Ba}$  with the calculated ones that were estimated by using the statistical model code HIVAP. Error bars represent not only the statistical contribution but also the systematical one of 40%.

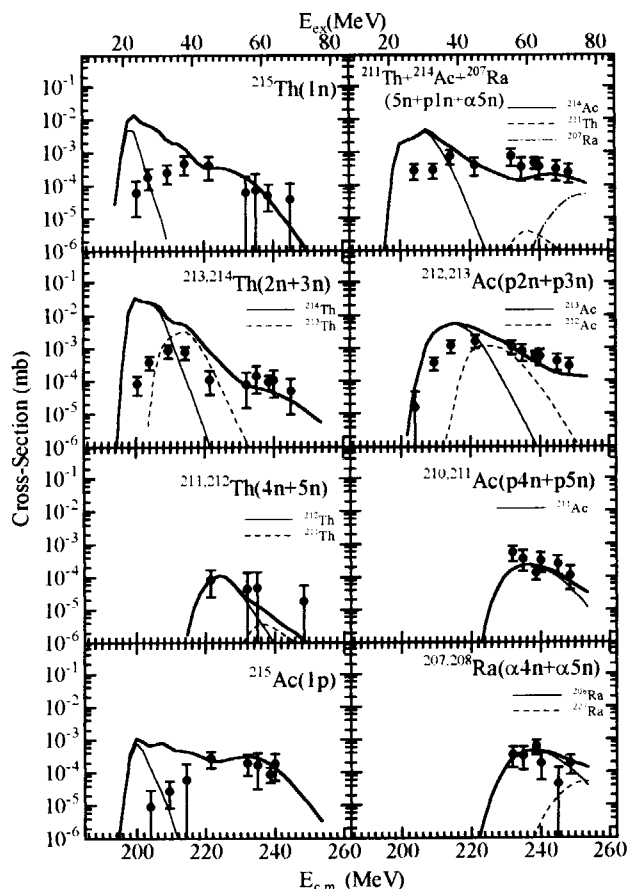


Fig. 2. Same as Fig. 1 except for the reaction  $^{82}\text{Se} + ^{134}\text{Ba}$ .

The thick curve in each channel is the calculated result including the components originating from the reactions  $^{82}\text{Se} + ^A\text{Ba}$ , where  $A \geq 135$ . The thin curve shows the component originating from the reaction  $^{82}\text{Se} + ^{134}\text{Ba}$ .

The extracted fusion probability from the obtained ER cross sections are compared with those of the asymmetric reactions  $^{40}\text{Ar} + ^{176,180}\text{Hf}$  ( $Z_p Z_t = 1296$ ) [4] and the more symmetric reactions  $^{124}\text{Sn} + ^{92,96}\text{Zr}$  ( $Z_p Z_t = 2000$ ) [5], where the same compound nuclei  $^{216}\text{Th}$  and  $^{220}\text{Th}$  as in the present reaction systems are produced. The fusion probability for the reaction  $^{82}\text{Se} + ^{138}\text{Ba}$  is consistent with that of the reaction  $^{40}\text{Ar} + ^{180}\text{Hf}$  and also the calculation. On the other hand, the fusion probability for the reaction  $^{82}\text{Se} + ^{134}\text{Ba}$  is rather close to that of the reaction  $^{124}\text{Sn} + ^{92}\text{Zr}$ . These results indicate the existence of fusion hindrance for the reaction  $^{82}\text{Se} + ^{134}\text{Ba}$ , while not for the reaction  $^{82}\text{Se} + ^{138}\text{Ba}$ .

The present result suggests that the fusion of massive reaction systems strongly depends on the shell structure of colliding partners. The experiment of the fusion reaction of heavier system  $^{86}\text{Kr} + ^{134,138}\text{Ba}$  ( $Z_p Z_t = 2016$ ) is now proceeding to investigate the dependence of fusion on the shell structure more detailed.

## References

- [1] K. Satou, H. Ikezoe, S. Mitsuoka, K. Nishio, and S. C. Jeong, Phys. Rev. C 65 (2002) 054602.
- [2] J. O. Fernández Niello, C. H. Dasso, and S. Landowne, Comput. Phys. Commun. 54 (1989) 409.
- [3] W. Reisdorf, and M. Schädel, Z. Phys. A 343 (1992) 47.
- [4] H.-G. Clerc, J. G. Keller, C.-C. Sahm, K.-H. Schmidt, H. Schulte, and D. Vermeulen, Nucl. Phys. A 419 (1984) 571.
- [5] C.-C. Sahm, H.-G. Clerc, K.-H. Schmidt, W. Reisdorf, P. Armbruster, F. P. Hessberger, J. G. Keller, G. Münzenberg, and D. Vermeulen, Nucl. Phys. A 441 (1985) 316.

### 3.2 MASS DIVISION OF $^{240}\text{Pu}$ FOLLOWING $\beta$ -VIBRATIONAL RESONANCE

K. NISHIO, H. IKEZOE, Y. NAGAME, S. MITSUOKA, L. DUAN<sup>1</sup>, I. NISHINANA,  
K. SATOU, M. ASAI, H. HABA, K. TSUKADA, N. SHINOHARA, S. ICHIKAWA,  
and S. GOTO<sup>2</sup>,

For a neutron induced fission of  $^{239}\text{Pu}$  using an explosive nuclear reaction, there is an investigation on the fission fragment mass distribution, in the form of the ratio of  $^{99}\text{Mo}$  to  $^{115}\text{Cd}$ , following the  $J^\pi=1^+$  resonance at 0.3 eV [1]. The distribution was found to form an enhanced asymmetric fission yield ( $^{99}\text{Mo}$ ) relative to the symmetric yield ( $^{115}\text{Cd}$ ), compared to the thermal neutron induced fission of  $^{239}\text{Pu}$ , which has a mixed state of  $J^\pi=0^+$  and  $1^+$ . This was interpreted in ref.[2] that fission through the octupole vibrational state ( $K^\pi=1^+$ ) on the saddle point would act on the motion of the system so as to proceed to the asymmetric fission valley. It can then be speculated that the  $\beta$ -vibrational state with  $K^\pi=0^+$  is populated in the middle stage of the fission process, the resulting mass distribution would have larger symmetric fission component. In order to determine the mass distribution following the  $\beta$ -vibrational state, the present measurement was made.

The  $\beta$ -vibrational state is formed on the 2nd minimum of the double-humped fission barrier, whose structure comes from the deformation dependent shell-correction energy applied to the liquid-drop potential. The  $\beta$ -vibrational state is observed under the threshold energy in the form of the enhanced barrier penetrability (fission cross section) due to resonance tunneling induced when the excitation energy ( $E_{\text{ex}}$ ) of the compound nucleus matches the level. By gating this resonance, the fission fragment mass distribution was measured.

The  $\beta$ -vibrational state of  $^{240}\text{Pu}$  was populated by  $^{239}\text{Pu}(\text{d},\text{p})$  reaction. A 13.5 MeV deuteron beam with about 5 nA was supplied by the JAERI Tandem accelerator and irradiated the  $^{239}\text{Pu}$  target. The excitation energy of  $^{240}\text{Pu}$  was specified by measuring the energy of outgoing protons. The proton was detected by a  $\Delta E$ -E telescope detector consisting of 300 and 1500  $\mu\text{m}$  thick silicon detectors. Two fission fragments were coincidentally measured by a silicon PIN diode to determine the fragment mass number.

Figure 1 shows the proton-fission coincidence events plotted as a function of fragment mass. The resonance fission is observed at 5.1 MeV. The resonance position is the same as that reported in ref.[3,4].

The mass distribution following the 5.1 MeV resonance was obtained by selecting the events in  $4.78 < E_{\text{ex}} < 5.30$  MeV as shown in Fig. 2. Even though the statistical error is large, the asymmetric fission character is evident. The distribution agrees with that for  $^{239}\text{Pu}(\text{n}_{\text{th}},\text{f})$  shown by the solid curve [5]. In this work, we cannot observe the significant enhancement of the symmetric fission component within statistical error. Penetrating the 2nd fission barrier from the  $\beta$ -vibrational state, the system should come out in the asymmetric potential valley identical to that the  $^{239}\text{Pu}(\text{n}_{\text{th}},\text{f})$  system descent.

1 Institute of Modern Physics, Chinese Academy of Sciences, 730000 Lanzhou, China

2 Department of Chemistry, Niigata University

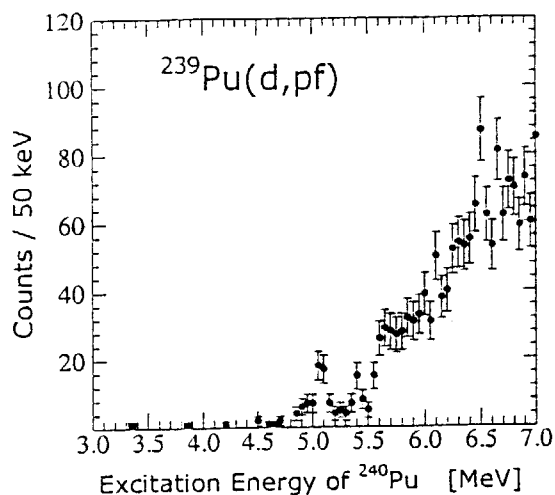


Fig.1. Proton-fission coincidence events as function of excitation energy of  $^{240}\text{Pu}$ .

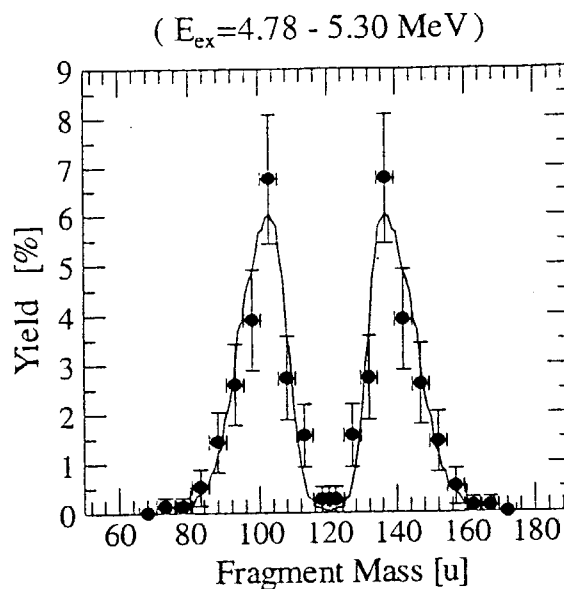


Fig.2. Mass distribution for the fission through the  $\beta$ -vibrational resonance.

#### References

- [1] G. A. Cowan, B.P. Bayhurst, R.J. Prestwood, J.S. Gilmore, and G.W. Knobeloch, *Phys. Rev.*, **144** (1966) 979.
- [2] A. Michaudon, *Advances in Nuclear Physics*, Plenum Press.
- [3] P. Glassel, H. Rosler and H.J. Specht, *Nucl. Phys.* **A256** (1976) 220.
- [4] M. Hunyadi, D. Gassmann, A. Krasznahorkay, D. Habs, P.G. Thirolf, M. Csatlos, Y. Eisermann, T. Faestermann, G. Graw, J. Gulyas, R. Hertenberger, H.J. Maier, Z. Mate, A. Metz, M.J. Chromik, *Phys. Lett. B*, **505** (2001) 27.
- [5] C. Wagemans, E. Allaert, A.J. Deruytter, R. Barthelémy, and P. Schillebeeckx, *Phys. Rev. C*, **30** (1984) 218.

### 3.3 MEASUREMENT OF THE $^{16}\text{N}(\alpha, n)$ CROSS SECTION

H. ISHIYAMA<sup>1</sup>, T. HASHIMOTO<sup>2,7</sup>, T. ISHIKAWA<sup>2</sup>, T. KAWAMURA<sup>2</sup>, H. MIYATAKE<sup>1</sup>, M. H. TANAKA<sup>1</sup>, Y. FUCHI<sup>1</sup>, N. YOSHIKAWA<sup>1</sup>, S. C. JEONG<sup>1</sup>, Y. WATANABE<sup>1</sup>, H. KAWAKAMI<sup>1</sup>, I. KATAYAMA<sup>1</sup>, T. NOMURA<sup>1</sup>, S. MITSUOKA, K. NISHIO, M. MATSUDA, S. ICHIKAWA, H. IKEZOE, T. FURUKAWA<sup>3</sup>, H. YANO<sup>3</sup>, H. IZUMI<sup>3</sup>, Y. MIZOI<sup>4</sup>, M. TERASAWA<sup>5</sup>, T. FUKUDA<sup>6</sup>, K. NAKAI<sup>2</sup>, and T. SHIMODA<sup>3</sup>

Recently, it has been discussed that the *r* (rapid)-process occurs in so-called “hot-bubble” under explosive conditions in the universe. In such conditions, nuclear reactions involving light neutron-rich nuclei play an important role as the *r*-process starting point [1]. We have tried to acquire directly systematical nuclear cross sections data of  $(\alpha, n)$  reactions using low energy ( $E = 1\text{--}2\text{ MeV/u}$ ) light neutron-rich radioactive nuclear beams (RNB). At first, the cross section of the  $^{16}\text{N}(\alpha, n)$  reaction has been measured successfully at JAERI-TANDEM.

As for the production of the low energy RNB, one of the powerful method is utilizing inversion kinematics [2]. In order to suppress the particles of the primary beam, the large solid angle recoil mass separator, JAERI-RMS has been used [3-4]. The  $d(^{18}\text{O}, ^{16}\text{N})\alpha$  reaction was selected as the production reaction of the  $^{16}\text{N}$ -RNB. The production target is a gas target filled with  $\text{D}_2$  gas ( $p = 1\text{ atm}$ ,  $L = 5\text{ cm}$ ). The intensity of the primary  $^{18}\text{O}^{6+}$ -beam is about 400 enA and the energy is 73 MeV. The energy of  $^{16}\text{N}$ -RNB becomes 32 MeV at the exit of the gas target. As a result, the intensity of the produced  $^{16}\text{N}$ -RNB is 4.7 kpps / 300 enA  $^{18}\text{O}^{6+}$ -beam at the focal plane of the RMS. The contamination ratio of  $^{18}\text{O}$  ions to  $^{16}\text{N}$  measured by a dE-E telescope becomes 1.5%.

For the measurement of the  $^{16}\text{N}(\alpha, n)$  cross section, a detector system has been installed at a focal plane of the RMS, consisting of a MCP, a PPAC, a “Multi-Sampling and Tracking Proportional Chamber” (MSTPC)[5] and a neutron detector array. The neutron counter consists of 28 pieces of plastic scintillators which covers 35% solid angles of  $4\pi$ . The total efficiency for a neutron at an energy region of 1.0-10 MeV is about 10%. The  $^{16}\text{N}$ -beam transported by the RMS is directly

---

<sup>1</sup> Institute of Particle and Nuclear Studies, KEK

<sup>2</sup> Tokyo University of Sciences

<sup>3</sup> Osaka University

<sup>4</sup> RIKEN

<sup>5</sup> University of Tokyo

<sup>6</sup> Osaka Electro-Communication University

<sup>7</sup> Research Fellow of the Japan Society for the Promotion of Science.



injected into the MSTPC filled with  $^4\text{He}+\text{CO}_2$  (10%) gas at 129 torr. The MSTPC can trace multiple charged particle trajectories with those  $dE/dx$  information. So, we can obtain the energy and position where the reaction occurs by detecting the  $dE/dx$  change with the MSTPC.

We have been analyzing the measured nuclear reaction events. Fig.1 shows the energy distribution of the selected  $^{16}\text{N}$  ( $\alpha$ , n) reaction events. The excitation function of the  $^{16}\text{N}$  ( $\alpha$ , n) reaction will be determined in the energy region of  $E_{\text{cm}} = 1.5 - 4.0$  MeV, correspond to the Gamov peak energy  $T_9 = 1 - 5$ . Further analysis is in progress in order determine the absolute cross section and the astrophysical nuclear reaction rate of  $^{16}\text{N}$  ( $\alpha$ , n) reaction.

### References

- [1] M. Terasawa, et. al., Nucl. Phys. A688(2001)581c.
- [2] T. Yamaya, et. al., Nucl. Instrum. Methods. B70(1992)374.
- [3] H. Ikezoe, et. al., Nucl. Instrum. Methods. A376(1996)470.
- [4] T. Kuzumaki, et. al., Nucl. Instrum. Methods. A437(1999)107.
- [5] Y. Mizoi, et. al., Nucl. Instrum. Methods. A 431(1999)112.

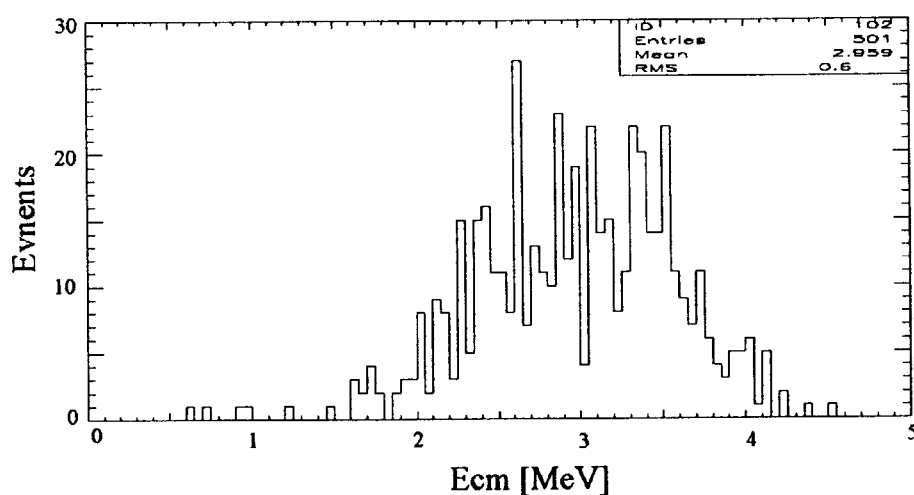


Fig.1 The preliminary result for the center-of-mass energy distribution of the selected  $^{16}\text{N}$  ( $\alpha$ , n) reaction events. These events are selected by the main gate condition that the  $dE/dx$ -change gap is larger than 0.15 MeV.

### 3.4 ANOMALOUS EXCITATION ENERGY DEPENDENCE OF SHELL EFFECTS IN ASYMMETRIC FISSION MODE

I. NISHINAKA, M. TANIKAWA<sup>1</sup>, S. GOTO<sup>2</sup>, Y. NAGAME,  
K. NISHIO, A. YOKOYAMA<sup>3</sup>, M. ASAI, H. HABA<sup>4</sup>, S. ICHIKAWA,  
K. TSUKADA, K. AKIYAMA, A. TOYOSHIMA<sup>5</sup>, and H. KUDO<sup>2</sup>

Shapes of nuclei are governed by shell effects of proton and neutron. Shell effect is expected to play a decisive role in fission process. However it is still unknown how shell effect influences deformation and mass division during descent from the saddle point to scission in the fission process. In general shell effect disappears with increasing excitation energy [1]. Thus we investigated how shell effect is responsible for mass division by measuring mass and kinetic energy distributions at several excitation energies. We reports anomalous excitation energy dependence of spherical shell effects of  $Z=50$  and  $N=82$  and deformed shell effect of  $N=86-88$  [2] in the asymmetric fission mode.

In the fission of  $p + {}^{232}\text{Th}$ , pair fission fragments were detected in coincidence by a double time-of-flight method. Mass and total kinetic energies of pair fragments were obtained from measured flight-time [3]. Total fission events of  $2.4 \times 10^6$ ,  $3.8 \times 10^6$  and  $4.7 \times 10^6$  were accumulated at incident proton energies of 10.0, 11.5 and 13.0 MeV, respectively.

Figure 1 shows the mass yield curves normalized to 200% as a function of heavy fragment mass number. Lines represent the mass yield curves decomposed into those of the symmetric and asymmetric fission modes by the two-component analysis of the mass and total kinetic distributions[3]. It is evident that the symmetric fission mode becomes more dominant with increasing excitation energy than the asymmetric fission mode as well observed in fission of actinides [4]. In order to illustrate variation of the mass yield curves of the asymmetric fission mode with excitation energy, Fig. 2. shows the mass yield ratios of the asymmetric fission mode at incident proton energies of 11.5 and 13.0 MeV to that of 10.0 MeV as a function of heavy fragment mass number. With increasing incident proton energy, the mass yield ratios at  $A \sim 143$  become smaller than  $A \sim 132$ . The fragments with  $A \sim 143$  and  $A \sim 132$  correspond to the deformed shell of  $N = 86-88$  and the spherical shells of  $Z = 50$  and  $N = 82$ , respectively. It is clear that deformed shell fragments with  $N=86-88$  vanish faster with excitation energy than spherical shell fragments with  $Z = 50$  and  $N = 82$  in the asymmetric fission mode. The nuclei with  $Z=50$  and  $N = 82$  have much larger negative shell correction energies than those with  $N=86-88$  [5]. It is expected that increasing excitation energy influences adversely shell effects of  $Z = 50$  and  $N = 82$  compared with those of  $N = 86-88$ . Hence it is found that observed excitation energy dependence is anomalous in view of fragment shell effects. Similar excitation energy dependence of the mass yields was observed in the photofission of  ${}^{232}\text{Th}$  [6]. The reason of this anomalous excitation energy dependence of fragment shells is not known, but shell structure of fissioning nuclei,  ${}^{232}\text{Th}(N=142)$  [6] and  ${}^{233}\text{Pa}(N=142)$ , this work), seems to influence mass division. In view of shell structure of neutron of fissioning nuclei, we plan an experiment in the proton induced fission of uranium isotopes in near future.

<sup>1</sup>School of Science, University of Tokyo

<sup>2</sup>Department of Chemistry, Niigata University

<sup>3</sup>Department of Chemistry, Faculty of Science, Kanazawa University

<sup>4</sup>Radioisotope Technology Division, Cyclotron Center, RIKEN

<sup>5</sup>Department of Chemistry, Graduate School of Science, Osaka University

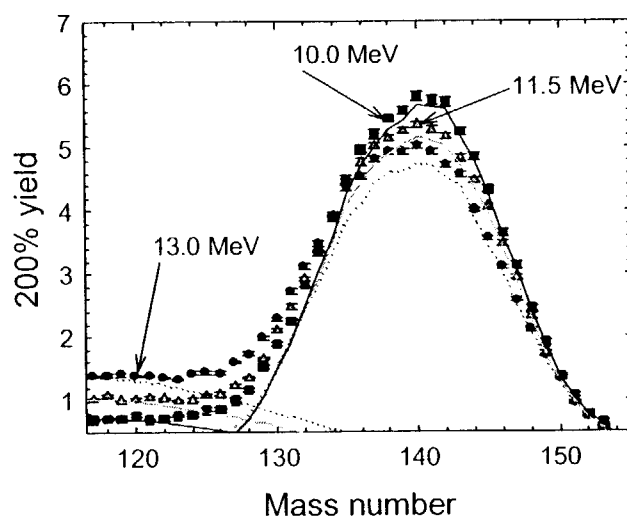


Fig. 1. Mass yield curves (200%) as a function of heavy fragment mass number in the proton induced fission of  $^{232}\text{Th}$ . Incident proton energies are 10.0 MeV (squares and solid line), 11.5 MeV (triangles and dashed-line) and 13.0 MeV (circles and dotted-line).

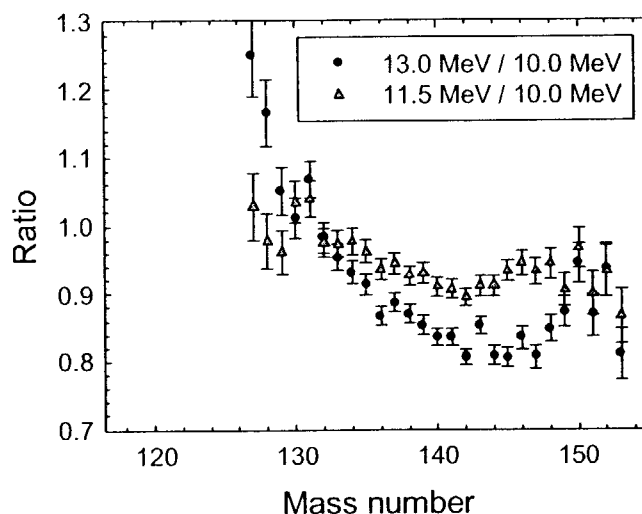


Fig. 2. The mass yield ratios of the asymmetric fission mode.

## References

- [1] A. V. Ignatyuk, G. N. Smirenkin, and A. S. Tishin. Sov. J. Nucl. Phys., **21** (1975) 255.
- [2] B. D. Wilkins, E. P. Steinberg, and R. R. Chasman, Phys. Rev. C **14** (1976) 1832.
- [3] Y. Nagame, I. Nishinaka, K. Tsukada, S. Ichikawa, H. Ikezoe, Y. L. Zhao, Y. Oura, K. Sueki, H. Nakahara, M. Tanikawa, T. Ohtsuki, K. Takamiya, K. Nakanishi, H. Kudo, Y. Hamajima, and Y. H. Chung, Phys. Lett. B **387** (1996) 26.
- [4] T. Ohtsuki, Y. Nagame, K. Tsukada, N. Shinohara, S. Baba, K. Hashimoto, I. Nishinaka, K. Sueki, Y. Hatsukawa, K. Hata, T. Sekine, I. Kanno, H. Ikezoe, and H. Nakahara, Phys. Rev. C **44** (1991) 1405.
- [5] P. Möller, J. R. Nix, W. D. Myers, and W. J. Swiatecki, At. Data Nucl. Data Tables **59** (1995) 185.
- [6] M. Piessens, E. Jacobs, S. Pomme, and D. De Frenne, Nucl. Phys. A **556** (1993) 88.

### 3.5 SUB-BARRIER FUSION OF $^{82}\text{Se}+^{176}\text{Yb}$

S. MITSUOKA, H. IKEZOE, K. NISHIO, and K. SATOU

In order to investigate experimentally the gentle fusion or the hugging fusion which have been theoretically proposed as a new approach to the superheavy-element production, we have studied the effect of nuclear deformation on the sub-barrier fusion in the reactions between heavy projectiles and well deformed targets of  $^{32}\text{S}+^{182}\text{W}$  and  $^{60,64}\text{Ni}+^{154}\text{Sm}$  [1,2],  $^{28}\text{Si}+^{198}\text{Pt}$  and  $^{76}\text{Ge}+^{150}\text{Nd}$  [3], and  $^{82}\text{Se}+^{nat}\text{Ce}$  [4]. It was found that the fusion probability in the low energy region, where only collision at the tip of the deformed targets is possible, was significantly hindered, while the fusion hindrance was negligible in the high energy region where side collisions become possible. This supports the original idea of the hugging fusion that the compact touching configuration in the side collision is more favorable for complete fusion than the elongated configuration in the tip collision.

The next step is to apply the hugging fusion to the production of superheavy elements ( $Z>100$ ). We attempt the hugging fusion reactions of  $^{82}\text{Se}+^{176}\text{Yb}$  and  $^{86}\text{Kr}+^{176}\text{Yb}$  to produce superheavies of  $^{258}\text{Rf}$  ( $Z=104$ ) and  $^{262}\text{Sg}$  ( $Z=106$ ), which were synthesized in the cold fusion reactions of  $^{50}\text{Ti}+^{208}\text{Pb}$  and  $^{54}\text{Cr}+^{208}\text{Pb}$ , respectively. The well deformed  $^{176}\text{Yb}$  target ( $400\mu\text{g}/\text{cm}^2$ ) was bombarded by  $^{82}\text{Se}$  beam from the JAERI tandem-booster accelerator. The beam energy was selected for the maximum cross section in 2 or 3 neutron-evaporation channel. The evaporation residues were separated in flight by the JAERI-RMS [5] and then identified by the correlation analysis of  $\alpha$ -decay and spontaneous fission.

In the very preliminary results, no evaporation residues was observed in the  $^{82}\text{Se}+^{176}\text{Yb}$  reaction. The upper limits of the cross section for 2n and 3n channels were 1.0 nb and 0.8 nb, respectively. Further analysis and some developments of the detector system are in progress.

#### References

- [1] S. Mitsuoka et al., Phys. Rev. C **62** (2000) 054603.
- [2] S. Mitsuoka et al., Phys. Rev. C **65** (2002) 054608.
- [3] K. Nishio et al., Phys. Rev. C **62** (2000) 014602.
- [4] K. Nishio et al., Phys. Rev. C **63** (2001) 044610.
- [5] H. Ikezoe et al., Nucl. Instrum. and Methods A376 (1996) 420.

### 3.6 MONITORING AND REJECTION OF BACKGROUND PARTICLES USING A PPAC INSTALLED IN THE JAERI-RECOIL MASS SEPARATOR IN THE MEASUREMENT OF FUSION EVAPORATION RESIDUES

K. NISHIO, L. DUAN<sup>1</sup>, K. SATOU, S. MITSUOKA and H. IKEZOE

The JAERI-Recoil Mass Separator (JAERI-RMS) [1] has been used for the measurement of fusion evaporation residues. In order to obtain the cross section of a low production rate, the background particles which cannot be rejected by the RMS and are transported to the focal plane must be suppressed before reaching the focal plane detector. We have determined the origin of the background particles by measuring the spectrum of transversal position,  $P(X)$ , using a parallel plate avalanche counter (PPAC) designed for this purpose and installed at the exit of the  $Q_4$  magnet. The experiment was performed in the reaction  $^{136}\text{Xe} + ^{124}\text{Sn}$ , which is of special interest as the reverse process of the fission of  $^{260}\text{Rf}$ . It was found that the background did not show an uniform  $P(X)$  spectrum but formed a strong bump at a certain position. The spectrum was reproduced by a simulation based on the GIOS code with assuming the background particle to be  $^{136}\text{Xe}$ .

The PPAC with active area of  $120 \times 50 \text{ mm}^2$  has an anode wire plane sandwiched by two cathode planes. The distance between the anode and the cathode is 3.2 mm. The Au-coated tungsten wire with  $20 \mu\text{m}$  diameter is stretched with 2 mm pitch, each of them are connected by  $50 \Omega$  resistance to give the position ( $X$ ) by charge division method. The bias of +480 V is applied to the anode. The cathode planes are made by gold coated Mylar film ( $0.9 \mu\text{m}$ ) and are grounded. The PPAC is operated with isobutane gas (330 Pa). Entrance and the exit windows are also made with  $0.9 \mu\text{m}$  Mylar film.

The 615 MeV  $^{136}\text{Xe}$  beam was supplied by the tandem-booster accelerator and irradiated the  $^{124}\text{Sn}$  target. An aluminum degrader of  $5.5 \mu\text{m}$  was attached to a rotating target apparatus. The RMS was set to transport the particle ( $M, E$ ) = (259u, 115MeV) with charge setting value  $Q_{\text{set}} = 33.8^+$ . The position spectrum recorded by the PPAC is shown by dash-dotted curve in Fig. 1 (a). The position is viewed from the downstream of the PPAC. The bulk of back ground particles are seen at around  $X = 40 \text{ mm}$ . By changing the charge setting down to  $Q_{\text{set}} = 32.8^+$ , we obtained the spectrum shown in Fig. 1 (b)–(f). One can find the variation of the bulk position with decreasing  $Q_{\text{set}}$ . In order to simulate this trend, the calculation was made in the assumption that the  $^{136}\text{Xe}$  beam was generated at the target having a broad energy spectrum ranging from 0 to 150 MeV and an uniform angular distribution within  $\pm 2.0^\circ$ , corresponding to the aperture angle used in this experiment. The results are shown in Fig. 1 by stepwise spectrum. The calculation reproduced the experimental data, identifying the origin of the background particles. Special importance is the rejection of background without loss of fusion evaporation residues by masking the background region. This is simulated in Fig. 1 (g), where the calculated  $^{136}\text{Xe}$  ( $17^+$ ) spectra and the  $^{259}\text{Rf}$  ( $32^+$  and  $33^+$ ) are shown. Masking the region  $60 < X < 78 \text{ mm}$  in front of the PPAC reduces the background events down to 1 / 6.

1 Institute of Modern Physics, Chinese Academy of Sciences, 730000 Lanzhou, China

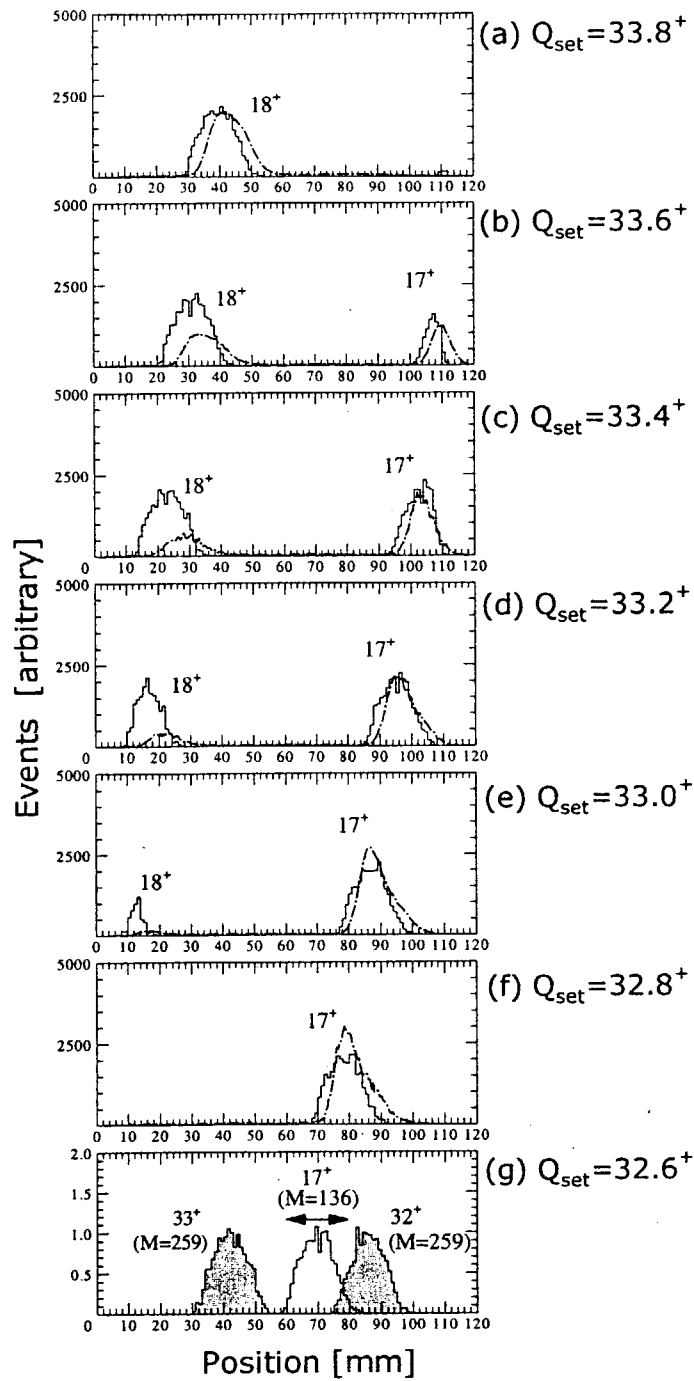


Figure 1 (a)-(f) Transversal ( $X$ ) position spectrum obtained by the PPAC (dash-dotted) for the reaction  $^{136}\text{Xe} + ^{124}\text{Sn}$ . The central trajectory corresponds to  $X=60$  mm. The charge state setting for the JAERI-RMS  $Q_{\text{set}}$  is indicated. The background  $^{136}\text{Xe}$  with charge state  $17^+$  or  $18^+$  forms a bulk, whose position varies with  $Q_{\text{set}}$ . This trend is simulated by the calculation (stepwise function). The figure (g) shows the calculated spectrum for  $Q_{\text{set}}=32.6^+$ . By masking the region shown by the arrow, the background  $^{136}\text{Xe}(17^+)$  is reduced to be 1 / 6 without missing the fusion residues  $^{259}\text{Rf}$  having charge states of  $32^+$  and  $33^+$  (shown by shadowed area).

## References

- [1] H. Ikezoe, Y. Nagame, T. Ikuta, S. Hamada, I. Nishinaka, and T. Ohtsuki, Nucl. Instrum. Methods. Phys. Res. A, **376** (1996) 420.

## **4. Nuclear Chemistry**

This is a blank page.



#### 4.1 SEARCH FOR "MISSING" $\alpha$ -EMITTERS FOR THE MASS MAPPING OF SUPERHEAVY ELEMENTS

N. SHINOHARA, Yu. N. NOVIKOV<sup>1</sup>, G. MÜNZENBERG<sup>2</sup>, H. WOLLNIK<sup>3</sup>,  
Y. HATSUKAWA, M. ASAI, K. TSUKADA, A. OSA, M. OSHIMA, H. HABA,  
S. ICHIKAWA, Y. NAGAME, A. V. POPOV<sup>1</sup> and D. M. SELIVERSTOV<sup>1</sup>

The discovery of new Super Heavy Elements (SHE) with atomic numbers up to  $Z=112$  [1] and a claim for the observation of heavier SHE announced recently [2] brought new excited interest to the problem on the existence of a mountain island of SHE peaked at a new "magic number". The observation of long-lived nuclides in the island can manifest the existence of shell stabilizing factors in the region of superheavy nuclei. The answers to the question how strong this stabilization is and how large the magic island is have been expected to lie in the investigation of the experimental mass surface of SHE.

To evaluate the masses of SHE, one must determine all  $\alpha$ -decay energies,  $Q_\alpha$ , in the linked  $\alpha$ -decay chains that reach the region of ordinal heavy-nuclides with known mass values. The  $\alpha$ -decay chains starting from SHE, that connect these to the transuranium nuclides whose masses are already known, can not be established so far since there are breaks in the chains. If the "missing"  $\alpha$ -emitters would be observed experimentally and the  $Q_\alpha$  values determined, the mass values of SHE can be obtained.

We started this program by search for the one of the "missing"  $\alpha$ -emitters:  $^{239}\text{Cm}$ . From the  $Q_\alpha$  value of  $^{239}\text{Cm}$  whose  $\alpha$ -branching ratio was expected to be very small, i.e. less than 0.001, the mass values of the nuclides starting from  $^{267}110$  nuclide can in principle be evaluated. The "broken"  $\alpha$ -decay chain is shown in Fig. 1. This work is a new approach to the mass mapping of the region of superheavy nuclides by searching for "missing"  $\alpha$ -emitters.

In this study the  $^{239}\text{Cm}$  was produced by irradiating  $^{232}\text{Th}$  with 75-MeV  $^{12}\text{C}$  ions for 5 hours at the JAERI tandem accelerator. Measurement for  $\alpha$ - and  $\gamma$ -rays from the chemically-separated curium fraction was carried out to confirm the formation of  $^{239}\text{Cm}$ . The determined half-life of  $^{239}\text{Cm}$  is  $2.5 \pm 0.4$  h by observing Am  $K_{\alpha 1}X$  and  $\gamma$ -rays (see Fig.2). Measurements of very weak  $\alpha$ -emission from  $^{239}\text{Cm}$  are now in progress.

<sup>1</sup> Petersburg Nuclear Physics Institute, Gatchina, 188300, Russia

<sup>2</sup> Gesellschaft für Schwerionenforschung, 64291 Darmstadt, Germany

<sup>3</sup> Giessen University, 35392 Giessen, Germany

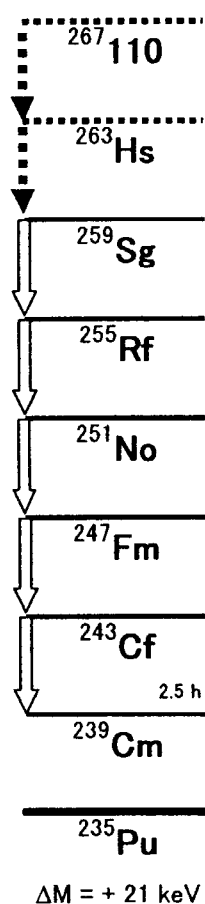


Fig. 1. The “broken”  $\alpha$ -decay chain starting from  $^{267}\text{110}$  nuclide. No  $\alpha$ -ray has been observed from the daughter nuclide  $^{263}\text{Hs}$  [3]. The experimental half-life measured in this study and the precision of reported mass value of  $^{235}\text{Pu}$  are also shown in the figure.

### References

- [1] S. Hofmann and G. Münzenberg, *Rev. Mod. Phys.* **72** (2000) 733.
- [2] Yu. Ts. Oganessian et al., *Phys. Rev. C* **63** (2000) 011301-1-2.
- [3] A. Ghiorso et al., *Nucl. Phys. A* **583** (1995) 861.

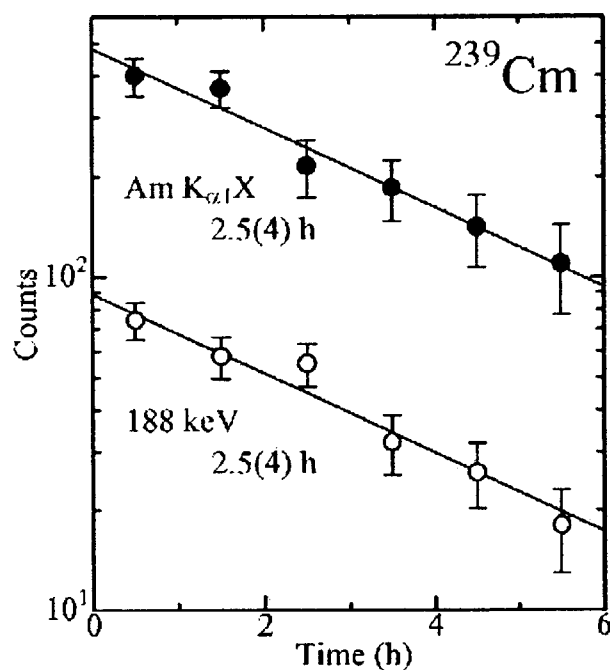


Fig. 2. Decay curves of Am  $K_{\alpha 1}$ X-ray and 188-keV  $\gamma$ -ray from  $^{239}\text{Cm}$  purified in the chemical sample.

## 4.2 ANION EXCHANGE BEHAVIOR OF Rf IN HCl AND HNO<sub>3</sub>

H. HABA<sup>1</sup>, K. TSUKADA, M. ASAI, I. NISHINAKA, S. GOTO<sup>2</sup>, A. TOYOSHIMA<sup>3</sup>, K. AKIYAMA, M. HIRATA, S. ICHIKAWA, Y. NAGAME, Y. SHOJI<sup>3</sup>, M. SHIGEKAWA<sup>3</sup>, T. KOIKE<sup>3</sup>, M. IWASAKI<sup>3</sup>, A. SHINOHARA<sup>3</sup>, T. KANEKO<sup>2</sup>, T. MARUYAMA<sup>2</sup>, S. ONO<sup>2</sup>, H. KUDO<sup>2</sup>, Y. OURA<sup>4</sup>, M. SAKAMA<sup>5</sup>, A. YOKOYAMA<sup>6</sup>, K. SUEKI<sup>7</sup>, H. NAKAHARA<sup>4</sup>, J. V. KRATZ<sup>8</sup> and M. SCHÄDEL<sup>9</sup>

The first transactinide element, rutherfordium (Rf), is expected to be a group-4 member in the periodic table with a ground state electronic configuration of  $[Rn]5f^{14}6d^27s^2$ , though the relativistic calculations have predicted conflicting configurations such as  $6d^27s^2$ ,  $7s^27p^2$ , and  $6d^17s^27p^1$  [1]. The nuclide  $^{261}\text{Rf}$  produced in the  $^{248}\text{Cm}(^{18}\text{O},5n)$  reaction has been used for chemical studies of Rf. The production yield of 78-s  $^{261}\text{Rf}$  is the order of one atom per minute, which forces us to perform rapid and repetitive chromatographic experiments with single atoms. Chemical behavior of Rf in HCl solutions has been studied to extract information on chloride complexation and hydrolysis [1]. Some of these experiments, however, showed conflicting results and some of them were criticized due to adsorption problems [1]. An anion-exchange experiment on Rf allows us to study the formation of chloride complexes in more detail and to verify the previous results from different viewpoints. On the other hand, the chemical behavior of Rf in HNO<sub>3</sub> had not been studied before. Recently, we have successfully investigated the anion-exchange behavior of Rf together with its homologues Zr, Hf, and Th in 4.0–11.5 M HCl and 8.0 M HNO<sub>3</sub> solutions [2,3] using the JAERI tandem accelerator. The following is a short review of our current studies.

The isotope  $^{261}\text{Rf}$  was produced by the  $^{248}\text{Cm}(^{18}\text{O},5n)$  reaction using a 94 MeV  $^{18}\text{O}$  beam from the JAERI tandem accelerator. Beam intensities were 200–300 particle nA. The  $^{248}\text{Cm}$  target of 610  $\mu\text{g}/\text{cm}^2$  thickness was prepared by electrodeposition onto a 2.4  $\text{mg}/\text{cm}^2$  thick beryllium foil. This target contained Gd (39.3%-enriched  $^{152}\text{Gd}$ ) of 36  $\mu\text{g}/\text{cm}^2$  thickness to produce Hf isotopes simultaneously and to monitor the behavior of Hf in the identical experimental condition as  $^{261}\text{Rf}$ . Reaction products recoiling out of the target were transported by the He/KCl gas-jet system to the Automated Ion-exchange separation apparatus coupled with the Detection system for Alpha spectroscopy (AIDA) [4].  $^{261}\text{Rf}$  and  $^{169}\text{Hf}$  deposited on the collection site of AIDA were dissolved with 170  $\mu\text{L}$  of 11.5 M HCl and fed into an anion-exchange column (MCI GEL CA08Y, 1.6 mm i.d.  $\times$  7 mm) at a flow rate of 1.0 mL/min. The effluent was collected on a Ta disk as Fraction 1 and was evaporated to dryness with hot He gas and a halogen heat lamp. The Rf and Hf remaining in the column were eluted with 230  $\mu\text{L}$  of 4.0 M HCl, and the effluent was collected on another Ta disk as Fraction 2. In the experiments at 4.0, 7.0, 8.5, 9.0, and 9.5 M HCl, Rf and Hf

<sup>1</sup> Cyclotron Center, RIKEN

<sup>2</sup> Department of Chemistry, Faculty of Science, Niigata University

<sup>3</sup> Department of Chemistry, Graduate School of Science, Osaka University

<sup>4</sup> Department of Chemistry, Graduate School of Science, Tokyo Metropolitan University

<sup>5</sup> Department of Radiologic Science and Engineering, School of Health Sciences, University of Tokushima

<sup>6</sup> Department of Chemistry, Faculty of Science, Kanazawa University

<sup>7</sup> Department of Chemistry, Tsukuba University

<sup>8</sup> Institut für Kernchemie, Universität Mainz

<sup>9</sup> Gesellschaft für Schwerionenforschung

were first fed into the column with 170  $\mu\text{L}$  of 11.5 M HCl and the effluent was discarded. Then, 290  $\mu\text{L}$  of 4.0–9.5 M HCl was pumped to the column and the effluent was collected on the Ta disk as Fraction 1. The remaining Rf and Hf were eluted with 250  $\mu\text{L}$  of 4.0 M HCl as Fraction 2. In the  $\text{HNO}_3$  experiment, Rf and Hf, dissolved in 190  $\mu\text{L}$  of 8.0 M  $\text{HNO}_3$ , were fed into the column and the effluent was collected as Fraction 1. Then, 220  $\mu\text{L}$  of 4.0 M HCl was used as Fraction 2. Each pair of Ta disks, Fractions 1 and 2, were automatically subjected to  $\alpha$  spectrometry with eight 600  $\text{mm}^2$  PIPS detectors. In order to investigate the behavior of Zr,  $^{85}\text{Zr}$  and  $^{169}\text{Hf}$  were produced simultaneously by the  $^{nat}\text{Ge}(^{18}\text{O}, xn)$  and  $^{nat}\text{Gd}(^{18}\text{O}, xn)$  reactions, respectively. The anion-exchange experiments with  $^{85}\text{Zr}$  and  $^{169}\text{Hf}$  were performed under the same experimental conditions as those with  $^{261}\text{Rf}$ . The effluents collected in polyethylene tubes were assayed by  $\gamma$ -ray spectrometry with Ge detectors.

The ion-exchange experiments of 245, 366, 400, 395, 328, and 159 runs were performed at 11.5, 9.5, 9.0, 8.5, 7.0, and 4.0 M HCl, respectively. In total, 186  $\alpha$  events from 78-s  $^{261}\text{Rf}$  (8.28 MeV) and its daughter 25-s  $^{257}\text{No}$  (8.22, 8.27, 8.32 MeV) were registered in the energy range of 8.00–8.36 MeV, including 35 time-correlated  $\alpha$  pairs. From the activities  $A_1$  and  $A_2$  observed in Fractions 1 and 2, respectively, the percent adsorption on CA08Y was calculated by the equation:  $\%ads = 100A_1/(A_1 + A_2)$ . The  $\%ads$  values of  $^{261}\text{Rf}$ ,  $^{169}\text{Hf}$ , and  $^{85}\text{Zr}$  at 11.5 M HCl were  $97^{+3}_{-6}$ ,  $98 \pm 4$ , and  $96 \pm 2\%$ , respectively. These high adsorptions indicate that the loading of these elements onto the column with 11.5 M HCl is completely done in the experiments at 4.0–9.5 M HCl. In Fig. 1, the variation of the  $\%ads$  values is shown as a function of HCl concentration. The  $\%ads$  values of Rf increase steeply with an increase of HCl concentration, indicating that the anionic chloride complexes of Rf are formed. This adsorption behavior of Rf is very similar to that of the group-4 homologues Zr and Hf, and is quite different from that of the pseudo-homologue Th(IV): the  $\%ads$  values for Th are estimated to be  $\sim 0\%$  from low  $K_d$  values [3]. It is noted that the adsorption order is  $\text{Rf} > \text{Zr} > \text{Hf}$ . This indicates that the chloride complexing strength in group-4 elements decreases in this order. Also noted is that the  $\%ads$  values at 4.0 M HCl are low enough for these elements to be stripped from the column. For 8.0 M  $\text{HNO}_3$ , the anion-exchanges of 217 runs were performed and a total of 20  $\alpha$  events from  $^{261}\text{Rf}$  and  $^{257}\text{No}$  were registered including 5  $\alpha$ - $\alpha$  correlations. The  $\%ads$  values of Rf, Hf, and Zr are  $13^{+11}_{-7}$ ,  $2.9 \pm 1.7$ , and  $5.5 \pm 1.3\%$ , respectively, and that of Th was separately determined to be  $99 \pm 3\%$  in the off-line experiments using a radiotracer of  $^{234}\text{Th}$ . These results imply that Rf forms cationic or neutral species in 8.0 M  $\text{HNO}_3$  like Zr and Hf but not like Th(IV):  $[\text{Th}(\text{NO}_3)_6]^{2-}$ .

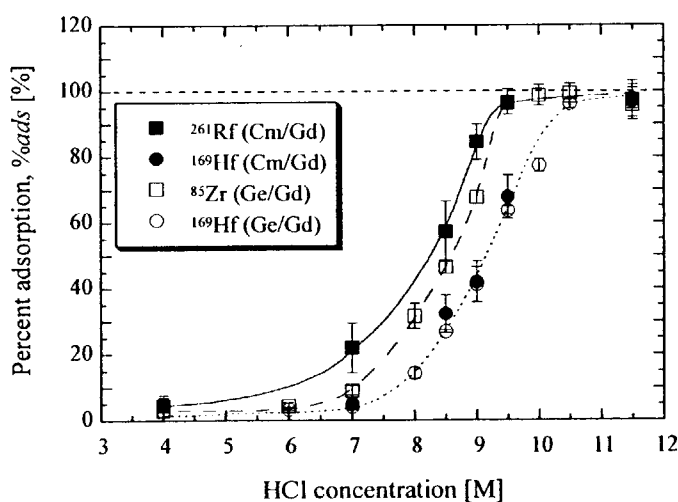


Fig. 1. Variation of the percent adsorption ( $\%ads$ ) for Zr, Hf, and Rf on CA08Y as a function of HCl concentration.

## References

- [1] J. V. Kratz, *Heavy Elements and Related New Phenomena, Vol. 1*, edited by W. Greiner and R. K. Gupta (World Scientific, Singapore, 1999), p. 129.
- [2] H. Haba *et al.*, *Radiochim. Acta* **89**(2001)733.
- [3] H. Haba *et al.*, *J. Nucl. Radiochem. Sci.* **3**(2002)143.
- [4] K. Tsukada *et al.*, a separate paper of this JAERI-Review.

### 4.3 DEVELOPMENT OF AUTOMATED LIQUID CHROMATOGRAPHY APPARATUS COUPLED WITH AN ON-LINE ALPHA-PARTICLE DETECTION SYSTEM

K. TSUKADA, I. NISHINAKA, M. ASAI, S. GOTO<sup>1</sup>, M. SAKAMA<sup>2</sup>,  
H. HABA, S. ICHIKAWA, Y. NAGAME, and M. SCHÄDEL<sup>3</sup>

To investigate the aqueous chemistry of the transactinide elements, such as  $^{104}\text{Rf}$  and  $^{105}\text{Db}$ , at JAERI, we have developed the Automated Ion exchange separation apparatus coupled with the Detection system for Alpha spectroscopy (AIDA). AIDA enables us to perform cyclic discontinuous column chromatographic separations of transactinide elements in aqueous phase and automatic detection of  $\alpha$ -particles within a typical cycle time of 1-2 minute.

AIDA consists of a modified ARCA (Automated Rapid Chemistry Apparatus) [1] which is the computer controlled apparatus for fast and repetitive High Performance Liquid Chromatography (HPLC) separation coupled with a He/KCl gas-jet transport system and an automated on-line  $\alpha$ -particle detection system with 8 PIPS detectors. The schematic view of the modified ARCA part and the whole system are shown in Figs.1 and 2, respectively. The reaction products were transported to AIDA by the He/KCl gas-jet system and deposited onto a PCTFE slider. The slider is mechanically moved on the top of one of the micro-columns and the deposited products are then dissolved, complexed, and eluted. The flow of solutions was directed through a micro-column by computer controlled chromatographic pumps, valves, and mechanical sliders. There is

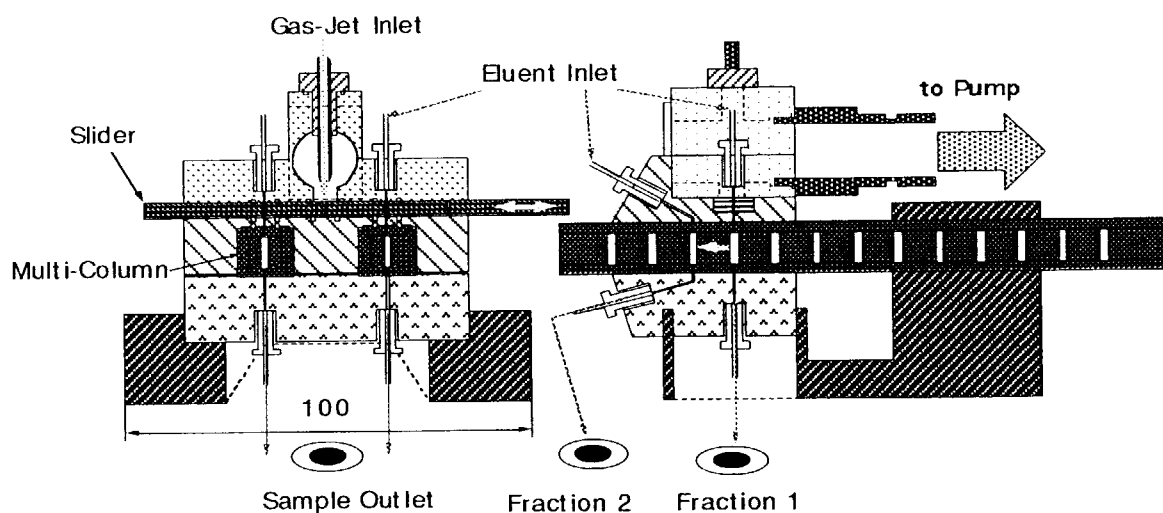


Fig.1. Schematic view of a modified ARCA (Automated Rapid Chemistry Apparatus).

<sup>1</sup> Department of Chemistry, Niigata University

<sup>2</sup> Department of Radiologic Science and Engineering, The University of Tokushima

<sup>3</sup> Gesellschaft für Schwerionenforschung (GSI)

a notable feature in AIDA that two different paths to flow the solution are available; in the first path the solution goes through the flit to the micro-column and in the other path another solution is directed through to the micro-column without the flit. In the anion exchange study of Rf in variable concentration of HCl solution, three kinds of solutions were used [2]. The first solution was charging solution, conc. HCl, to dissolve and adsorb all Rf to the micro-column using the first path. The second solution of 1-11 M HCl was used to examine adsorption behavior of Rf and finally the washing solution of 4 M HCl was used to remove all Rf from the micro-column using the 2nd path. The effluent collected on a Ta disk was evaporated to dryness using hot He gas stream and a halogen heat lamp. There are eight vacuum chambers to detect  $\alpha$ -particles and SF events in AIDA. Each Ta disk was mechanically transported to the selected vacuum chamber and subjected to alpha spectrometry by 600mm<sup>2</sup> PIPS detectors. Measured pulse-height data of  $\alpha$ -particles were recorded by event by event together with time information. In this anion exchange study of Rf in the HCl solution, the elution cycle was about 2 min, and the whole procedures from the dissolution to the beginning of the measurement for the 1st and 2nd samples were automatically completed in about 80 s and 100 s, respectively.

## References

- [1] M. Schädel et al., *Radiochim. Acta* **48** (1989) 171.
- [2] H. Haba et al., *J. Nucl. Radiochem. Sci.* **3** (2002) 143.

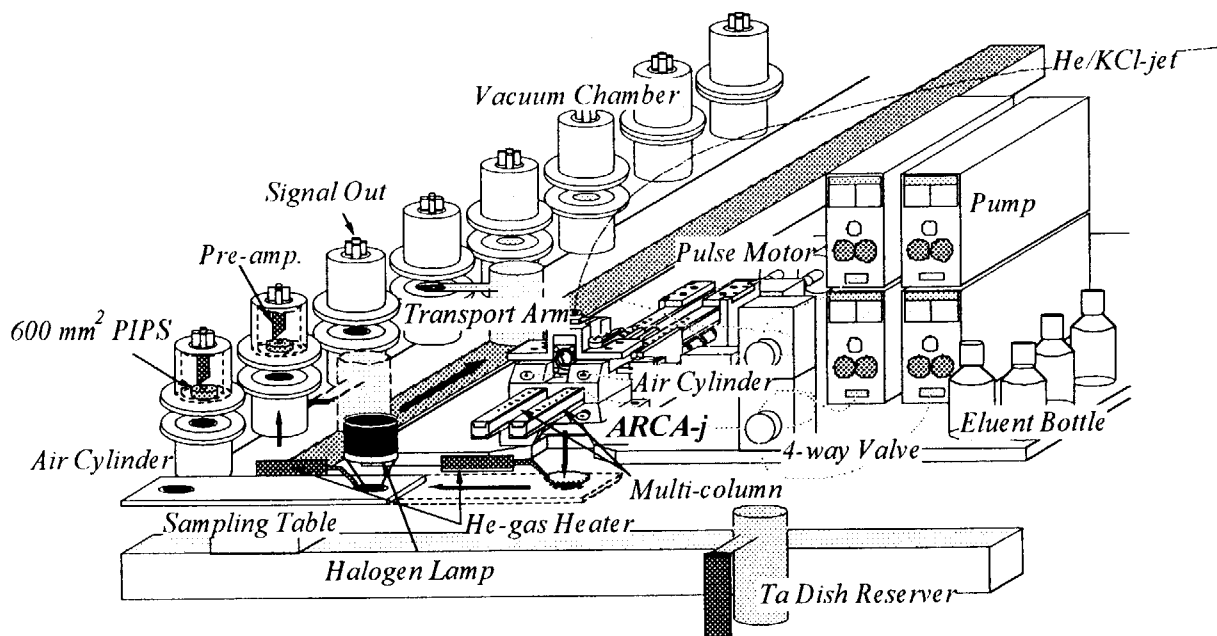


Fig.2. Schematic view of an Automated Ion exchange separation apparatus coupled with the Detection system for Alpha spectroscopy (AIDA).

#### 4.4 NEW TECHNIQUE FOR DETERMINATION OF TRACE ELEMENTS USING MULTIPARAMETER COINCIDENCE SPECTROMETRY -ULTRA SENSITIVE MEASUREMENT OF Ir -

Y. HATSUKAWA, Y. TOH, M. OSHIMA, T. HAYAKAWA,  
N. SHINOHARA, and K. TOYOTA\*

In the case of neutron activation analysis, measurements of  $\gamma$ -rays from trace elements are strongly interfered by the  $\gamma$ -rays from major elements, e.g.,  $^{24}\text{Na}$ ,  $^{56}\text{Mn}$ , etc. Therefore, chemical separation processes are usually required to eliminate the contribution from such major elements. The application of multiparameter coincidence spectroscopy using two Ge detectors for neutron activation analysis was already reported[1]. This method, however, has a disadvantage of low detection efficiency. In this study, to improve the low efficiency of multiparameter coincidence spectrometry, an array of twelve Ge detectors with BGO Compton suppressors, GEMINI[2] was used. The measurement of coincident  $\gamma$ -rays reduces significantly the background and allows clear detection of  $\gamma$ -rays with small intensities without chemical separations.

Geological samples were irradiated in a JAERI's research reactor. Gamma-gamma coincidence of multiple  $\gamma$ -rays from the radioisotopes produced by neutron capture reactions was measured with the array of the twelve Ge detectors [3, 4]. Iridium is an interested element in the field of geochemistry. In generally, contents of iridium in geological samples are very low, less than 1 ppb. Therefore, chemical separation procedures are generally required to eliminate the interference from major elements, such as Cr and Sc, in  $\gamma$ -ray spectroscopy. In this study, to determine contents of iridium in geological samples, rock samples were irradiated and  $\gamma$ - $\gamma$  coincidence measurements were also carried out with no chemical separation.

Iridium contents of nine standard rock samples (PTM-1, PTC-1, WMS-1, SARM-7, WPR-1, JP-1, DNC, BIR-1, W-2) were measured by the multiparameter coincidence method without any chemical separation. Thirty to fifty mg of each sample was sealed in quartz tube, and irradiated for 1 or 15 hours. 100 – 200 ng of iridium standard samples were also prepared and irradiated together with the rock samples. After irradiation,  $\gamma$ - $\gamma$  coincidence of multiple  $\gamma$ -rays from the radioisotopes produced by the neutron capture reactions was measured with GEMINI. Each sample was measured for 6 – 24 hours at GEMINI after 2-12 weeks of irradiation.

The results of iridium measurements for the standard rock samples are shown in Table 1, and

---

\*Hokkaido University, Sapporo, Hokkaido 060-0810, Japan

the reference values are also listed in this table. All results were in good agreement with previous data. A few ppt of iridium in geological sample can be determined by this method.

### References

- [1] G. Meyer, *J. Radioanal. Nucl. Chem.*, 114(1987) 223.
- [2] K. Furuno, M. Oshima, T. Komatsubara, K. Furutaka, T. Hayakawa, M. Kidera, Y. Hatsukawa, M. Matsuda, S. Mitarai, T. Shizuma, T. Saito, N. Hashimoto, H. Kusakari, M. Sugawara, T. Morikawa, *Nucl. Instr. and Meth. A* 421(1999) 211.
- [3] Y. Hatsukawa, M. Oshima, T. Hayakawa, Y. Toh, N. Shinohara, *J. Radioanalytical , Nucl. Chem.* 248(2001) 121.
- [4] Y. Hatsukawa, M. Oshima, T. Hayakawa, Y. Toh, N. Shinohara, *Nucl. Inst. Meth A* 482, (2002) 301.
- [5] *Geochemical Reference Material Compositions*, P. J. Potts, A.G. Tindal, P.C. Webb, CRC Press, USA, (1992).

Table 1 Iridium concentration in standard rock samples.

Sample	This work (ppb)	Reference value(ppb)*
PTM-1	$430 \pm 15$	300
PTC-1	$301 \pm 16$	
WMS-1	$104 \pm 10$	100
SARM-7	$87 \pm 14$	74
WPR-1	$16.4 \pm 1.4$	
JP-1	$2.2 \pm 0.6$	2
DNC	$0.55 \pm 0.04$	0.52
BIR-1	$0.20 \pm 0.05$	0.15
W-2	$0.08 \pm 0.01$	
*ref (5)		



## 4.5 SYNTHESIS OF PULTONIUM METALLOFULLERENE

K. AKIYAMA, K. SUEKI<sup>1</sup>, H. HABA, K. TSUKADA, M. ASAI, I. NISHINAKA, K. KIKUCHI<sup>2</sup>,  
S. ICHIKAWA, Y. NAGAME, H. NAKAHARA<sup>2</sup>, and M. KATADA<sup>2</sup>

A metallofullerene is a clathrate compound with one or more metal atoms encapsulated in the fullerene cage, and its unique structure has attracted many scientists to the study of its physical and chemical properties. It has been reported, for example, that the encapsulated metal atoms often take unique chemical states due to the  $\pi$  electrons of the surrounding carbon atoms which can rarely be observed in the atmosphere of air [1]. For this reason, it is significant to investigate the chemical states of the actinide atoms in the fullerene cages for probing a new field of the actinide science. Previously, we reported the HPLC elution behavior of the Th, Pa, U, Np, and Am metallofullerenes and the UV/vis/NIR absorption spectra of the Th@C<sub>84</sub> and U@C<sub>82</sub> species [2]. In this report, the HPLC elution behavior of the Pu metallofullerene investigated in the radiotracer technique.

The fullerenes encapsulating Pu atoms were synthesized by the arc discharge method. The anode for the discharge was made from a porous carbon rod (size: 10 mm $\phi$   $\times$  40 mm) which absorbed about 1 mL of the ethanol solution of La(NO<sub>3</sub>)<sub>3</sub> mixed with the radiotracer of <sup>237</sup>Pu, and was sintered at 800 °C under the He atmosphere. This anode was set in the chamber for the generation of fullerenes and discharged in the 400 Torr He with the direct current of 110 A. The soot containing Pu metallofullerenes was recovered from the chamber and dissolved in CS<sub>2</sub>. This CS<sub>2</sub> solution was filtered for removing the insoluble substance and condensed. The condensed solution was injected to a 5PBB (Pentabrombenzyle stationary phase) column and developed with the flow rate of 2 mL/min. The effluent from the column was collected for every 1 min and monitored by the on-line UV absorption detector. The HPLC elution behavior of the Pu fullerenes was monitored by the X-ray detection of the Np KX-ray following the EC decay of <sup>237</sup>Pu in each fraction.

Figure 1 shows the HPLC elution behavior of the Pu metallofullerene, which was obtained from the X-ray measurements of the eluant. For comparison, the HPLC chromatogram monitored by the UV absorption detector and the elution behavior of the metallofullerenes of Ce, Np and Eu are also plotted in this figure. As the results of the X-ray and  $\gamma$ -ray measurements for a series of HPLC fractions, the 101 keV Np K $\alpha_1$  X-ray was observed around the retention time of 13.5 to 18.5 min. The  $\gamma$ -ray spectrum of this region is shown in the inset at the upper right Fig. 1. More detailed measurements were performed on this region and the amount of Pu was estimated to be under the detection limit in the fractions of 13.5 min and 16.5 to 18.5 min but to be slightly over the detection limit in the fractions of 14.5 and 15.5 min.

The HPLC elution behavior of the metallofullerenes has been well investigated, [3,4] especially for the lanthanide metallofullerenes. The main product in the crude extracts of lanthanide metallofullerenes is M@C<sub>82</sub>, and, accordingly, the dominant HPLC elution peak in the chromatogram is due to this species. The retention time of a series of the lanthanide M@C<sub>82</sub> is affected by the topological structure of the fullerene cage and by the oxidation state of the encapsulated metal atom for some lanthanides. The M@C<sub>82</sub> of Sm, Eu, Tm and Yb takes a formal

<sup>1</sup> Department of Chemistry, University of Tsukuba

<sup>2</sup> Department of Chemistry, Tokyo Metropolitan University

charge of  $M^{2+}@C_{82}^{2-}$  as a result of the charge transfer interaction between the encapsulated metal atom and the  $C_{82}$  fullerene cage and have three topological isomers [1, 5]. On the other hand, the  $M@C_{82}$  species encapsulating the other lanthanides takes the formal charge of  $M^{3+}@C_{82}^{3-}$  and has an aerobic stable isomer and an unstable one which have topological differences [6-8]. These differences of the charge state on the cage and topological structure of the  $M@C_{82}$  cause the difference of the retention time of  $M@C_{82}$ . The retention time of  $M@C_{82}$  encapsulating the latter group of lanthanides is almost the same as that of  $C_{86}$  on 5PBB column, so, these  $M@C_{82}$  elute with  $C_{86}$  on this column. In the previous paper, we pointed out that the component of the dominant HPLC elution peak of the metallofullerenes encapsulating U, Np and Am was confirmed to be the latter type of  $M@C_{82}$  from the similarity of HPLC elution behavior and the TOF/MS measurement of the U species. The retention time of the Pu metallofullerene is confirmed to be within 14.5 to 15.5 min, and it approximately coincides with that of the  $C_{86}$ . If the Pu metallofullerene were of the former type of  $M@C_{82}$ , the activity from Pu must have been observed in the fraction of 13.5 min with the same level as that of 14.5 min. Moreover, if the  $M@C_{84}$  type metallofullerene similar to the Th metallofullerene were formed for Pu, the fractions collected at 16.5 and 17.5 min would have been active [9]. From these results, it is suggested that the component of the dominant HPLC elution peak is  $Pu@C_{82}$  and that the oxidation state of the encapsulated Pu is 3+.

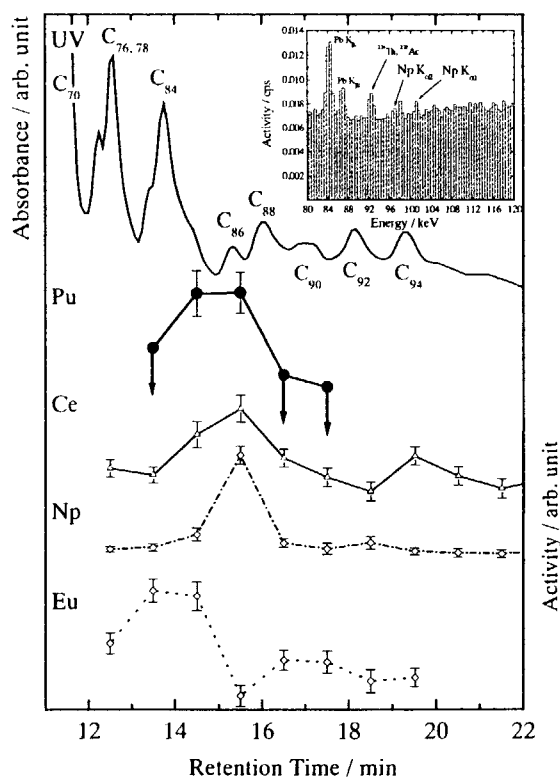


Fig. 1. HPLC elution behavior of Pu metallofullerene

## References

- [1] T. Okazaki *et al.*, *Chem. Phys. Lett.*, **320**, (2000) 435.
- [2] K. Akiyama *et al.*, *J. Am. Chem. Soc.*, **123** (1), (2001) 181.
- [3] K. Sueki, K. Akiyama, T. Yamauchi, W. Sato, K. Kikuchi, S. Suzuki, M. Katada, Y. Achiba, H. Nakahara, T. Akasaka and K. Tomura, *Fullerene Sci. Technol.*, **5** (1997) 1435.
- [4] D. Fuchs, R. Hermann, R. H. Michel, A. Fischer, P. Weis, M. M. Kappes, *J. Phys. Chem.*, **100** (1996) 725.
- [5] U. Kirbach and L. Dunsch, *Angew. Chem. Int. Ed. Engl.*, **35** (1996) 2380.
- [6] T. Akasaka, S. Okubo, M. Kondo, Y. Maeda, T. Wakahara, T. Kato, T. Suzuki, K. Yamamoto, K. Kobayashi and S. Nagase, *Chem. Phys. Lett.*, **319** (2000) 153.
- [7] K. Yamamoto, H. Funasaka, T. Takahashi and T. Akasaka, *J. Phys. Chem.*, **98** (1994) 2008.
- [8] S. Ohkubo, T. Kato, M. Inakuma and H. Shinohara, *New Diamond Front. Carbon Technol.*, **11** (2001) 285.
- [9] K. Akiyama, K. Sueki, Y.-L. Zhao, H. Haba, K. Tsukada, T. Kodama, K. Kikuchi, T. Ohtsuki, Y. Nagame, H. Nakahara, and M. Katada, *ISNM 2001 AIP Conf. Proc. 590, NANONETWORK MATERIALS: Fullerenes, Nanotubes and Related Systems* (AIP, New York, 2001), p. 437.

#### 4.6 DETERMINATION OF DISINTEGRATION RATE AND GAMMA-RAY EMISSION PROBABILITIES FOR $^{66}\text{Ga}$ SOURCE

H. MIYAHARA<sup>1</sup>, K. KATOH<sup>2</sup>, K. FUJIKI<sup>2</sup>,  
H. HABA, M. ASAI, K. TSUKADA and S. ICHIKAWA

Gallium-66 is a noticeable nuclide for application in radiation measurement and nuclear medicine because of high-energy gamma-ray emission. The half-life of  $^{66}\text{Ga}$  is 9.49 h and it decays by electron capture or beta emission. Though the emission probabilities of high-energy gamma-rays are evaluated with relatively small uncertainties [1], the experimental data which were referred in Ref. 1 were not certain in high energy region [2,3]. Source of  $^{88}\text{Y}$  was used as a gamma-ray emitter with the highest energy in calibration of detection efficiency in Ref. 3. The highest gamma-ray energy that the detection efficiency was determined by the  $^{88}\text{Y}$  source was 1.8 MeV and the detection efficiencies above 2 MeV were determined by linear extrapolation in both logarithmic scales. In Ref. 2 the similar method was also used. To improve the certainty of the detection efficiencies for high-energy gamma-rays,  $^{56}\text{Co}$  standard source was used in this measurement and the detection efficiency at 3.5 MeV was experimentally determined. Using  $^{66}\text{Ga}$  sources the disintegration rate and gamma-ray emission probabilities of  $^{66}\text{Ga}$  were measured in this study.

Sources of  $^{66}\text{Ga}$  were produced by proton irradiation of enriched  $^{66}\text{Zn}$  powder (enrichment : 99.29%) for 25 to 40 min and the proton energy was about 13 MeV previously determined [4]. The irradiated powder was dissolved in dilute HCl solution and sources for  $4\pi$  beta-gamma coincidence measurement were prepared on thin metallised VYNS films stretched on brass mounts. The  $4\pi$  beta-gamma coincidence apparatus was composed from a  $4\pi$ -beta pressurised proportional counter, an HPGe gamma-ray detector with relative efficiency of 23%, and coincidence apparatus using a two-dimensional data-acquisition system [5].

Gamma-ray detection efficiencies were determined from the gamma-ray intensities and disintegration rates measured for sources of  $^{56}\text{Co}$ ,  $^{133}\text{Ba}$ ,  $^{134}\text{Cs}$  and  $^{152}\text{Eu}$ . The gamma-ray emission probabilities adopted for these standard sources were the evaluated values taken from an IAEA report [6]. The data corrected for cascade summing effect were fitted to a fourth-order polynomial equation as a function of energy in both logarithmic scales by a method of least squares using a covariance matrix. Detection efficiencies above 3.5 MeV were evaluated by extrapolation.

The gamma-ray spectrum of the  $^{66}\text{Ga}$  source showed no impurity peak. An example of coincidence efficiency function to determine the disintegration rate of  $^{66}\text{Ga}$  is shown in Fig. 1, where gate was set on the photopeak of the 1039 keV gamma-ray. The efficiency of  $4\pi$ -beta counter was below 50%, because probability of electron capture is about 45% and specific activity of the sample source was low. However, the uncertainty of disintegration rate was about 1.5%, and final uncertainty of the source deduced from twice measurements and coincidence function obtained from gates set for the 1039 and 2752 keV gamma-rays was about 1%.

<sup>1</sup> Department of Radiological Technology, School of Health Sciences, Nagoya University

<sup>2</sup> Department of Nuclear Engineering, Graduate School of Engineering, Nagoya University

The emission probabilities of the principal gamma-rays from  $^{66}\text{Ga}$  were calculated from the disintegration rate, gamma-ray intensities and gamma-ray detection efficiencies. The measurements were carried out four times and two sources were used in each run. The results are shown in Table 1 together with the evaluated data. The values at low energy region agree with each other, but the evaluated values in high energy region are larger than the present values by 5 to 10%. In addition, the present work gives small uncertainties of 0.7 to 2%.

## References

- [1] H.R. Bhat, Nucl. Data Sheets **83** (1998) 789.
- [2] P.M. Endt and C. Alderliesten, Nucl. Phys. **A575** (1994) 297.
- [3] D.C. Camp and G.L. Meredith, Nucl. Phys. **A166** (1971) 349.
- [4] K. Katoh, H. Miyahara et al., J. Nucl. Sci. Technol. **39** (2002) 329.
- [5] H. Miyahara, K. Ikeda and N. Marnada, J. Nucl. Sci. Technol. **38** (2001) 270.
- [6] IAEA, *X-ray and gamma-ray standards for detector calibration*, IAEA-TECDOC-619, (IAEA, Vienna, 1991).

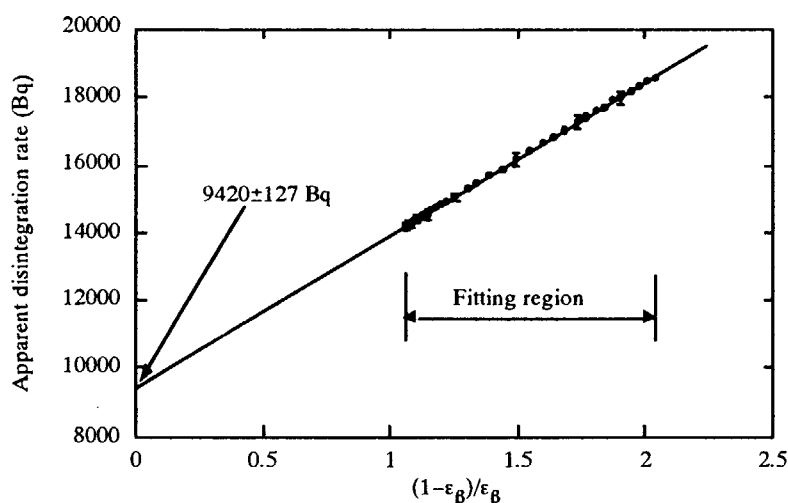


Fig. 1 An example of coincidence efficiency function of  $^{66}\text{Ga}$  source obtained for gate set of the 1039 keV gamma-ray, where  $\epsilon_\beta$  means detection efficiency of beta-counter

Table 1 Measured and evaluated emission probabilities (%) of the principal gamma-rays from  $^{66}\text{Ga}$

Gamma-ray energy (keV)	Evaluated value [1]	Present work
833	$5.89 \pm 0.18$	$5.96 \pm 0.04$
1039	$37.0 \pm 1.1$	$37.15 \pm 0.25$
2190	$5.60 \pm 0.18$	$5.29 \pm 0.04$
2752	$23.4 \pm 0.7$	$22.40 \pm 0.16$
4296	$4.05 \pm 0.13$	$3.68 \pm 0.07$

## **5. Nuclear Theory**

This is a blank page.

## 5.1 EXTREME LOCATION OF THE FLUORINE DRIP LINE AND THE $N = 20$ SHELL GAP

Y. UTSUNO, T. OTSUKA,<sup>1</sup> T. MIZUSAKI<sup>2</sup> and M. HONMA<sup>3</sup>

In neutron-rich nuclei, the magic number can shift from that of stable nuclei to another. For instance, the  $N = 20$  magic number disappears at around  $Z = 12$ , and a new  $N = 16$  one appears near oxygen [1]. The location of the drip line sensitively reflects the magic structure. In this direction, the drip line of fluorine isotopes with  $Z = 9$  attracts much interest: the drip line is located at  $N = 16$  for  $Z = 6, 7$ , and  $8$ , while it extends farther to  $N = 22$  or more for  $Z = 9$  [2]. In this study, we investigated how the drip line suddenly extends in fluorine isotopes based on large-scale shell-model calculations using the Monte Carlo shell model (MCSM) [3], as described in Ref. [4] in detail. Because the model space and the effective interaction are the same as those used in a study of the yrast properties of O, Ne, Mg, and Si isotopes [5], the present study can give a unified picture of this region in going from stable to unstable nuclei. This interaction is designed to reproduce the drip line of O isotopes with  $N = 16$ .

The two-neutron separation energies of  $N = 20$  isotones were calculated from  $Z = 9$  to  $14$ , as shown in Fig. 1 (a). For  $Z = 10$  to  $14$ , the agreement between the experiment and the calculations with full configurations is excellent. By comparing the full calculations with those in which the configuration is truncated within the 0-particle 0-hole excitation ( $0p0h$ ) from the  $N = 20$  core, the importance of the  $2p2h$  excited configurations is clearly seen, as shown in the ground-state probabilities in Fig. 1 (b). The dominance of the  $2p2h$  configurations at  $Z = 11$  and  $12$  obtained in the present calculation justifies the assumption of the so-called “island of inversion” [6], where no mixing between different configurations is included. To be more interesting, the  $4p4h$  configurations rather increase for smaller  $Z$ . The  $N = 20$  nucleus,  $^{29}\text{F}$ , is not bound against two-neutron emission unless the  $4p4h$  configurations are taken into account. This binding mechanism of  $^{29}\text{F}$ , i.e., large  $4p4h$  contribution to the ground state, which is small for  $N \neq 20$  nuclei, is in sharp contrast to the previous picture [6]. The “island of inversion” picture [6] results in the ground state of  $^{29}\text{F}$  having the  $0p0h$  configurations, and fails to reproduce unbound  $^{26}\text{O}$  and bound  $^{29}\text{F}$  simultaneously [6, 7]. In the present calculation,  $^{29}\text{F}$  gains correlation energy through mixing among the  $0p0h$ ,  $2p2h$ , and  $4p4h$  configurations, and becomes a bound nucleus in a natural way. By the mixing of the  $4p4h$ , the deformation is not so enhanced, but the pairing correlation plays a significant role.

Large  $4p4h$  mixing occurs due to a narrowing  $N = 20$  “effective” shell gap for smaller  $Z$ . The effective shell gap is defined by the difference in the *effective single-particle energies* [5] between the *sd* and *pf* shells. Owing to difference in the contribution of the two-body interaction between different nuclei, the effective single-particle energy varies as the proton or neutron number changes. In this case, the narrowing shell gap is caused by a sharp lowering of the neutron  $0d_{3/2}$  orbit as protons occupy the  $0d_{5/2}$  orbit, being essential in both the disappearance of the  $N = 20$  magic number and the appearance of the  $N = 16$  one. Direct evidence about the narrowing shell gap, such as the negative-parity energy levels, has not yet been observed experimentally. However, it seems that the extreme location of fluorine isotopes indicates this narrowing, because, provided that it is absent, the bound fluorine must stop at  $N = 18$ .

<sup>1</sup> Department of Physics, University of Tokyo

<sup>2</sup> Institute of Natural Sciences, Senshu university

<sup>3</sup> Center for Mathematical Sciences, University of Aizu

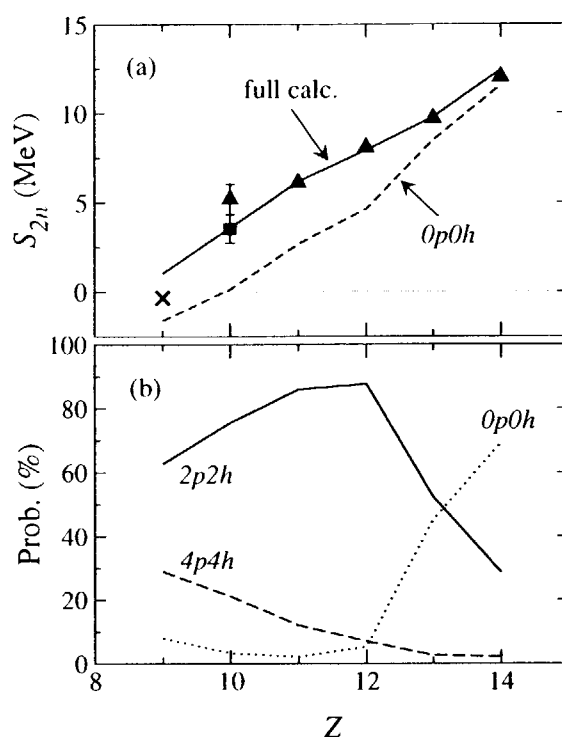


Fig. 1. (a) Two-neutron separation energies of  $N = 20$  isotones from F to Si compared between experiments (the triangles and the square) and shell-model calculations with various truncation schemes. The cross in  $^{29}\text{F}$  represents the  $0p0h + 2p2h$  calculation. (b) Probabilities of the  $npnh$  ( $n = 0, 2, 4$ ) configurations in their ground states.

## References

- [1] A. Ozawa, T. Kobayashi, T. Suzuki, K. Yoshida, and I. Tanihata, Phys. Rev. Lett. **84** (2000) 5493.
- [2] H. Sakurai *et al.*, Phys. Lett. B **448** (1999) 180.
- [3] T. Otsuka, M. Honma, T. Mizusaki, N. Shimizu, and Y. Utsuno, Prog. Part. Nucl. Phys. **47** (2001) 319.
- [4] Y. Utsuno, T. Otsuka, T. Mizusaki, and M. Honma, Phys. Rev. C **64** (2001) 011301(R).
- [5] Y. Utsuno, T. Otsuka, T. Mizusaki, and M. Honma, Phys. Rev. C **60** (1999) 054315.
- [6] E.K. Warburton, J.A. Becker, and B.A. Brown, Phys. Rev. C **41** (1990) 1147.
- [7] E. Caurier, F. Nowacki, A. Poves, and J. Retamosa, Phys. Rev. C **58** (1998) 2033.



## 5.2 POSSIBILITY OF $\Lambda\Lambda$ PAIRING IN $NA$ MATTER

T. TANIGAWA,<sup>1</sup> M. MATSUZAKI,<sup>2</sup> and S. CHIBA

Superfluidity in hadronic matter is one of the important issues in the physics of neutron stars. This is expected to be responsible for well-known phenomena such as their cooling processes and pulsar glitches. Unlike nucleonic pairing, there are a few studies on hyperonic pairing as to be mentioned later. Recently, the so-called “NAGARA” event was observed to unambiguously determine the binding energy of the two  $\Lambda$  hyperons  $B_{\Lambda\Lambda}$  in  ${}^6_{\Lambda\Lambda}\text{He}$  [1]. This leads to negation of its larger value (*i.e.* strong attraction) presented about three decades ago. The weaker attractive  $\Lambda\Lambda$  interaction newly observed has a significant impact on the microscopic understanding of the properties of neutron stars.

Up to now, two groups have studied the  $\Lambda\Lambda$  pairing in dense nuclear matter [2, 3]. They used realistic hyperon-hyperon ( $YY$ ) interactions based on the old data and reported sizable  $\Lambda\Lambda$  pairing gaps. The “NAGARA” event, however, imposes a strong constraint on them and may result in reduction or even vanishing of the pairing gap. We thus study the  $\Lambda\Lambda$  pairing in symmetric nuclear matter, adopting a phenomenological one-boson-exchange (OBE)  $\Lambda\Lambda$  interaction which includes a relativistic “medium effect” via a scalar mean field inherent in relativistic approaches owing to the Lorentz covariance. The strength of the  $\Lambda\Lambda$  attraction is determined so that it approximately reproduces the smaller bond energy  $\Delta B_{\Lambda\Lambda} = B_{\Lambda\Lambda} - 2B_{\Lambda}$ ,  $B_{\Lambda}$  being the binding energy of  $\Lambda$ , within relativistic mean field (RMF) calculations [4]. To treat pairing correlations, we use a relativistic Hartree-Bogoliubov (RHB) model which has been successful to describe many non-strange finite nuclei and some hypernuclei.

Figure 1 shows the resulting  ${}^1S_0$   $\Lambda\Lambda$  pairing gap at the Fermi surface with nucleon background of different densities  $\rho_N$  equal to 0,  $\rho_0$ ,  $2.5\rho_0$ , and  $5\rho_0$ , where  $\rho_0$  is the saturation density of symmetric nuclear matter. As nucleon density increases,  $\Lambda\Lambda$  pairing gap is more and more suppressed. It should be mentioned that since there are probably no  $\Lambda$ 's at  $\rho_N = 0$  and  $\rho_0$  in neutron star matter, the pairing gaps at these densities are quite hypothetical. At  $\rho_N = 2.5\rho_0$ , where  $\Lambda$  already appears in some models [5], the maximum pairing gap is less than 0.5 MeV. This is due to weakness of the attraction adopted here.

A mechanism of this suppression is originated from decrease of baryon mass, which has an important role if we admit its use in the baryon spinor. A fine example is the Dirac-Brueckner-Hartree-Fock approach for nucleon. Requirement of the self-consistency for the nucleon spinor, that is, the use of the Dirac effective mass in the nucleon spinor, effectively gives repulsion to the binding energy of symmetric nuclear matter [6]. Consequently, the theoretical saturation point goes toward the empirical one. It seems that our finding is similar to this repulsive effect. Moreover, the mechanism is apparently not restricted to the  $\Lambda\Lambda$  pair. It is probable that other kinds of hyperon-hyperon pairs have the same trend.

<sup>1</sup>Japan Society for the Promotion of Science and JAERI

<sup>2</sup>Department of Physics, Fukuoka University of Education

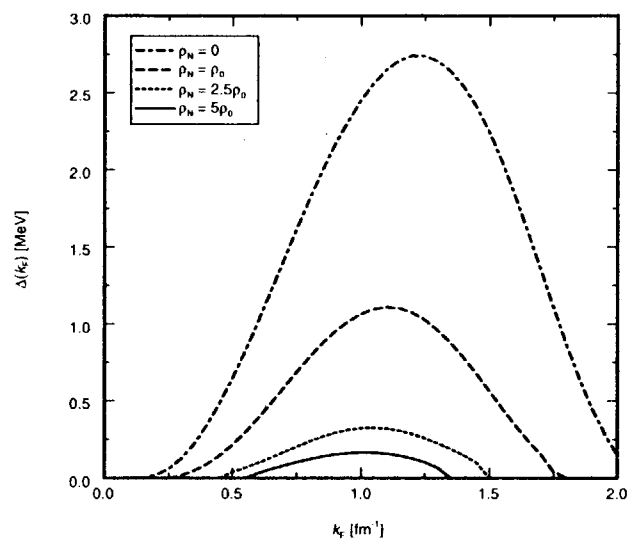


Figure 1:  $\Lambda\Lambda$  pairing gap at the Fermi surface of  $\Lambda$  for various background densities of symmetric nuclear matter.

In summary, we have investigated  $\Lambda\Lambda$  pairing in binary mixture matter of nucleons and lambdas. We have used the RHB model with the OBE interaction both in the particle-hole and particle-particle channels to naturally incorporate the medium effect into the latter via the scalar mean field, in other words, Dirac effective mass of  $\Lambda$ . We have found that the value of  $\Lambda\Lambda$  pairing gap decreases as the background nucleon density increases. This is the result opposite to the one reported in Ref. [2]. Furthermore, at physical densities of background, the pairing gap is so small that it is likely to vanish with the parameters other than the one used in this study. At present, unfortunately, our knowledge of  $YY$  interaction is somewhat limited. We notwithstanding expect that qualitative trends presented in this study survive in more refined models, and also in pairing of another hyperonic species.

## References

- [1] H. Takahashi *et al.*, Phys. Rev. Lett. **87** (2001) 212502.
- [2] S. Balberg and N. Barnea, Phys. Rev. C **57** (1998) 409.
- [3] T. Takatsuka and R. Tamagaki, Prog. Theor. Phys. **102** (1999) 1043.
- [4] S. Marcos, R. J. Lombard, and J. Mareš, Phys. Rev. C **57** (1998) 1178.
- [5] J. Schaffner and I. N. Mishustin, Phys. Rev. C **53** (1996) 1416.
- [6] R. Brockmann and R. Machleidt, Phys. Rev. C **42** (1990) 1965.

### 5.3 FORMATION AND DECAY OF SUPER HEAVY SYSTEMS

T. MARUYAMA, A. BONASERA<sup>1</sup>, M. PAPA<sup>2</sup> and S. CHIBA

The search for the super heavy elements (SHEs) is mainly carried out using complete fusion or nearly-complete fusion reactions. Since the “fusion” of very heavy nuclei (e.g. Au+Au) where the fission barrier no more exists is thought to be ineffective[1], the total mass number of the system used for SHE production is very close to the aimed one. However, the reaction mechanism of very heavy nuclei has not been discussed by fully dynamical models. We study the possible molecule-like states of heavy nuclei and the time scale of formed very heavy composite system.

For these problems we use constraint molecular dynamics (CoMD)[2], which takes into account the Fermionic nature of nucleons and is feasible for heavy systems. By using the CoMD model we simulate collisions of Au+Au system at  $E_{\text{lab}} = 5 \sim 35$  MeV/u. Here we use interaction parameter set slightly different from the original one[2]; the fusion cross section of Ca+Ca reactions is well reproduced. A typical collision event of Au+Au system is displayed in Fig. 1. A deformed composite system is formed and stays very long time before fission occurs. We note the average fission time amounts to  $10^3$  fm/c.

Assuming a very simple form of the time-dependent fission width  $\Gamma(t) = \Gamma_f \theta(t - T_d)$ , the averaged fission time  $T_{\text{fiss}}$  can be obtained by the survival probability of the compound system against two-body process  $P_{\text{surv}}$  as

$$P_{\text{surv}} = \exp[-(t - T_d)\Gamma_f/\hbar], \quad (1)$$

$$T_{\text{fiss}} \equiv T_d + \hbar/\Gamma_f \quad (2)$$

where  $T_d$  is the delay time and  $\Gamma_f$  is the “fission width” after the delay time. The probability  $P_{\text{surv}}(t)$  is obtained directly by the simulation. In Fig. 2 (a) we plot the fission time of the formed heavy systems. With the interaction parameters originally used in CoMD[2] we observe still longer fission time. Here we stress that such a long life time of very heavy system is interesting and important for the possible spontaneous  $e^+e^-$  production by a static QED process[3].

As mentioned above, production of SHE is one of the most important subjects in the heavy-ion collision problem. Besides cold- and hot-fusion, mass transfer in collision of very heavy nuclei was tried before. One could produce, e.g. up to Fm ( $Z = 100$ ) in U+U system, or Md ( $Z = 101$ ) in U+Cm system, by such a mechanism[1]. The incident energy, however, was very close to the Coulomb barrier and the reaction was rather gentle with the transfer of  $\sim 20$  nucleons. In our CoMD calculation for  $E_{\text{lab}} \geq 7$  MeV/nucleon, the reaction mechanism is more violent and there happens the transfer of much more nucleons though the mass loss from the system is also large. In Fig. 2 (b) plotted is the mass-asymmetry  $(A_1 - A_2)/(A_1 + A_2)$  of the fission process in CoMD calculation, where  $A_1$  and  $A_2$  are the largest and the second largest fragment mass when the fission occurs. The mass-asymmetry increases with the incident energy. At  $E_{\text{lab}} = 7$  MeV/nucleon, the asymmetry amounts to about 0.1 and at 10 MeV/nucleon almost 0.2 as average. If we simply assume no proton loss and asymmetry of 0.2 the largest fragment charge will be 112 for U+U system. Of course we should consider

<sup>1</sup> INFN-LNS, Via S. Sofia 44, Catania 95123, Italy.

<sup>2</sup> INFN-Sezione di Catania, Corso Italia 57, Catania 95129, Italy

the thermal mass loss and subsequent fission due to the excitation of fragments. However, such a kind of fusion-fission mechanism at around 10 MeV/nucleon should be taken into account for the SHE production. The new  $4\pi$  detectors can accumulate lots of statistics plus they can make coincidence studies to see if the fragments come from fission.

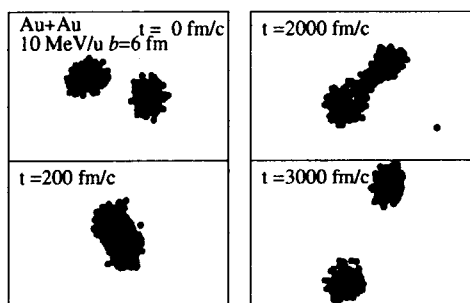


Figure 1: Snapshot of  $^{197}\text{Au}+^{197}\text{Au}$  at  $E_{\text{lab}} = 10 \text{ MeV/u}$   $b = 6 \text{ fm}$ .

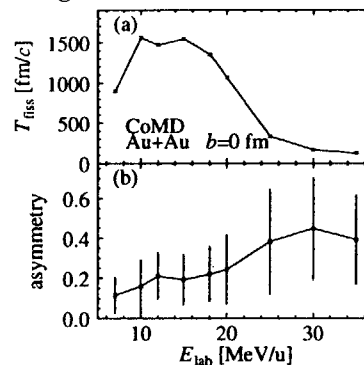


Figure 2: (a) The averaged fission time of composite system and (b) the fragment mass asymmetry.

## References

- [1] H. Gaggeler et al., Proc. 4th Int. Conf. on Nuclei Far From Stability, L.O. Skolen, Helsingør 1981, CERN 81-09, p 763; G. Herrmann, Proc. 4th Int. Conf. on Nuclei Far From Stability, L.O. Skolen, Helsingør 1981, CERN 81-09, p 772.
- [2] M. Papa, T. Maruyama and A. Bonasera, Phys. Rev. C. 64 (2001) 024612.
- [3] "Quantum Electrodynamics of Strong Fields", ed. W. Greiner, Plenum Press New York and London, 1983.

## 5.4 FIRST ORDER PHASE TRANSITION OF EXPANDING MATTER

S. CHIKAZUMI,<sup>1</sup> A. IWAMOTO

Fragmentation occurring in non-equilibrium system has some connection with a dynamical phase transition which is outside the scope of usual thermal physics. In order to study such non-equilibrium phenomena, it is advisable to resort to a molecular dynamics (MD) simulation under adequate conditions. Now, we are interested in expanding matter like a fire ball considered to be generated in heavy ion reactions. In the previous study [1, 2], we have proposed expanding nuclear matter model based on quantum molecular dynamics (QMD) to simulate nuclear matter with expanding motion. Dynamical aspects of nuclear matter have been an attractive topic in nuclear physics. Expanding matter model is such a model that we can investigate energetic nuclear matter where a new kind of phase transition might occur due to the expanding motion.

What kind of phase transition occurs can be inferred by seeing what kind of fragment mass distribution is observed. In some heavy ion reaction experiments with relatively low energy, a power law distribution is observed [3, 4], which indicates that there is a universal feature in the phenomenon. For this reason, it is often considered that the power law corresponds to a second order of a liquid-gas phase transition which can be explained by the theory for equilibrium system [5]. However, it is not necessarily certain that the liquid-gas phase transition can proceed free from the expanding motion even how low energy the system has.

Our purpose is to elucidate how the expanding motion affects the liquid-gas phase transition. It is clear that we do not have to use complicated QMD interactions. Thus, we introduce expanding matter with Lennard-Jones (LJ) potential [6, 7, 8], which ensures that liquid-gas phase transition occurs as long as expanding motion is slow enough to be regarded as quasi-static. In addition, it is possible to calculate the exact liquid-gas coexistence curve for the LJ matter by the Gibbs ensemble method [9]. During the time evolution of the expanding matter, we calculate the effective temperature as a function of density, which is compared with the coexistence curve.

Figure 1 shows the calculated temperature for the matter with the initial temperatures  $T_{\text{ini}} = 5$  (broken line), 3 (thin line) and 1 (solid line) in reduced units. The coexistence curve is represented by the open circles. The left figure is for quasi static expanding matter ( $h = 0.001$ ), where  $h$  is a parameter for the expanding speed which increases with the increase of  $h$ . The time evolution proceeds from right to left with the decrease of the density. For  $h = 0.001$ , it is found that each temperature decreases until it reaches the coexistence curve. However, the temperature remains constant just after the system enters the coexistence region. In other words, the phase separation into liquid and gas proceeds with the constant temperature. This is a typical feature of a first order phase transition.

On the other hand, the right hand side shows the case that the matter has the speed which is 100 times as rapid as the speed with  $h = 0.001$ . In this case, the dependence of the temperature on the density is quite different from that of the quasi-static expanding matter. The coexistence curve is not the border of a phase transition any more. The temperature still decreases after the system crosses over the coexistence curve. We can see that the expanding motion affects the process of the phase transition.

<sup>1</sup>Institute of Physics, University of Tsukuba

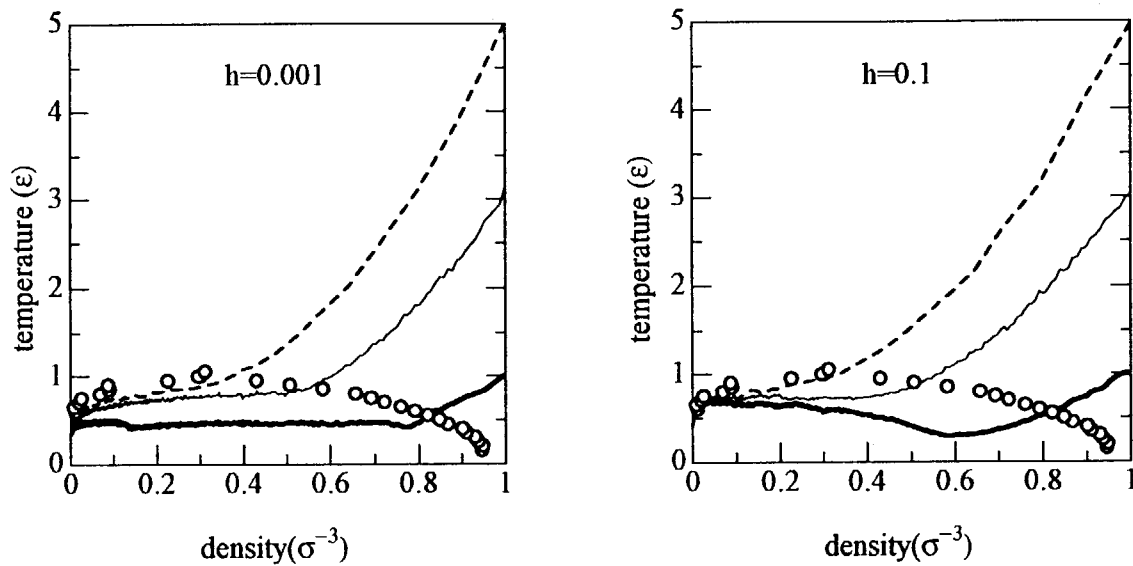


Figure 1: The effective temperature as a function of average density  $\rho$ . The left hand side is for  $h = 0.001$  and the right hand side is for  $h = 0.1$ . The broken line is for  $T_{\text{ini}} = 5$ , the thin solid line is for  $T_{\text{ini}} = 3$ , and the bold line is for  $T_{\text{ini}} = 1$ . The open circles are calculated by the Gibbs ensemble method and form a liquid-gas coexistence curve.  $\epsilon$  is unit of energy and  $\sigma$  is unit of length used in the LJ system.

## References

- [1] S. Chikazumi, T. Maruyama, K. Niita, A. Iwamoto, Phys. Lett. B, 476 (2000) 273.
- [2] S. Chikazumi, T. Maruyama, S. Chiba, K. Niita, A. Iwamoto, Phys. Rev. C, 63 (2001) 024602.
- [3] M. L. Gilkes, et al., Phys. Rev. Lett., 73 (1994) 1590.
- [4] P. F. Mastinu, et al., Phys. Rev. Lett., 76 (1996) 2646.
- [5] M. E. Fisher, Rep. Prog. Phys., 30 (1967) 615.
- [6] S. Toxvaerd, Phys. Rev. E, 58 (1998) 704.
- [7] W. T. Ashurst, B. L. Holian, Phys. Rev. E, 59 (1999) 6742.
- [8] S. Chikazumi, A. Iwamoto, Phys. Rev. C, 65 (2002) 067601.
- [9] D. Frenkel, B. Smit, Understanding Molecular Simulation, Academic Press, 1996.

## 5.5 RATIO OF THE r- AND s-PROCESS IN THE SOLAR SYSTEM

T. HAYAKAWA and T. SHIZUMA

Nucleosynthesis of heavy elements is important for understanding of the site mechanism in the stellar and cosmochronology [1]. The nuclei heavier than iron have been mainly synthesized by s- and r-process of the neutron capture ( $n, \gamma$ ) reaction. It has recently been discussed the s-process in thermally pulsing stars on the asymptotic giant branch [2]. The isotopes have also been produced by the  $\beta^-$  decay after the r-process, which have been considered to be happened in the Type II supernovae explosion [3]. In order to understand the role of each process, we estimated a model independent ratio between the s- and r-process corresponding to the proton number in the solar system. The r/s ratio is derived from the division of abundance of s-nuclei and r-nuclei. There are three type of the combinations, which are the pure s- and r-nuclei, pure s-nuclei and mixed nuclei, pure r-nuclei and mixed nuclei. These ratios are derived from the followed equations.

$$R = \frac{A(r)}{A(s)}$$

$$R = \frac{A(r+s) - A(s)}{A(s)}$$

$$R = \frac{A(r)}{A(r+s) - A(r)}$$

The  $A$  means the avrage of isotopes abundance of the s- or r-nuclei. Fig. 1 shows the plot of the r/s ratio corresponding to the proton number.

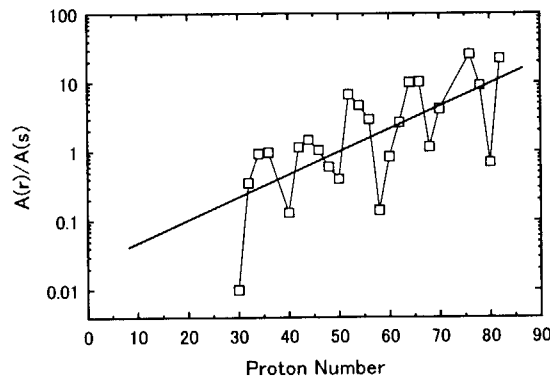


**Fig. 1** Ratio between r- and s nuclei.

We got a following equation from the  $\chi^2$  fitting. The  $z$  is proton number.

$$R(z) = 0.0234e^{0.0749z}$$

### Reference

- [1] W.A.Foler, Rev. Mod. Phys. 55 (1984) 149.
- [2] L.-S.The, *et al.*, Astrophys. J. 533 (2000) 998.
- [3] R.D.Hoffman, *et al.*, Astrophys. J. 521 (1999) 735.

## 5.6 CLUSTERING PROPERTIES IN NEUTRON-RICH NUCLEAR MATTER IN LOW DENSITY REGION

M. FUKUSHIMA, H. TAKEMOTO, S. CHIBA, H. HORIUCHI<sup>1</sup> and Y. AKAISHI<sup>2</sup>

We consider clusterization of neutron-rich nuclear matter in low-density region. As a variational function to describe structure of nucleon matter, we adopt a Bloch function (B.F.) with a simple cubic periodicity [1], which has two extreme states, an aggregation of isolated clusters and uniform matter in low- and high-density limit, respectively. Here, the width parameter of clusterings can be determined variationally depending on the density. In this paper, we extend the Bloch function up to the linear combination of  $p$ -wave function orthogonal to that of  $s$ -wave function to describe excess neutrons, which may occupy  $p$ -orbit above  $s$ -orbit in a cluster. First of all we will give the explanation of such an extension, and show the existence of the  $^{10}\text{He}$ -cluster-like density fluctuated state in asymmetric nuclear matter with  $N/A = 0.8$ . We will also discuss  $^{16}\text{O}$ -cluster-like density fluctuations as well as  $\alpha$ -cluster-like one in the symmetric case.

We take a linear combination of atomic orbit as a variational wave function in analogy with electrons in lattice as follows:

$$\Psi = \mathcal{A} \prod_{i=1}^A \psi_{\vec{c}\vec{k}_i}(\vec{r}_i) \cdot \chi_i(\sigma_i, \tau_i), \quad (1)$$

where  $\psi_{\vec{c}\vec{k}}$  and  $\chi_i$  are the spatial and spin-isospin parts of single-particle wave functions, respectively. When the crystallized nuclear matter consists of  $\alpha$  cluster,  $\psi_{\vec{c}\vec{k}}$  is constructed by the linear combination of  $s$ -wave function  $\psi_{s\vec{k}}(\vec{r}) = \phi_{sk_x}(x) \cdot \phi_{sk_y}(y) \cdot \phi_{sk_z}(z)$  with

$$\phi_{sk_x}(x) = \left(\frac{a}{L}\right)^{1/2} \left(\frac{1}{N_{sk_x}}\right)^{1/2} \sum_m e^{ik_x ma} \varphi_s(x - ma), \quad \varphi_s(x) = \left(\frac{1}{\sqrt{\pi}b}\right)^{1/2} \exp\left[-\frac{x^2}{2b^2}\right], \quad (2)$$

where  $a$  is the periodic distance,  $L^3$  is the normalization volume, and  $N_{sk_i}$  is the normalization factor of  $\phi_{sk_i}$  ( $i = x, y, z$ ) [1]. For the purpose of describing asymmetric nuclear matter, we prepare a B.F. of the linear combination of  $p$ -wave function  $\psi_{p\vec{k}}(\vec{r}) = \phi_{pk_x}(x) \cdot \phi_{pk_y}(y) \cdot \phi_{pk_z}(z)$ , because excess neutrons may occupy  $p$ -orbit above  $s$ -orbit in an isolated cluster.

$$\phi_{pk_x}(x) = \left(\frac{a}{L}\right)^{1/2} \left(\frac{1}{N_{pk_x}}\right)^{1/2} \sum_m e^{ik_x ma} \varphi_p(x - ma), \quad \varphi_p(x) = \left(\frac{1}{\sqrt{\pi}b}\right)^{1/2} \frac{\sqrt{2}}{b} x \exp\left[-\frac{x^2}{2b^2}\right]. \quad (3)$$

However this  $p$ -wave B.F. is not orthogonal to  $s$ -wave B.F. Therefore we define the orthogonal  $p$ -wave ( $op$ -wave) B.F. to  $s$ -wave one as  $\psi_{op\vec{k}}(\vec{r}) = \phi_{opk_x}(x) \cdot \phi_{sk_y}(y) \cdot \phi_{sk_z}(z)$ , with

$$\phi_{op,k_x}(x) = \left(\frac{1}{N_{opk_x}}\right)^{1/2} [\phi_{pk_x}(x) - \langle \phi_{sk_x} | \phi_{pk_x} \rangle \phi_{sk_x}(x)]. \quad (4)$$

$\psi_{op\vec{k}}$  and  $\psi_{op\vec{k}}$  are also defined in the similar way.  $\{\psi_{s,\vec{k}}, \psi_{op,\vec{k}}\}$  is the normalized orthogonal set, and satisfies the relation  $\langle \psi_{s',\vec{k}'} | \psi_{s,\vec{k}} \rangle = \delta_{ss'} \delta_{\vec{k}\vec{k}'}$ . In this description there are two parameters, one is the lattice spacing,  $a$ , which corresponds to the density of matter, and the other is the width of Gaussian,  $b$ , which corresponds to the size of a cluster. B.F. is characterized by the ratio of  $a$  to  $b$ . In the limit  $a/b \rightarrow 0$  density fluctuation vanishes and nuclear matter becomes uniform,

<sup>1</sup>Department of Physics, Kyoto University, Kyoto 606-8502, Japan

<sup>2</sup>Institute of Particle and Nuclear Studies, KEK, Japan



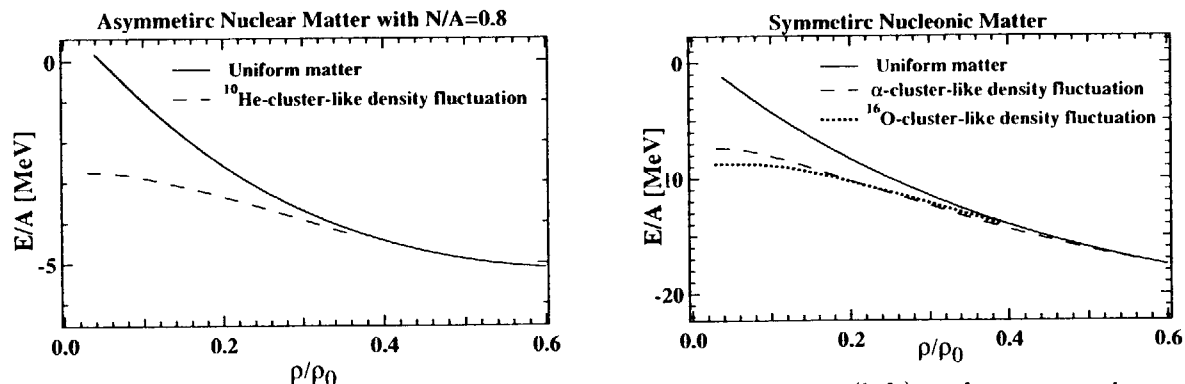


Figure 1: Density-dependence of energy per nucleon of symmetric (left) and asymmetric nuclear matter (right) with consideration of the spurious energy arising from the c.m. motion of a cluster approximately. Solid lines indicate those of uniform nuclear matter.  $\rho_0$  is the saturation density and equal to  $0.26 \text{ fm}^{-3}$  in the use of the Modified Volkov force.

while in the limit  $a/b \rightarrow \infty$  nuclear matter becomes an aggregation of isolated clusters fixed at lattice sites. We determine the width  $b$  under the variational analysis with respect to the following total energy per nucleon. As an effective interaction we use the modified Volkov (MV) force which consists of two-range Gaussian type two-body part and delta-type three-body part [3]. Total energy per nucleon is given by  $E/A = \langle \hat{T} \rangle / A - \langle \hat{T}_{\text{c.m.}} \rangle / A + \langle \hat{U}_2 \rangle / A + \langle \hat{U}_3 \rangle / A$ , where the first term represents the kinetic energy, the second comes from the center-of-mass (c.m.) motion, the third stands for the two-body interaction energy and the last term is the three-body interaction energy. It is noted here that we estimate the spurious energy approximately. At extremely low density, that is, at the isolated cluster limit  $a/b \rightarrow \infty$  the overlap between clusters placed at different lattice sites is practically zero, and therefore each cluster should have zero-point oscillation energy of its c.m. motion. For very high density ( $a/b$  is small) the overlap is so large that no spurious energy arises due to clustering. We estimate  $T_0/A$  at intermediate densities approximately as follows:  $T_0/A \approx \frac{3\hbar^2}{2M_c} \frac{1}{b^2} \left( 1 - \exp\left[-\frac{1}{4} \left(\frac{a}{b}\right)^2\right] \right)$ .

Figure 1 shows results taking account of the spurious energy approximately. At the limit of  $\rho \rightarrow 0$  ( $a \rightarrow \infty$ ), energies of density-fluctuated states approaches those of isolated cluster. except for the Coulomb energy, which are indicated by arrows, and approximated spurious energies become near critical densities. The critical densities increase up to  $\sim 0.4\rho_0$ ,  $\sim 0.6\rho_0$ , and  $\sim 0.4\rho_0$  in  $^{10}\text{He}$ ,  $\alpha$ , and  $^{16}\text{O}$  cluster-like density fluctuated states, respectively, compared with cases of no subtraction of the spurious energy. This subtraction tends to cause density fluctuations because of enlargement of binding energy of each cluster, and its effect becomes more for lighter cluster-like density fluctuation because the spurious energy is proportional to the inverse of mass of a cluster.  $\alpha$  and  $^{16}\text{O}$  cluster-like density-fluctuated states almost degenerate in the region between  $0.2\rho_0$  and  $0.4\rho_0$ . It indicates that amorphous states may exist in this region. Such a situation will arise in the crust region of neutron stars where the properties of neutron-rich nuclear matter is highly relevant to thermal and mechanical properties of neutron stars. However, in order to evaluate critical densities quantitatively, it is necessary to estimate this spurious energy as precisely as possible at the intermediate density.

## References

- [1] Y. Akaishi and H. Bandō, Prog. Theor. Phys. **41** (1969) 1594.
- [2] D.M. Brink and J.J. Castro, Nucl. Phys. **A216** (1973) 109.
- [3] T. Ando, K. Ikeda, and A. Tohsaki-suzuki, Prog. Theor. Phys. **64** (1980) 1608.

This is a blank page.

## **6. Atomic Physics and Solid State Physics**

This is a blank page.

## 6.1 HIGH-RESOLUTION ZERO-DEGREE ELECTRON SPECTROSCOPY OF HIGHLY CHARGED ARGON ION

M. IMAI<sup>1</sup>, M. SATAKA, K. KAWATSURA<sup>2</sup>, K. TAKAHIRO<sup>2</sup>,  
K. KOMAKI<sup>3</sup> and H. SHIBATA<sup>4</sup>,

Penetration of ions through solid target has been investigated in many aspects. Production of Rydberg states of fast projectiles interacting with foil target has been providing attractive subjects among these investigations [1]. The method of zero-degree electron spectroscopy [2] has proved to be one of the excellent tools to study these phenomena by measuring the secondary electrons emitted from the projectile and/or electrons captured from or lost to the continuum. We have measured Coster-Kronig (C-K) electrons from  $S^{12+}$  [3] and  $Si^{5+}$  [4] ions excited through He or C-foil target, and have succeeded in reproducing the experimental spectra by using C-K electron energies calculated by perturbation theory of Z-expansion method (MZ code), where we have assumed ion charge distributions “inside” the foil [5]. Based on the previous studies, we have extended our work to another projectile(s) to study Rydberg ion structures systematically, the preliminary result of which is presented here for 80 MeV  $Ar^{14+}$  ion penetrating through C-foil target.

The experiment was performed at HIR2-2 beam line of the 20UR Tandem Accelerator Facility. As the experimental apparatus has already been presented previously [3,4,6] only the major parameters are given here. Measured are the electrons emitted from argon projectile passing through C-foil of  $6.9 \mu\text{g}/\text{cm}^2$ . A beam of 2.0 MeV/u  $Ar^{6+}$  were provided by the accelerator using the terminal ECR ion source and post-stripped to form  $Ar^{14+}$  beam before entering the switching magnet. Electrons emitted from the projectile were energy-analyzed by a tandem electrostatic analyzer at zero degrees. The laboratory frame spectrum, which had a famous cusp-shaped peak centered at 1.1001 keV and C-K electron peaks on both wings of the cusp, was obtained by scanning the retarding potential between the first and the second analyzers. The projectile rest frame spectrum, obtained by converting the laboratory frame spectrum into the projectile rest frame, resulted in the energy resolution of  $0.02 \sim 0.2 \text{ eV}$ .

In the figure is shown the high energy wing electron spectrum from 2.0 MeV/u  $Ar^{14+}$  through C-foil of  $6.9 \mu\text{g}/\text{cm}^2$  in thickness. The repetitive peaks are assigned to 5 series of C-K transitions as marked (a), (a'), (b), (b') or (b'') in the figure. Each series comes from transitions of

- (a)  $Ar^{14+} 1s^2 2p(^2P_{3/2}^o)nl - 1s^2 2s(^2S_{1/2})\epsilon l'$  (35.04 eV),
- (a')  $Ar^{14+} 1s^2 2p(^2P_{1/2}^o)nl - 1s^2 2s(^2S_{1/2})\epsilon l'$  (31.88 eV),
- (b)  $Ar^{13+} 1s^2 2s 2p(^3P_2^o)nl - 1s^2 2s^2(^1S_0)\epsilon l'$  (31.33 eV),
- (b')  $Ar^{13+} 1s^2 2s 2p(^3P_1^o)nl - 1s^2 2s^2(^1S_0)\epsilon l'$  (29.24 eV),
- (b'')  $Ar^{13+} 1s^2 2s 2p(^3P_0^o)nl - 1s^2 2s^2(^1S_0)\epsilon l'$  (28.35 eV),

where  $n$  starts from 10 and counts up as the peak energy grows for all transitions. The energy values in parenthesis give the series limits. The marked energies are obtained as

$$E = \Delta E - Q^2 Ry / 2n^2,$$

where  $\Delta E$  is the energy level of the initial core configuration counted from ground (final) configuration,  $Q$  the effective charge of the core configuration (assumed to be +15 and +14 for (a)

<sup>1</sup> Department of Nuclear Engineering, Kyoto University

<sup>2</sup> Department of Chemistry and Materials Technology, Kyoto Institute of Technology

<sup>3</sup> Institute of Physics, Graduate School of Arts and Sciences, University of Tokyo

<sup>4</sup> Research Center for Nuclear Science and Technology, University of Tokyo

and (b) series, respectively), and  $Ry/2$  the Rydberg energy 13.606 eV. For  $\Delta E$ , compiled level data for Ar XV and Ar XVI taken from “NIST Atomic Spectra Database” [7] are used. These assignments show that both  $Ar^{14+} 1s^2 2p(^2P)$  and  $Ar^{13+} 1s^2 2s 2p(^3P)$  states play an important role in penetrating  $Ar^{14+}$  ions through thin carbon film.

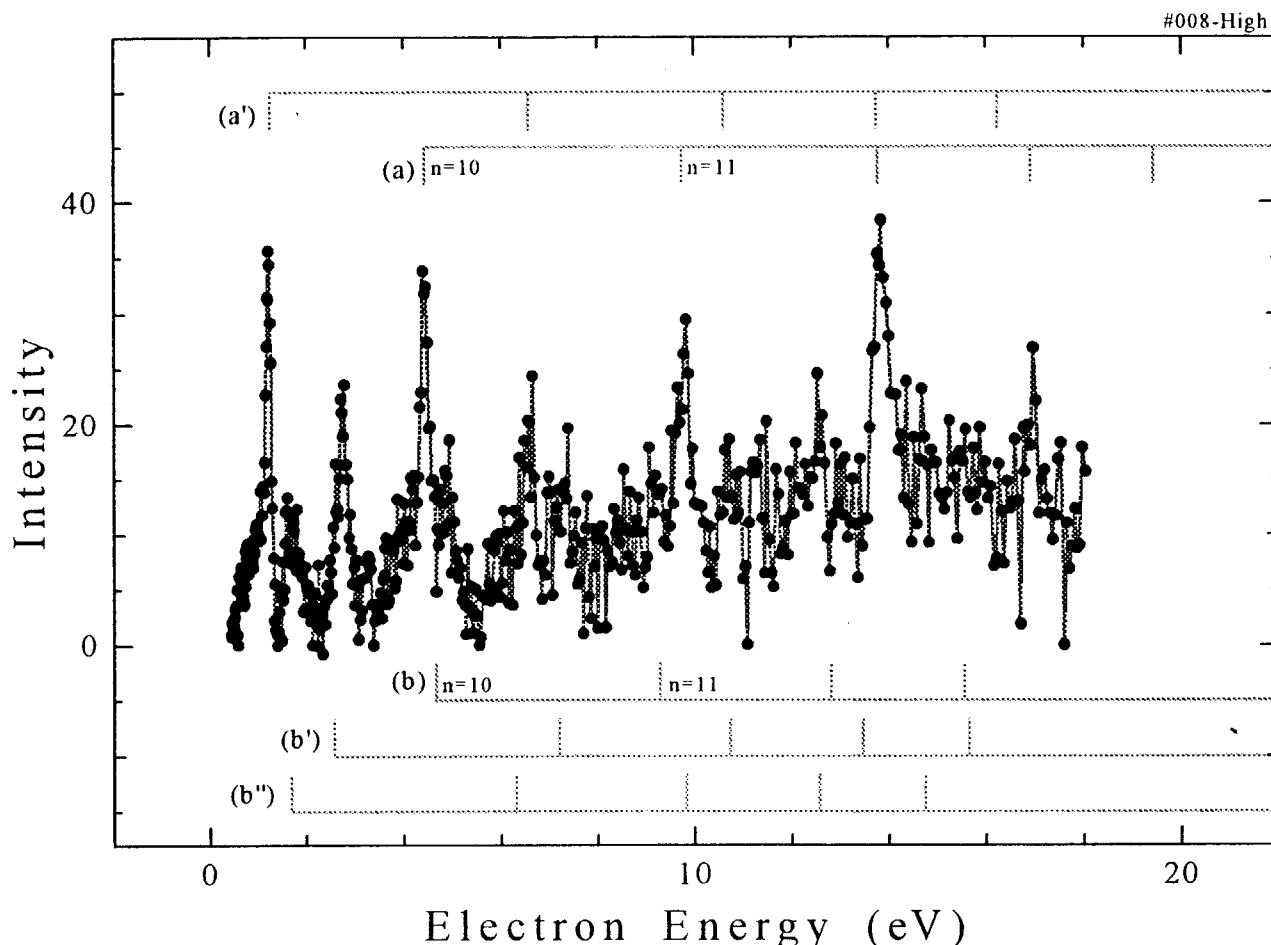


Fig. 1 Spectrum of electrons ejected at 0 degrees in 2.0 MeV/u  $Ar^{14+}$  + C-foil ( $6.9 \mu g/cm^2$ ) collisions. Energy refers to the projectile rest frame.

#### References

- [1] Y. Yamazaki, Nucl. Instrum. Methods **B96**, 517 (1995).
- [2] N. Stolterfoht, Phys. Rep. **146**, 315 (1987).
- [3] K. Kawatsura *et al.*, Nucl. Instrum. Methods **B48**, 103 (1990); Nucl. Instrum. Methods **B53**, 421 (1991); M. Imai *et al.*, Nucl. Instrum. Methods **B67**, 142 (1992); K. Kawatsura *et al.*, Nucl. Instrum. Methods **B124**, 381 (1997); M. Imai *et al.*, Nucl. Instrum. Methods **B193**, 674 (2002).
- [4] M. Imai *et al.*, Physica Scripta **T73**, 93 (1997).
- [5] M. Sataka *et al.*, J. Phys. **B35**, 267 (2002); Phys. Rev. **A65**, 052704 (2002).
- [6] M. Sataka *et al.*, Phys. Rev. **A44**, 7290 (1991); K. Kawatsura *et al.*, J. Electron Spectr. and Relat. Phenomena **88–91**, 83 (1998); K. Kawatsura *et al.*, J. Electron Spectr. and Relat. Phenomena **88–91**, 87 (1998).
- [7] Available free online at [http://physics.nist.gov/cgi-bin/AtData/main\\_asd](http://physics.nist.gov/cgi-bin/AtData/main_asd).

## 6.2 STUDIES ON THE DIFFUSION PROCESSES IN SOLID MATERIALS BY RADIOACTIVE NUCLEAR BEAMS

S.C. JEONG<sup>1</sup>, I. KATAYAMA<sup>1</sup>, H. KAWAKAMI<sup>1</sup>, H. ISHIYAMA<sup>1</sup>, H. MIYATAKE<sup>1</sup>,  
M. SATAKA, A. IWASE, S. OKAYASU, H. SUGAI, S. ICHIKAWA, K. NISHIO,  
Y. SUGIYAMA<sup>2</sup>, K. TAKADA<sup>3</sup>, M. WATANABE<sup>3</sup>

Under the collaboration between KEK-IPNS and JAERI-TOKAI, a radioactive nuclear beam facility is under construction at JAERI Tandem Accelerator Facility. In the facility, various radioactive nuclear beams accelerated up to 1MeV/u will be available in JFY 2004. For an interdisciplinary application of the radioactive nuclear beams, we have tried to measure diffusion constants of short-lived radioactive nuclei implanted in a solid material of interest. Especially, we are interested in the diffusion of Li in LiCoO<sub>2</sub>, which is one of the positive electrode materials of the Li ion batteries. For the measurement of the diffusion constant, we are going to use <sup>8</sup>Li as a tracer of the Li movement in the materials; <sup>8</sup>Li is a beta delayed alpha particle emitter. In this year, we concentrated on the production of <sup>8</sup>Li by using the JAERI-ENMA, and examined the feasibility of the measured, time-dependent alpha spectra as a measure of the diffusion of <sup>8</sup>Li in the materials of interest, reflecting the temporal evolution of the density distribution of the <sup>8</sup>Li primarily implanted in the material.

The radioisotope of <sup>8</sup>Li( $T_{1/2}=0.838$ s) was produced by bombarding <sup>7</sup>Li of 24MeV on <sup>9</sup>Be target of 42μm in thickness. In order to effectively single out and collect <sup>8</sup>Li on a sample with a size of less than 10mm in diameter, we used the JAERI-ENMA. ENMA is a magnetic spectrograph for analyzing reaction products, especially resulting from the light-ion induced nuclear reaction, and thus operating in a dispersive mode in order to maximize the momentum resolution of the reaction products of interest. For the present purpose, however, the reaction products, <sup>8</sup>Li, emitted in a large angular region with different energies, should be collected simultaneously on the sample of interest. We have examined an achromatic operation of ENMA for the effective collection of <sup>8</sup>Li on the sample. As a result, more than 600 nuclei/s of <sup>8</sup>Li were routinely collected on the sample with an intensity of 200nA of <sup>7</sup>Li. In this case, the energy spreading of <sup>8</sup>Li is

---

<sup>1</sup> Institute for Particle and Nuclear Studies, KEK

<sup>2</sup> Japan Advanced Technology

<sup>3</sup> National Institute for Materials Science (NIMS)

close to the energy acceptance of ENMA, about 10% in FWHM, and almost the same amount of contaminations, light particles and  $^7\text{Li}$ , was observed.

The experimental set-up for the diffusion measurement is shown in Fig. 1, installed nearly at the focal position of ENMA. The  $^8\text{Li}$  beam of 16.6MeV with about 1MeV in FWHM, analyzed by ENMA in an achromatic way, was implanted in the sample, after being properly energy-degraded. The energy degrader is made of an Al foil of 35 $\mu\text{m}$  in thickness and the actual thickness passed through by the incident beam can be adjusted by rotation as shown in Fig.1. An Al foil, 5 $\mu\text{m}$  thick, was used as the sample for test. The density distribution of the implanted  $^8\text{Li}$  in the sample was estimated by examining, as a function of the thickness of the energy degrader as shown in Fig.2, the yields of decay alpha particles measured by a SSD located in front of the sample at off-axis position: The width of the distribution in FWHM is about 4 $\mu\text{m}$  and the implanted depth is, on the average, about 2.5 $\mu\text{m}$  estimated by the range of the decay alpha particles in the sample. This shows good agreement with the estimation of SRIM2000.

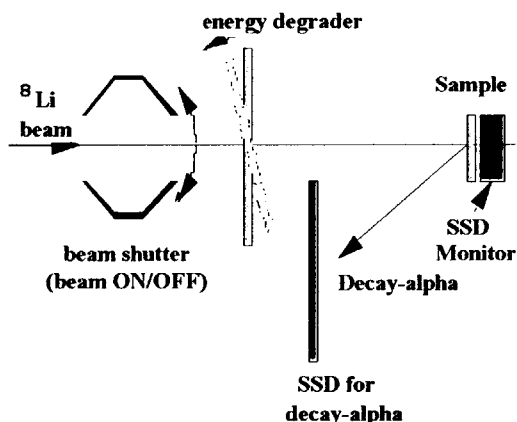


Fig.1 Experimental set-up

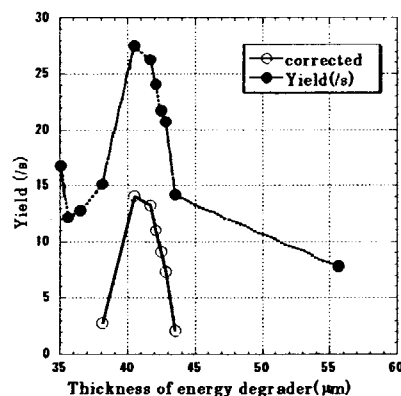


Fig.2 Decay alpha yields(●) from  $^8\text{Li}$  implanted in the sample (Al: 5 $\mu\text{m}$ ), obtained by subtracting the beta-yields of  $^8\text{Li}$  from the measured yields (○)

We have recently performed experiments to measure the diffusion constants of Li in samples such as  $\text{LiCoO}_2$  and  $\text{LiAl}$ , by using  $^8\text{Li}$  beam developed in this way. Though the data analysis is under progress, it should be worthwhile to mention the characteristics of our method: (1) It is a completely non-destructive method. (2) The temporal movement of Li in the sample could be observed in an order of ms, although significantly influenced by the experimental limitations like the energy width of the incident  $^8\text{Li}$  at the instant of implantation and the natural energy width of decay alphas.



### 6.3 A COMPARISON BETWEEN B- AND n-IRRADIATION ON $\text{MgB}_2$ BULK SAMPLES

S. OKAYASU, M. SATAKA, H. IKEDA<sup>1</sup> and R. YOSHIZAKI<sup>1</sup>

A comparison of irradiation effects between neutron and high-energy boron-ion (45MeV) irradiation on  $\text{MgB}_2$  bulk samples was investigated. The irradiation doses were  $8 \times 10^{17} \text{ n/cm}^2$  (thermal neutron) and  $2 \times 10^{15} \text{ ion/cm}^2$  (B ion), respectively. Although the amount of defects are almost the same of the order ( $10^{-2} \text{ dpa}$ ) for both two cases, irradiation effects on superconducting properties of the material are completely different.

Fig.1 shows the temperature dependence of susceptibilities before and after the irradiation. No change on the transition temperature  $T_c$  can be observed for the boron irradiated case, but a significant decrease for the neutron. This is because that leading process of defect formation is entirely different between the two cases. For the B-irradiation, nuclear collisions among bombarding ions and lattice atoms are dominant for the defect formation processes. Primary knock-on atoms flick out about 10 surrounding atoms and defect will be formed. In this situation, however, the flicked atoms remain near their original positions. The overall crystal structure may not be damaged severely.

For the neutron case, on the other hand, the defect formation is mainly originated in the most probable nucleus reaction  $^{10}\text{B}(n, \alpha)^7\text{Li}$ . A  $^{10}\text{B}$  atom captures a thermal neutron (cross section  $3.8 \times 10^{-25} \text{ m}^2$ ), and this process makes two high energetic particles, 1.7MeV- $\alpha$  and 1MeV- $^7\text{Li}$ , respectively. It is worth emphasizing that the B site is certainly affected with the reaction. As the result of this reaction, the boron atom in the crystal structure is replaced to a lithium atom, and band structure of  $\text{MgB}_2$  will be affected seriously. M. Eisterer et al. compared irradiation effects between fast and thermal neutron [1]. Due to a low nuclear reaction cross section between a fast neutron and a boron atom or a magnesium atom, defect formation process of the former is similar to B-irradiated case, i. e. nuclear collisions. No decrease of  $T_c$  is observed for the fast neutron irradiation. The transition temperature decreases for the thermal neutron case only. It is obvious that the nuclear reaction above mentioned plays an important role for the deterioration of superconductivity of this material.

---

<sup>1</sup>Univ. of Tsukuba, Tsukuba, Ibaraki 305-8577, Japan

Thus the following important conclusion is derived from the above that the B-originated fermi surfaces are important for the appearance of the superconductivity on  $\text{MgB}_2$ . This result is consistent with calculations for the band structure of this material representing superconducting gaps derived from boron band [2].

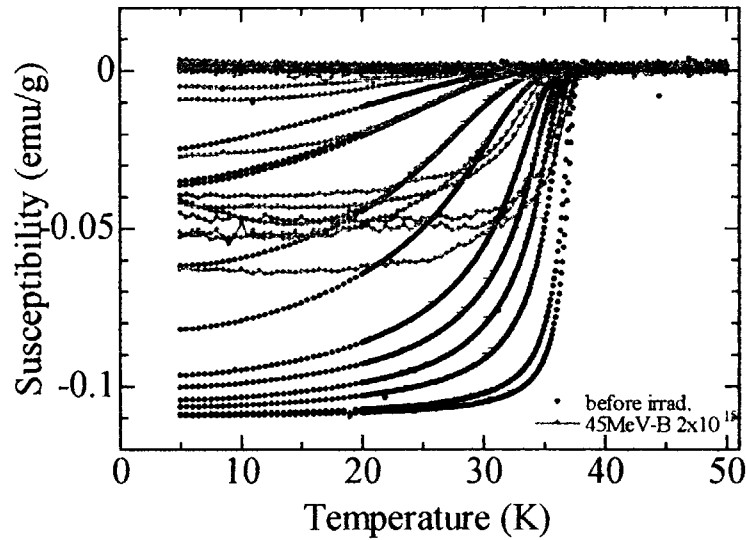


Fig.1 -a) Temperature dependence of susceptibilities at different external fields. Applied fields are (from light lower side to left upper) 5mT, 10mT, 30mT, 50mT, 70mT, 0.1T, 0.2T, 0.3T, 0.5T and 0.7T, respectively.

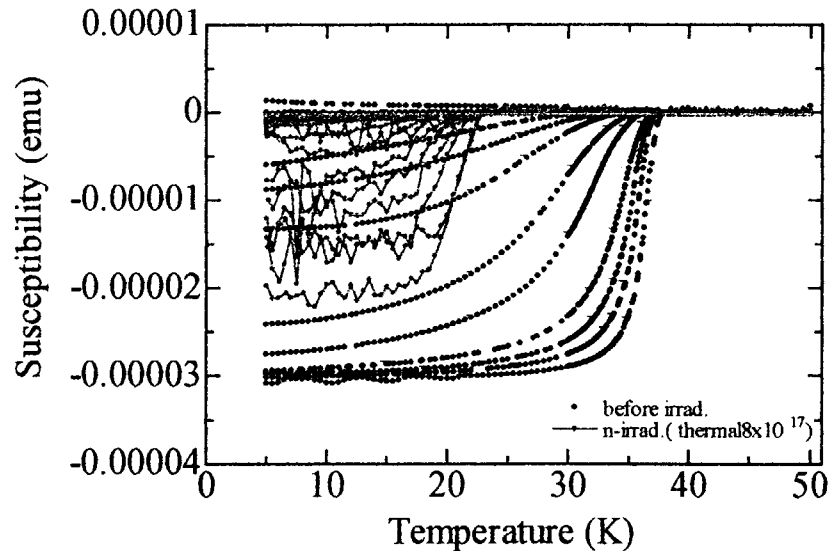


Fig.1 -b) Temperature dependence of susceptibilities at different external fields. Applied fields are (from light lower side to left upper) 5mT, 10mT, 30mT, 50mT, 70mT, 0.1T, 0.2T, 0.3T, 0.5T and 0.7T, respectively.

#### REFERENCES

- [1] M. Eisterer et al., Supercond. Sci. Technol. 15 (2002) L9
- [2] H.J. Choi et al., cond-mat/0111183

## 6.4 ELECTRONIC EXCITATION EFFECTS ON SECONDARY IONS EMISSION FROM CONDUCTIVE MATERIALS BOMBARDED BY HEAVY IONS

T. SEKIOKA<sup>1</sup>, M. TERASAWA<sup>1</sup> and M. SATAKA

The interaction between swift heavy ions and solids has been an active research area. One of the important problems has been whether electron excitations can induce the production of lattice defects in simple metals or not. In metals, it had been considered for a long time that on account of the great number of free conduction electrons and of their high mobility, inelastic interactions (electron excitation) could not cause any radiation damage or annealing process. In recent years, there have been extensive studies on the electronic excitation effect in metals irradiated by high-energy heavy ions (1-10 MeV/nucleon), where the electronic stopping power  $S_e = - (dE/dx)_e$  dominates the nuclear stopping power ( $S_n$ ) by a factor of about 100-1000 [1, 2]. We have studied the secondary ion mass spectrometry from thin conductive solid targets irradiated with heavy ion beams from the JAERI tandem accelerator in the energy region where the electronic stopping power is dominant.

An Au foil target of 2000 Å thickness evaporated on C-foils of 8.5 µg/cm<sup>2</sup> was irradiated with 240 MeV Au<sup>15+</sup> ion beam from the tandem accelerator. The secondary ions ejected from the front surface of the target were collected by a time of flight (TOF) mass spectrometer by applying an acceleration voltage of -500V and detected by an electron multiplier. Secondary electrons from the back side of the target were detected by another electron multiplier and this signal was used as the start signal of the TOF. Immediately before the measurement of the secondary Au<sup>+</sup> ion yield from the Au target, we cleaned the target by infrared radiation heating. We maintained the temperature of the target about 500°C for two hours in the vacuum of  $1.6 \times 10^{-6}$  Pa. Without cleaning, we could find no Au<sup>+</sup> secondary ion peak in the TOF spectrum because otherwise, the weak Au<sup>+</sup> peak is buried in the background mainly due to hydrocarbon contaminants.

Figure 1 shows the yield of the secondary ions of Au<sup>+</sup> from Au target normalized by the counts of secondary electron signal, together with the yield of the secondary ions of Cu<sup>+</sup> from Cu target as a function of the electronic stopping power. The values of the electronic stopping power are obtained from Ziegler's table by TRIM. The solid line in the figure represents the slope of  $(dE/dx)^2$  for the eye guide. The yield of the Au<sup>+</sup> secondary ions from Au target is very small as compared with the yield of the Cu<sup>+</sup> secondary ion from Cu target, though Cu and Au have the same electronic structure (<sup>2</sup>S<sub>1/2</sub>). The tendency of the target mass dependence of the secondary ion yield agrees with the experimental results on the damage creation in metals by high electronic excitation effect by swift heavy ion irradiation [1]: the comparison of two metals with similar electronic and atomic properties shows that the lower target atomic number corresponds higher sensitivity to damage creation by  $S_e$ .

To confirm these experimental results, it is important to study the secondary ions mass spectroscopy in a wide range of electronic stopping power with various combinations of projectiles and conductive targets.

<sup>1</sup> Faculty of Engineering, Himeji Institute of Technology

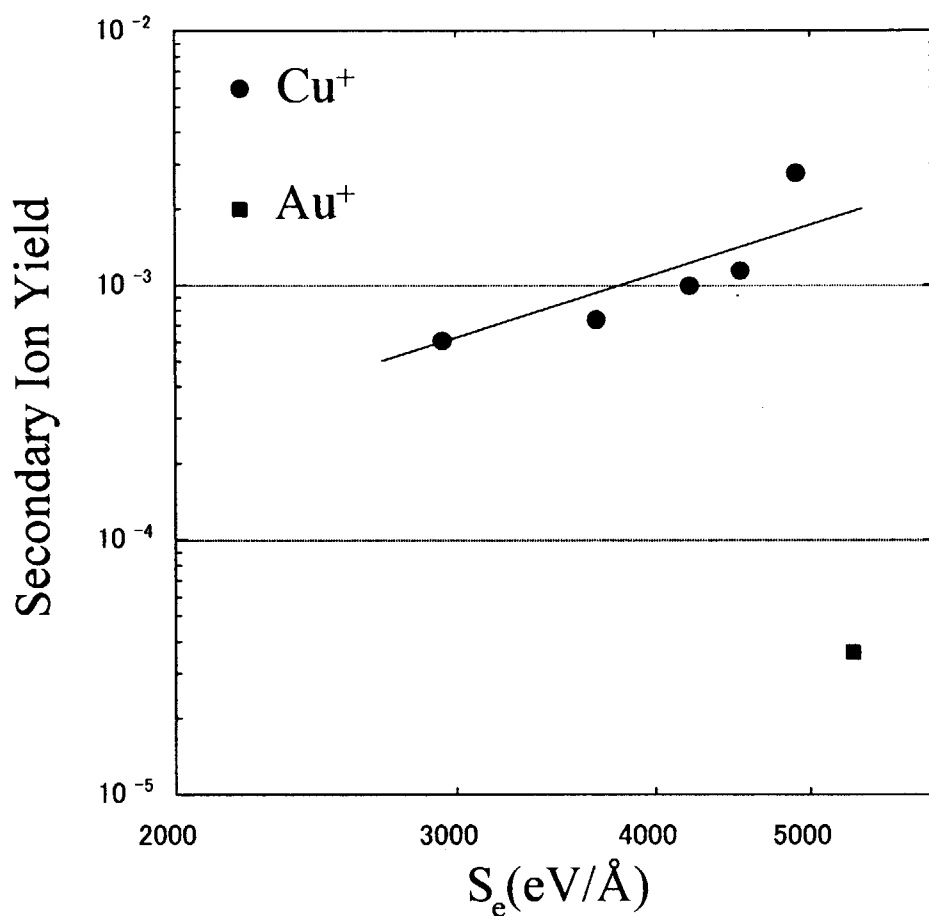


Fig. 1. The yield of the secondary ions of  $\text{Cu}^+$  and  $\text{Au}^+$  from Cu and Au target respectively normalized by the counts of secondary electrons, as a function of the electronic stopping power  $S_e$ . The values of the electronic stopping power are obtained by Ziegler's table (TRIM). The solid line shows the  $S_e^2$  dependence.

#### References

- [1] A. Dunlop and D. Lesueur, Radiat. Eff. Def. Solids 126 (1993) 123.
- [2] A. Iwase and T. Iwata, Nucl. Instr. and Meth. B 90 (1994) 322.

## **7. Radiation Effects in Materials**

This is a blank page.

## 7.1 ELECTRONIC SPUTTERING OF NON-CONDUCTIVE OXIDES BY HIGH ENERGY HEAVY IONS

N. MATSUNAMI<sup>1</sup>, M. SATAKA, A. IWASE and S. OKAYASU

We have measured sputtering yields of non-conductive oxides for systematic investigation of electronic excitation effects on atomic displacement by high energy heavy ions, applying carbon (C)-film collector method [1]. Samples of amorphous (a)-SiO<sub>2</sub>, SrCe<sub>0.95</sub>Yb<sub>0.05</sub>O<sub>3-δ</sub> (SCO), SrTiO<sub>3</sub> (STO), CeO<sub>2</sub>, Al<sub>2</sub>O<sub>3</sub>, MgO, TiO<sub>2</sub> and ZnO were irradiated by ions of 198 MeV Xe, 99 MeV Xe, 84 MeV I, 89 MeV Ni, 69 MeV Ni, 60 MeV Ar and 80 MeV S. Sputtered atoms collected in the C-films during ion irradiation (less than 10<sup>14</sup>/cm<sup>2</sup>) were analyzed by 1.8 MeV He Rutherford backscattering spectroscopy (RBS). The sputtering yield of each component was derived from the slope of the linear relationship between the amount of atoms in the C-film collector and the ion dose. Here, the collection efficiency of the C-films was calibrated as 0.35 (O), 0.48 (Si), 0.34 (Ti), 0.55 (Sr), 0.25 (Ce), 0.25 (Yb), 0.36 (Mg), 0.31 (Al) and 0.25 (Zn) [2, 3]. The validity of the C-film collector method is described in [4].

We find the followings. Sputtering yields of each component are roughly proportional to the composition (stoichiometric sputtering). The experimental sputtering yields  $Y$  (atoms per ion = sum of sputtering yield of each component) do not follow the nuclear stopping power and are larger by 30 - 2000 than the calculated values ( $Y_c$ ) based on the elastic collision cascades (Table 1). The sputtering yields do not follow the mean charge of ions after transmission through the C-film [3]. Hence the electronic excitation effects are dominant in the sputtering of the oxides (electronic sputtering). The electronic sputtering yields increase super-linearly with the electronic stopping power  $Se$  (Table 1). The exponent varies from 1.4 (Al<sub>2</sub>O<sub>3</sub>) to 4 (CeO<sub>2</sub>).

Figure 1 shows the band gap ( $E_g$ ) dependence of the representative sputtering yields taken at  $Se = 15$  keV/nm (medium  $Se$  in this study) [3]. It is suggested that the dotted line represents the maximum or upper limit of the electronic sputtering yields at the given electronic stopping power. The fourth-power dependence holds for  $Se = 5$ -20 keV/nm. It is assumed that the relaxation time from the highly excited states just after the ion impact to the low excited states is very short and thus the low excited states have the major contribution to the electronic sputtering. Then the available energy to the atomic displacement is due to the transition of electrons at low excited states to the ground states (recombination) and it is presumably determined by the band gap. Super-linear dependence of the electronic sputtering yields on the band gap suggests that the multiple excited states come into play.

The sputtering yields of Al<sub>2</sub>O<sub>3</sub>, MgO and CeO<sub>2</sub> are small, though their band gaps are large. Obviously, electron-phonon coupling is another factor for the electronic sputtering. No systematic trend is revealed by the mobility (a possible candidate of the electron-phonon coupling). This subject requires more detail investigation. Furthermore, the relation with the track formation and track volume are to be investigated.

<sup>1</sup> Dept. Energy Engineering and Science, School of Engineering, Nagoya University

The authors thank Prof. Y. Takai, Prof. H. Hosono, Prof. M. Ishigame and Dr. N. Sata, Prof. H. Iwahara and Dr. T. Shimura, Dr. A. Takahashi and Dr. T. Yamazaki for sample preparation of ZnO films, a-SiO<sub>2</sub>, SCO films, polycrystalline SCO, and CeO<sub>2</sub> films and SiO<sub>2</sub> films. They also thank Mr. T. Masuda for technical assistance of RBS and NRA.

## REFERENCES

- [1] N. Matsunami, M. Sataka, A. Iwase, Nucl. Instrum. Meth. B175-177(2001)56.
- [2] N. Matsunami, M. Sataka, A. Iwase, Nucl. Instrum. Meth. B(2002, in press).
- [3] N. Matsunami, M. Sataka, A. Iwase, S. Okayasu, Int. Conf. Swift Heavy Ions in Matter, Giardini Naxos, Taromina-Italy (2002, May 22-25).
- [4] N. Matsunami, M. Sataka, A. Iwase, T. Inami, M. Kobiyama, J. Nucl. Mater. 302(2002)206.

Table 1 Summary of electronic sputtering yields  $Y$ .  $B$  and  $n$  are the coefficients and exponent in the approximation:  $Y=(BSe)^n$ , with the representative yields at  $Se = 15\text{keV/nm}$ .  $Y$  values at  $Se \sim 15\text{ keV/nm}$  are compared with the calculated yields  $Y_c$ . Band gap  $E_g$  and a rough estimate of the electron mobility are given.  $2E3$  means  $2 \times 10^3$ .

Sample	$Y=(BSe)^n$ $n$	$B$	$Y(Se=15\text{ keV/nm})$	$Y/Y_c$	$E_g$ (eV)	mobility ( $\text{cm}^2\text{V}^{-1}\text{S}^{-1}$ )
a-SiO <sub>2</sub>	3	0.58	660	2E3	8.3	10
SCO	2.2	0.8	240	1.5E3	7.5	10
STO	3.6	0.14	14	200	3.4	10
CeO <sub>2</sub>	4	0.12	10	100	7.5	10
Al <sub>2</sub> O <sub>3</sub>	1.4	0.25	6.4	200	8.8	1
MgO	3	0.075	1.4	40	7.7	10
TiO <sub>2</sub>	2.5	0.18	12	350	3.2	0.1
ZnO	1.8	0.15	4.1	30	3.2	10

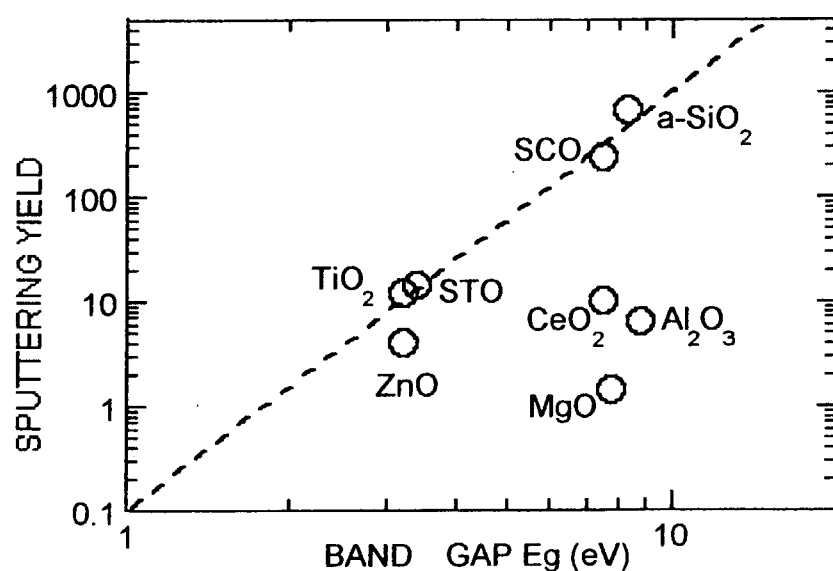


Fig. 1 Representative sputtering yields at electronic stopping power  $Se = 15\text{ keV/nm}$  as a function of the band gap  $E_g$ . The dotted line shows  $E_g^4$  dependence.



## 7.2 STRUCTURAL CHANGE BY HIGH-ENERGY IRRADIATION AND POST-ANNEALING IN $\text{EuBa}_2\text{Cu}_3\text{O}_y$

N. ISHIKAWA, H. SATO<sup>1</sup>, A. IWASE, Y. CHIMI, T. HASHIMOTO<sup>1</sup> and O. MICHIKAMI<sup>1</sup>

High-energy ion irradiation produces continuous linear defects along ion path by high-density electronic excitation in oxide superconductors. The production of the defects is often explained by the model that the electronic excitation causes effective temperature rise and thus creates defects [1,2]. If it is true, it is expected that the irradiation-induced damaged region mainly consists of deficiency of chain-site oxygen, which is movable at relatively low temperature ( $\sim 300^\circ\text{C}$ ), and it should cause the elongation of c-axis lattice parameter. When the chain-site oxygen is already removed by thermal treatment before irradiation, ion-irradiation would not cause the elongation of c-axis lattice parameter. Based on this recognition, we have compared the elongation of c-axis lattice parameter of sample that have the chain-site oxygen with that have no chain-site oxygen. The purpose of this study is to know whether the irradiation-induced damaged region is mainly composed of deficiency of chain-site oxygen or not.

The c-axis oriented films of  $\text{EuBa}_2\text{Cu}_3\text{O}_y$  (EBCO) oxide superconductor were prepared by dc-magnetron sputtering. The thickness of films was about 300 nm. The as-sputtered films are expected to have oxygen content of  $y \approx 7$ , since the superconducting transition temperature is around 90K. The samples with oxygen content of  $y \approx 6$  were prepared by thermal annealing. The annealed samples are expected to have oxygen content of  $y \approx 6$ , since their c-axis lattice parameter was larger by 1.2% than that of the sample with oxygen content of  $y \approx 7$  [3]. The samples were irradiated with 200 MeV Au ions from the direction parallel to the c-axis at room temperature. The irradiations were performed by using the tandem accelerator at JAERI-Tokai. We measured the X-ray( $\text{Cu K}\alpha$ ) diffraction pattern before and after the irradiations for estimating the c-axis lattice parameter. We subsequently performed the recovery treatment at an elevated temperature ( $550^\circ\text{C}$ ) following the procedure shown in Ref.[4]. We measured c-axis lattice parameter before and after the recovery treatment.

Figure 1 shows that the slope of elongation of c-axis lattice parameter for the sample with oxygen content of  $y \approx 6$  is almost the same as for the sample with oxygen content of  $y \approx 7$ . Figure 2 shows the c-axis lattice parameter after the recovery treatment. The c-axis lattice parameter of all samples is recovered to the same level as the sample with oxygen content of  $y \approx 7$ .

The above experimental results can be explained by the following consistent picture. The ion-irradiation produces the softly damaged region surrounding the thermally stable damaged region. The complete recovery of c-axis lattice parameter by the thermal treatment at  $550^\circ\text{C}$  shows that the softly damaged region, that is thermally unstable, is the origin of the irradiation-induced elongation of c-axis lattice parameter.

Then, what are the components of the softly damaged region? We expected that the softly damaged region consisted mainly of simple deficiencies of chain-site oxygen, since the

---

<sup>1</sup> Iwate University

chain-site oxygen is lighter and its bonding is weaker than the other elements. But, the present result shows that the irradiation effect of sample for  $y \approx 7$  and  $y \approx 6$  is almost same, although the sample for  $y \approx 6$  do not have chain-site oxygen before irradiation. Therefore, contrary to the above expectation, the softly damaged region is composed mainly of the defects of the elements other than the chain-site oxygen. Since the c-axis lattice parameter of all samples is recovered to the same level as the sample with oxygen content of  $y \approx 7$ , the recovery treatment is very effective for the control of softly damaged region.

## References

- [1] M. Toulemonde, J. M. Costantini, Ch. Dufour, A. Meftah, E. Paumier, and F. Studer, Nucl. Instr. Meth. **B116** (1996) 37.
- [2] ] M. Toulemonde, Ch. Dufour, Z. Wang, and E. Paumier, Nucl. Instr. Meth. **B112** (1996) 26.
- [3] W. R. McKinnon, M. L. Post, L. S. Selwyn, G. Pleizier, J. M. Tarascon, P. Barboux, L. H. Greene, and G. W. Hull, Phys. Rev. **B 38** (1988) 6543.
- [4] O. Michikami, H. Wakana, and K. Atsumi, Jpn. J. Appl. Phys. **38** (1999) 6674.

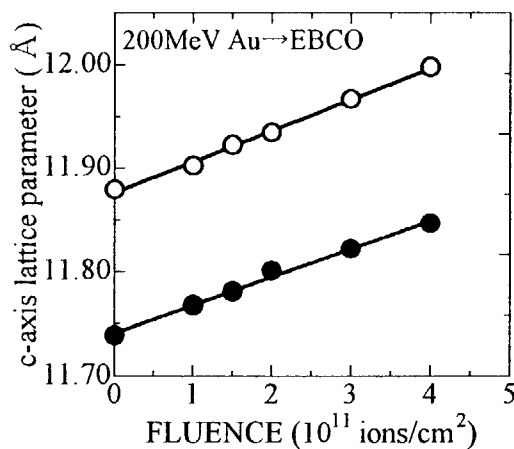


Fig. 1. Fluence dependence of c-axis lattice parameter for EBCO films irradiated with 200 MeV Au ion. Closed circles (●) are for the sample with oxygen content of  $y \approx 7$ , and open circles (○) are for the sample with oxygen content of  $y \approx 6$ .

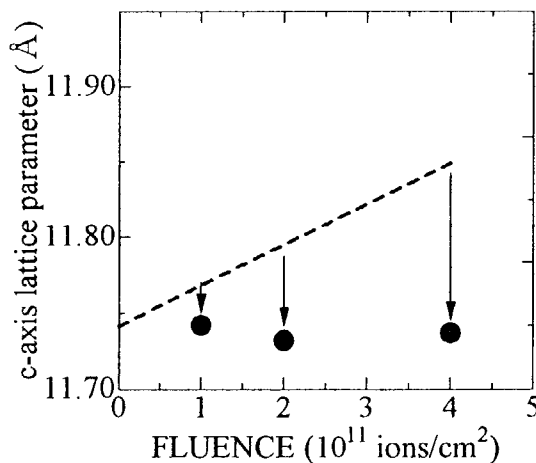


Fig. 2. Fluence dependence of c-axis lattice parameter after recovery treatment. Closed circles (●) are for the sample with oxygen content of  $y \approx 7$ . The data before recovery treatment are shown as dotted lines.

### 7.3 STRUCTURE OF BEAM TRACKS INDUCED BY SWIFT HEAVY ION IN Bi-2212

M. SASASE<sup>1</sup>, S. OKAYASU, H. YAMAMOTO, H. KURATA<sup>2</sup> and K. HOJOU

For high- $T_c$  superconductors, the columnar defects act as strong pinning centers of magnetic flux lines and enhance the critical current density ( $J_c$ ) [1, 2]. Previous results show that the diameter of the columnar defects affect the  $J_c$  [3]. If one can control the diameter of the columnar defect by changing the condition of ion irradiation, it is easy to obtain the optimum results of  $J_c$ . The understanding of the governing factors for the columnar defect formation is therefore important not only for basic investigations. It has been considered that the electronic stopping power ( $S_e$ ) mainly affects the defects formation through the swift heavy ion irradiation. However, our recent results suggest that the "ion-velocity" cannot be negligible for these phenomena [4]. These results suggest that parameters of ion irradiation other than  $S_e$  affect the formation. In the present study, the columnar defect diameters have been measured from the high resolution transmission electron micrographs (HRTEM) for various conditions of ion irradiation. From the obtained results, "ion-velocity" dependence of the defect diameters and their distributions have been discussed.

Specimens used in this study were  $\text{Bi}_2\text{Sr}_2\text{CaCu}_2\text{O}_8$  (Bi-2212) single crystals ( $T_c=90$  K). The specimens were irradiated with the following ions at room temperature; 60 and 180 MeV  $\text{Au}^+$  ions, 90 and 600 MeV  $\text{I}^+$ , 180 MeV  $\text{Ni}^+$  and 190 MeV  $\text{Br}^+$ , respectively, with a fluence of  $2.0 \times 10^{10}$  ions/cm<sup>2</sup> using Tandem accelerator at JAERI. The charge number was from 8 to 29. The range and stopping power ( $S_e$  and  $S_p$ ) of these ions in the Bi-2212 were calculated by using the TRIM codes [5]. The samples were peeled off in thin sheets having 50 nm thickness from bulk samples, before it had been damaged by the subsequent passage of high energy ions. Irradiation defects were observed by using TEM (JEOL JEM-2000F type) [6].

On the basis of observed results, the most probable diameter of the columnar defects  $R$  and standard deviation of the distribution  $\Delta R$  can be obtained as  $R \pm \Delta R = 9 \pm 4.1$  nm for 60 MeV  $\text{Au}^+$  and  $4 \pm 2.5$  nm for 180 MeV  $\text{Ni}^{11+}$ ,  $12 \pm 3.2$  nm for 180 MeV  $\text{Au}^{12+}$  and  $6.5 \pm 2.1$  nm for 600 MeV  $\text{I}^{29+}$ , respectively. These values for each ion energy were listed in Table 1. The obtained diameters  $R$  are plotted as a function of  $S_e$  in Fig. 1 with other data. The columnar defect formation has often been discussed in terms of  $S_e$  value, since such defects are observed only for high-energy heavy ion irradiation. On the other hand, ion-velocity dependence has also been observed in the defect formation under the fixed  $S_e$  conditions in recent studies [2~3, 7]. Figure 1 show that the observed diameter is quite different even at the same  $S_e$ . These results suggest that  $S_e$  is not only key parameter for columnar defect formation. Our previous results [4] show that the defect formation process drastically changes at the velocity around  $2 \times 10^9$  cm/sec. Even though the previous results have some ambiguities on the

<sup>1</sup> The Wakasa Wan Energy Research Center

<sup>2</sup> Kyoto University

physical meaning of this change, the obtained plots in Fig. 1 can be divided into two groups from the velocities. These are lower velocity ( $<2 \times 10^9$  cm/sec) and higher velocity ( $>2 \times 10^9$  cm/sec) groups shown in white and solid circles, respectively. These results reveal that irradiated ions which have higher ion-velocity produce smaller columnar defects under the fixed  $S_e$  conditions. When the ion-velocity increases, it is known that the component of the high-energy secondary electrons becomes larger even at the same  $S_e$  [8]. Since these high-energy secondary electrons go far from the ion path within the time scale of defect formation [9], these electrons have no contribution for the localized damage area along the ion path. The component of electrons which have the "effective" energy for the defect formation decreases with the increase of ion-velocity. The diameter of the columnar defects becomes therefore smaller for higher ion-velocities.

There is another ion-velocity effect is observed through the present experiments. Figure 2 shows the dependence of the standard deviations of the distribution  $\Delta R$  for the columnar defect diameters  $R$  on the ion-velocity. It is clearly shown that the  $\Delta R$  increases with the decrease of ion-velocity. Izui shows that effect of the nuclear collision cannot be neglected even for the high energy heavy ion irradiation in the range of several MeV or higher [10]. When nuclear collision takes place, collision cascade is formed near the path of irradiated ion as a branch of columnar defect. The formation of collision cascade will become a cause of  $\Delta R$  increase. In Izui's study, mean free path of nuclear collision for irradiated ions have been calculated as a function of ion energy and transferred energy through the collision. We have therefore paid attention to the effect of nuclear collisions and applied the calculation for the mean free path of nuclear collisions to the present experimental conditions. The possibility of collision cascade formation through the high energy ion irradiation has been estimated. The obtained results can be interpreted as the number of collision in the 50 nm film. For the lower velocity group, it is expected collision takes place several times. On the other hand, possibility of the collision is very low for the higher one, since the mean free path is quite larger than the film thickness. These calculations show that possibility of the nuclear collision increase with the decrease of ion-velocity even for the several MeV ion irradiation. From the cross-sectional TEM observation of the ion irradiated specimens, "spherical" collision cascade is observed along the ion path with the energy dissipation of irradiated ions [11]. On the other hand, the ion path shows an almost continuous column with a nearly uniform diameter for high velocity region. These results are consistent with the observed relationship between  $\Delta R$  and ion-velocity appeared in Fig. 2.

## References

- [1] J.R. Thompson, Y.R. Sun, H.R. Kerchner, D.K. Christen, B.C. Sales, B.C. Chakoumakos, A.D. Marwick, L. Civale and J.O. Thomson, *Appl. Phys. Lett.*, **60** (1992) 2306.
- [2] W. Jiang, N.-C. Yeh, S. Reed, U. Kriplani, D.A. Bean, M. Konczykowski, T.A. Tombrello and F. Holtzberg, *Phys. Rev. Lett.*, **72** (1994) 550.
- [3] L. Civale, A.D. Marwick, T.K. Worthington, M.A. Kirk, J.R. Thompson, L. Krusin-Elbaum, Y. Sun, J.R. Clem and F. Holtzberg, *Phys. Rev. Lett.*, **67** (1991) 648.
- [4] M. Sasase, S. Okayasu, H. Kurata and K. Hojou, *Physica C*, **357-360** (2001) 497.
- [5] J.F. Ziegler: *Handbook of Stopping Cross Section for Energetic Ions in All Elements*

(Pergamon, New York, 1980)

- [6] M. Sasase, S. Okayasu, H. Kurata, K. Hojou, J. Electron Microscopy, **51** (2002) S235.
- [7] N. Ishikawa, Y. Chimi, N. Kuroda, A. Iwase and T. Kambara, Physica Scripta, **T80** (1999) 559.
- [8] D.X. Huang, Y. Sasaki and Y. Ikuhara, Phys. Rev. **B59** (1999) 3862.
- [9] K. Izui, J. Phys. Soc. Jpn., **20** (1965) 915.
- [10] K. Izui, J. Phys. Soc. Jpn., **22** (1967) 85.
- [11] D.X. Huang, Y. Sasaki, S. Okayasu, T. Aruga, and Y. Ikuhara, Phys. Rev. **B57** (1998) 13907.

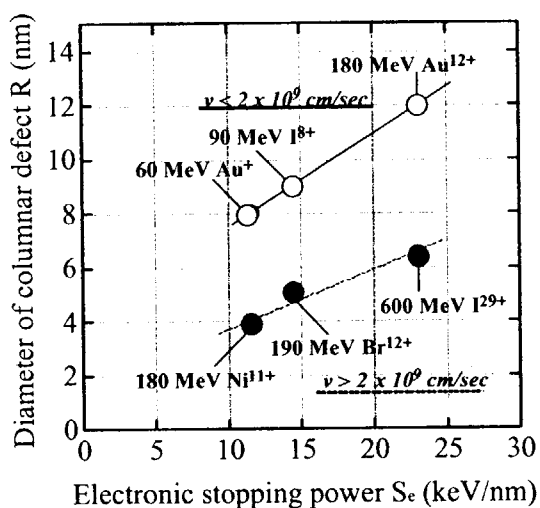


Fig. 1. Dependence of the columnar defect diameter  $R$  on the  $S_e$  in the Bi-2212.

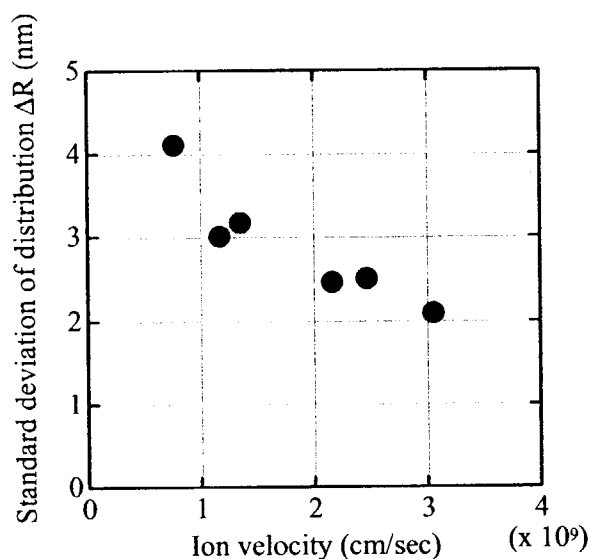


Fig. 2. Dependence of the standard deviations of the distribution  $\Delta R$  for the columnar defect diameters  $R$  on the ion-velocities.

Table 1 Irradiation parameter and measured data by TEM observation.

Ion	Energy (MeV)	velocity ( $\times 10^9$ cm/sec)	$S_e$ (keV/nm)	$R \pm \Delta R$ (nm)
Au <sup>+</sup>	60	0.76629	11.5	$9.0 \pm 4.1$
Ni <sup>11+</sup>	180	2.43242	11.5	$4.0 \pm 2.5$
I <sup>8+</sup>	90	1.16934	14.5	$9.0 \pm 3.0$
Br <sup>12+</sup>	190	2.14203	14.5	$5.0 \pm 2.5$
Au <sup>12+</sup>	180	1.32776	23.0	$12.0 \pm 3.2$
I <sup>29+</sup>	600	3.0192	23.0	$6.5 \pm 2.1$

## 7.4 DEFECT PRODUCTION INDUCED BY HIGH-DENSITY ELECTRONIC EXCITATION IN IRON

Y. CHIMI, A. IWASE, N. ISHIKAWA, and T. KAMBARA<sup>1</sup>

The contribution of high-density electronic excitation to defect production in iron has been studied [1]. Iron thin films were prepared on  $\alpha$ - $\text{Al}_2\text{O}_3$  single crystal substrates by rf magnetron sputtering. The film thickness was  $\sim 200\text{nm}$ . The specimens were irradiated at  $\sim 77\text{K}$  with the following energetic particles;  $2.0\text{MeV}$  electrons from a  $3\text{MV}$  single-ended accelerator at TIARA, JAERI-Takasaki,  $0.5$ - $2.0\text{MeV}$   $^1\text{H}$ - $^{40}\text{Ar}$  ions from a  $2\text{MV}$  Van de Graaff accelerator,  $84$ - $200\text{MeV}$   $^{12}\text{C}$ - $^{197}\text{Au}$  ions from a  $20\text{MV}$  tandem accelerator both at JAERI-Tokai, and  $3.1$ - $3.8\text{GeV}$   $^{136}\text{Xe}$ - $^{209}\text{Bi}$  ions from a ring cyclotron at RIKEN. The electrical resistivity of the specimen was measured in situ during each irradiation at appropriate fluence intervals. In metals, the increase in resistivity,  $\Delta\rho$ , is generally proportional to the concentration of irradiation-produced defects,  $C$ ;  $\Delta\rho = \rho_F C$ , where  $\rho_F$  is the resistivity of unit concentration of Frenkel pairs. In the present study, we adopted  $\rho_F = 1250\mu\Omega\text{cm}$  [2].

From an analysis of the fluence dependence of the defect concentration, we can obtain the information on kinetics of the defect production and annihilation by using a conventional rate equation [3]. In the present report, we deal with only the defect production. The defect annihilation have been described elsewhere [4]. According to careful consideration of the contribution of elastic collision and electronic excitation to the defect production and annihilation, the defect production cross-section through electronic excitation,  $\sigma_d^{\text{electronic}}$ , can be extracted in high- $S_e$  (electronic stopping power) region ( $S_e > \sim 20\text{MeV}/(\text{mg}/\text{cm}^2)$ ). The detailed procedure for the extraction will be published elsewhere. Fig. 1 shows  $\sigma_d^{\text{electronic}}$  for the irradiation in high- $S_e$  region plotted against  $S_e$ . Previous results by Dunlop et al. [5] are also shown in the figure. As can be seen in Fig. 1,  $\sigma_d^{\text{electronic}}$  for  $\sim 100\text{MeV}$  ion irradiations is larger than that for  $\text{GeV}$  ion irradiations even at the same  $S_e$  value. Since the ion velocity of  $\sim 100\text{MeV}$  ion is much lower than that of  $\text{GeV}$  ion, the difference in  $\sigma_d^{\text{electronic}}$  even at the same  $S_e$  is one of so-called 'the velocity effects'. The velocity effect was observed more clearly in the present systematical irradiations than in the previous irradiations with only  $\text{GeV}$  ions [5]. Thus,  $\sigma_d^{\text{electronic}}$  is not well correlated with  $S_e$ .

For describing the defect production induced by electronic excitation, we have proposed the primary ionization rate [6-8] as a scaling parameter;

$$\frac{dJ}{dx} = \frac{Z^*{}^2 \alpha}{I_0 v^2} \ln \left( \frac{2m_e v^2}{0.048 I_0} \right), \quad (1)$$

where  $Z^*$  is the ion effective charge,  $\alpha$  a constant depending on the target material,  $I_0$  the ionization potential of the most loosely bound electron,  $v$  the ion velocity, and  $m_e$  the electron mass. The ion effective charge proposed by Pierce and Blann [9] is used for the present data. We adopt  $I_0 = 7.87\text{eV}$  of the first ionization potential for an iron atom. Fig. 2 shows  $\sigma_d^{\text{electronic}}$  in high- $S_e$  region as a function of  $dJ/dx$ . An excellent correlation of  $\sigma_d^{\text{electronic}} \propto (dJ/dx)^3$  can be found in the figure. The  $dJ/dx$  means the number of iron atoms ionized by an incident ion per unit path

<sup>1</sup>Atomic Physics Laboratory, The Institute of Physical and Chemical Research (RIKEN)

length. Since the phenomenon can be well described not by deposited energy but by the number of primary ionization, it appears that the Coulomb repulsion between adjacent ionized iron atoms induces the atomic displacements in iron (what is called the Coulomb explosion mechanism). We can obtain an index of interpretation of the present result referring to the electronic sputtering yield in inorganic insulators. Applying the Coulomb explosion model and a shock wave mechanism for cluster emission [10], the sputtering yield may be proportional to  $(dJ/dx)^3$  [11]. We need further consideration for applying these models to metallic crystal targets.

## References

- [1] Y. Chimi, A. Iwase, N. Ishikawa, T. Kambara, Nucl. Instrum. Methods **B 193** (2002) 248.
- [2] P.G. Lucasson, R.M. Walker, Phys. Rev. **127** (1962) 485.
- [3] H.J. Wollenberger, in: A. Seeger, D. Schumacher, W. Schilling, J. Diehl (Eds.), Vacancies and Interstitials in Metals, North-Holland, Amsterdam, 1970, p. 215.
- [4] Y. Chimi, A. Iwase, N. Ishikawa, N. Kuroda, T. Kambara, Nucl. Instrum. Methods **B 164-165** (2000) 408.
- [5] A. Dunlop, D. Lesueur, P. Legrand, H. Dammak, J. Dural, Nucl. Instrum. Methods **B 90** (1994) 330.
- [6] R.L. Fleischer, P.B. Price, R.M. Walker, E.L. Hubbard, Phys. Rev. **156** (1967) 353.
- [7] H. Bethe, Ann. Phys. **5** (1930) 325.
- [8] N. Ishikawa, A. Iwase, Y. Chimi, O. Michikami, H. Wakana, T. Kambara, J. Phys. Soc. Jpn. **69** (2000) 3563.
- [9] T.E. Pierce, M. Blann, Phys. Rev. **173** (1968) 390.
- [10] I.S. Bitensky, E.S. Parilis, Nucl. Instrum. Methods **B 21** (1987) 26.
- [11] R.E. Johnson, J. Schou, Kgl. Danske Vidensk. Selsk. mat.-fys. Medd. **43** (1993) 403.

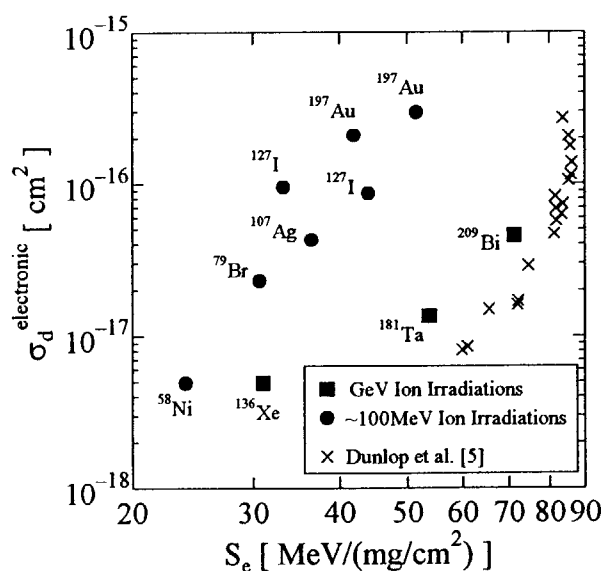


Fig. 1. Defect production cross-section through electronic excitation,  $\sigma_d^{\text{electronic}}$ , plotted against electronic stopping power,  $S_e$ , for the irradiation in high- $S_e$  region. Previous results by Dunlop et al. [5] are also shown.

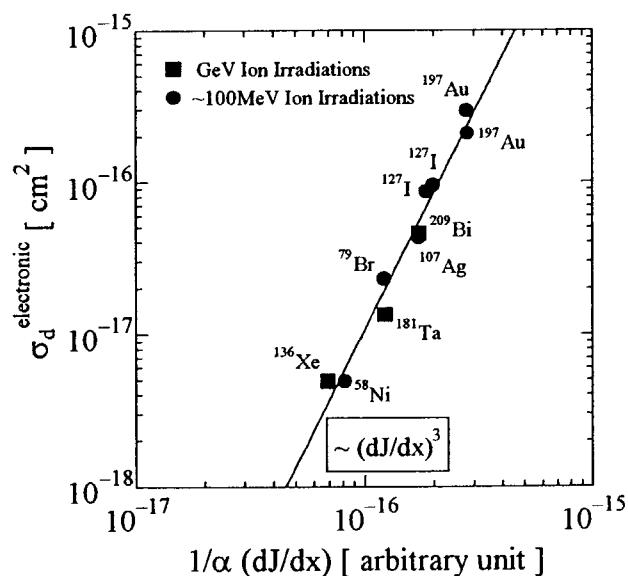


Fig. 2. Defect production cross-section through electronic excitation,  $\sigma_d^{\text{electronic}}$ , as a function of primary ionization rate,  $dJ/dx$ , for the irradiation in high- $S_e$  region.

## 7.5 ANOMALOUS SHIFT OF CURIE TEMPERATURE IN IRON-NICKEL INVAR ALLOYS BY HIGH-ENERGY HEAVY ION IRRADIATION

A. IWASE, Y. HAMATANI, Y. MUKUMOTO<sup>1</sup>, N. ISHIKAWA, Y. CHIMI and F. ONO<sup>1</sup>

Fe-Ni Invar alloys with Ni composition of ~ 32% were irradiated with 100-210 MeV Xe ions at room temperature by using the JAERI-tandem accelerator. Before and after irradiation, AC susceptibility was measured using a specially designed system for rapid measurements. Due to the existence of the demagnetizing factor, the susceptibility has a finite value below  $T_c$ , and it becomes zero above  $T_c$ . From this measurement, we determined the change in  $T_c$  by the irradiation. As the projected range of the Xe ions was smaller than the specimen thickness, only the surface region of the specimen was affected by the irradiation.

Experimental result for 210 MeV Xe irradiation is shown in Fig. 1. The figure clearly shows that the Curie temperature,  $T_c$ , for the irradiated area increases by increasing the ion fluence. The figure also shows that the value of  $T_c$  at the unirradiated region is not changed even after irradiation. The increase in  $T_c$  appears even at a low ion fluence ( $2 \times 10^{12}/\text{cm}^2$ ), implying that it is attributed to ion-induced high-density electronic excitation along the beam path. It is well known that  $T_c$  of such Fe-Ni Invar alloys strongly depends on the Ni concentration and the external pressure. With increasing the Ni concentration from ~30%,  $T_c$  increases, and with decreasing the lattice parameter by the pressure,  $T_c$  decreases. Therefore, the increase in  $T_c$  by high-energy ion irradiation can be explained as originating from the lattice expansion and/or the composition change, which are induced by the high-density electronic excitation.

This experiment shows that high energy heavy ion irradiation can be used as a method for the local modification of magnetic properties, which has never been realized by conventional metallurgical treatments.

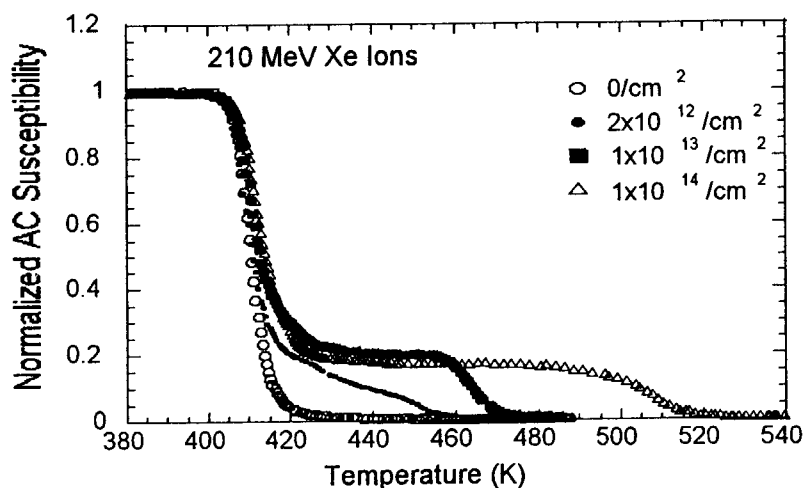


Fig. 1 AC susceptibility of FeNi invar alloy as a function of temperature. Values of AC susceptibility are normalized to unity at room temperature.

<sup>1</sup> Okayama University



## 7.6 SURFACE DAMAGES IN MgO IRRADIATED WITH ENERGETIC IODINE IONS

T. ARUGA, Y. KATANO, T. OHMICHII, S. OKAYASU and Y. KAZUMATA

In the studies investigating changes brought about in the near surface region of materials, amorphization behaviors of ceramic materials irradiated with highly energetic heavy ions have recently been paid a lot of attentions, especially to understand amorphization mechanisms due to high energy electronic excitations. We have reported that a polycrystalline aluminum oxide ( $\alpha$ - $\text{Al}_2\text{O}_3$ ) has been transformed into an amorphous phase under the 85 MeV iodine ion irradiation with a rate of an electronic deposition above 4-5 keV/nm and an accumulated dose above 1.5-2 GGy [1]. It is of a physical and practical interest to elucidate the relation between a bonding nature of oxides and the tendency for these oxides to be amorphized under swift ion irradiation.

In the present study, we examined radiation responses due to the high energy electronic excitations for oxide ceramics of MgO through a cross-sectional transmission electron microscopy (XTEM) and a X-ray diffractometry (XRD). Samples of polycrystalline sintered ceramics of MgO were irradiated at the ambient temperature with 85 MeV  $\text{I}^{7+}$  iodine ions to doses up to  $1.2 \times 10^{19}/\text{m}^2$ . X-ray diffraction patterns were measured using a Cu  $K\alpha$  radiation for MgO samples irradiated to each dose to  $1.2 \times 10^{19}/\text{m}^2$ , and the sample before irradiation as well. To avoid diffraction from the unirradiated portion of the samples, they were masked with a gold foil of 5  $\mu\text{m}$  thickness having an open square window with a side length of 2 mm. The intensities of diffraction peaks from the samples were normalized by the peak intensities of a specified diffraction from gold. Depth profiles of the energy deposition cross sections for 85MeV I-ions incident on MgO, along with stopped ion concentrations, from the calculation using the extended E-DEP-1 code[2], shows that the average projected range for the ions is 8.7  $\mu\text{m}$  and the stopped ion concentrations peak there to be about 130 atomic ppm, for the irradiation to  $1.2 \times 10^{19}/\text{m}^2$ . The dpa values peak to be 1 dpa around a depth of 8.5  $\mu\text{m}$ . Electronic stopping power is 17 keV/nm at the incident surface and decreases to 3-4 keV/nm at depths around 8  $\mu\text{m}$ .

No amorphization is observed for the MgO sample irradiated to  $1.2 \times 10^{19}/\text{m}^2$ , through XTEM. The fact demonstrates that a higher ionicity of chemical bonding and its more isotropic nature, as compared with those of  $\text{Al}_2\text{O}_3$  and  $\text{MgAl}_2\text{O}_4$ , instantly recover the lattice disorders produced by electronic energy depositions. Instead, XRD reveals an enhancement for the diffraction peak for (200), (400) reflections, as compared with those before irradiation. Figures 1 compare the X-ray diffraction patterns between 25 and 50 degrees of diffraction angles,  $2\theta$ , for the MgO sample before and after the irradiations to  $0.12 \times 10^{19}/\text{m}^2$  and  $1.2 \times 10^{19}/\text{m}^2$ , which are designated below as IR-1 and IR-4. In the figures, there appear two diffraction peaks from (111) and (200) reflections, which are ascribed to a fcc structure of MgO, within the limited range of diffraction angles shown. The peak height of (111) decreases slightly with an increase in the dose, while that of (200) increases noticeably. Large peaks designated with A and B are due to diffractions from the Au window foil and are used in the normalization for the peak intensities from the MgO samples. Figure 2 shows the ratios of peak intensities for the irradiated samples to those before irradiation as a function of  $2\theta$ , corresponding to reflections from (111) to (400), taking the dose as a parameter. If the present ion irradiation does not give any effect to MgO samples, as observed in the XTEM, the ratios should be one. Peak intensities of diffraction from (200) and (400) planes for IR-4 are observed to increase considerably, as compared with those before irradiation, as shown in Fig. 1 of the XRD patterns for the (200) peak. This suggests that in grains, which are randomly oriented in the polycrystalline MgO before irradiation, there seems to appear a volume of crystallites having a tendency, due to the irradiation, to be aligned (100) perpendicular to the incident beam direction. That is, an atomistic rearrangement may occur along ion's paths to form a new surface with the lowest surface energy or {100} planes from the ion-incident surface.

### References

- [1] T. Aruga, Y. Katano, T. Ohmichi, S. Okayasu, and Y. Kazumata, Nucl. Instr. Methods. Phys. Res. B 166-167 (2000) 913.

[2] T. Aruga, K. Nakata, and S. Takamura, Nucl. Instr. Methods Phys. Res. B 33 (1988) 748.

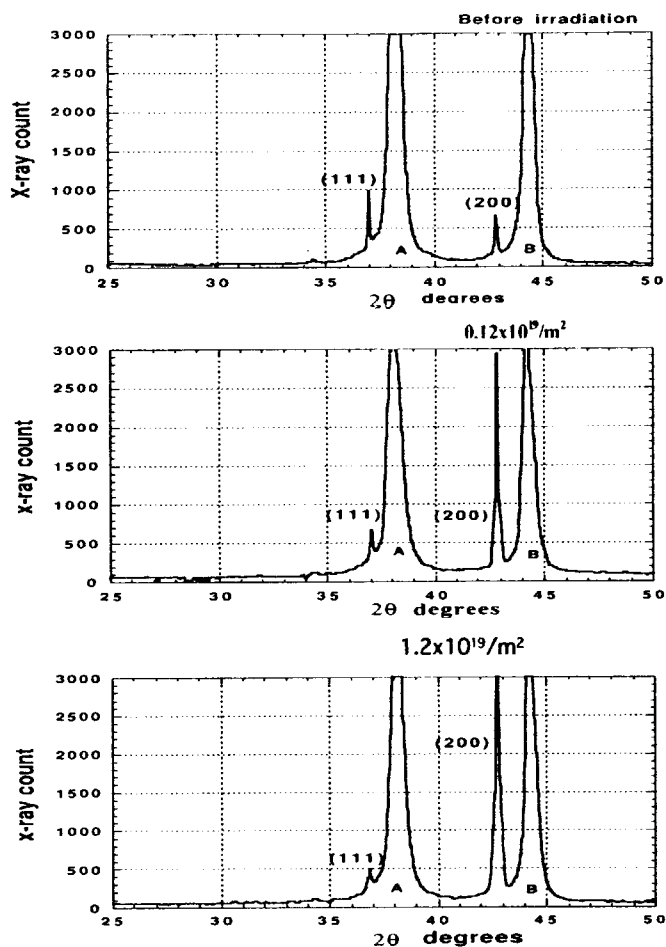


Fig. 1. XRD patterns of MgO before irradiation (top) are compared for diffraction angles  $2\theta$  of 25-55 degrees with those from the samples irradiated with 85 MeV iodine ions to each dose shown (middle, bottom).

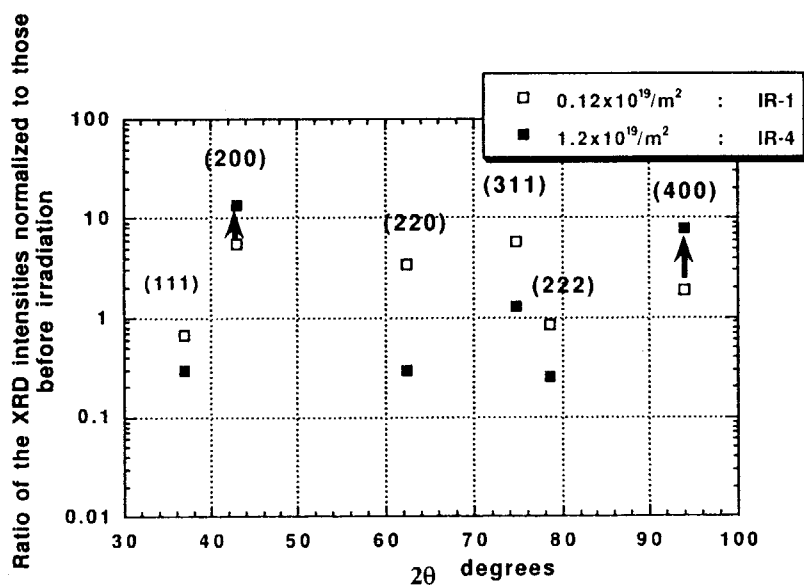


Fig. 2. Changes in X-ray diffraction peak intensities with an increase in the ion dose for MgO irradiated with iodine ions are shown as ratios to each peak intensity before irradiation. Arrows are used to specify the increased diffraction intensities.

## 7.7 STUDY OF RADIATION DAMAGE MECHANISMS IN STEELS USING HIGH ENERGY ION IRRADIATION

S. ISHINO<sup>1</sup>, A. IWASE, Y. CHIMI, N. ISHIKAWA, BAGIYONO,  
M. SUZUKI, T. TOBITA, K. AIZAWA

Mechanism of radiation embrittlement in pressure vessel steels is one of the most important subjects for plant life extension of a light water reactor. Role of point defects in copper clustering in Fe-Cu model alloys has been studied by electrical resistivity measurements *in-situ* under ion irradiation.

The specimens were prepared from two kinds of Fe-Cu alloys, the Cu concentrations of which were 0.02 and 0.6 wt.%, respectively. The final state of heat treatment was 850°C×10 minutes followed by quenching. The specimens were irradiated with 100MeV carbon ions at 300K using JAERI-Tokai tandem accelerator. The thickness of the specimen was about 30μm, which was much smaller than the range of 100MeV carbon ions. Irradiation dose (dpa) was calculated by using the measured ion fluence and the TRIM code [1]. The electrical resistivity was measured *in-situ* by a conventional four-probe method as a function of irradiation dose.

The results were compared with 2MeV electron irradiation data obtained using a single-end electron accelerator at TIARA. Fig.1 shows the dose dependence of resistivity change showing a comparison of ion irradiation data with electron irradiation data. The dose rates of both irradiations are almost the same, being  $(1.6 - 2) \times 10^{-9}$  dpa/s. Three things are immediately apparent from the figure: 1) The resistivity decreases with dose contrary to the irradiation at 7K [2]. This is due to radiation enhanced copper clustering. 2) The rate of change of resistivity is larger for electron irradiation than for ion irradiations. This seems to reflect the fact that freely migrating defect (FMD) fraction is less for ion irradiations than for electron irradiations. 3) There is an initial anomalous behavior in the resistivity change. The reason for this phenomenon has not been clarified yet. There might be a transient effect associated with nucleation process, often observed in an initial stage of age hardening. Another possibility is radiation-induced liberation of weakly trapped impurities as carbon or oxygen. The initial anomaly is removed by small amount of pre-irradiation. This is shown in Fig.2 for 100MeV carbon ion irradiation.

The effect of dose rate is a current subject of great concern for actual pressure vessel steels. Fig. 3 shows a comparison between high dose rate ( $\sim 10^{-8}$  dpa/s) and low dose rate ( $\sim 10^{-9}$  dpa/s) data for Fe-0.6 wt.%Cu alloy. Similar data have been obtained for electron irradiations. It is clearly observed that low dose rate gives higher rate of resistivity change.

Important concluding remarks are as follows: 1) Electrical resistivity is a very sensitive means to detect small changes of irradiation effects in a  $\mu$ dpa range, so that *in-situ* measurements of defect behavior under irradiation with a dose rate equivalent to that of a test reactor. 2) From the present experiment, efficiency of Cu atom removal from solid solution in terms of one displacement event can be estimated. The preliminary evaluation shows that the efficiency is very high and one vacancy may remove more than one copper atom from solid solution.

<sup>1</sup>Department of Applied Science, Tokai University

## References

- [1] J. P. Biersack and L. G. Hagmark, Nucl. Instrum. Methods, **174** (1980) 257.  
 [2] H. Hasegawa et al., JAERI Tandem Annual Report 2000, JAERI-Review 2001-030, 96-97.

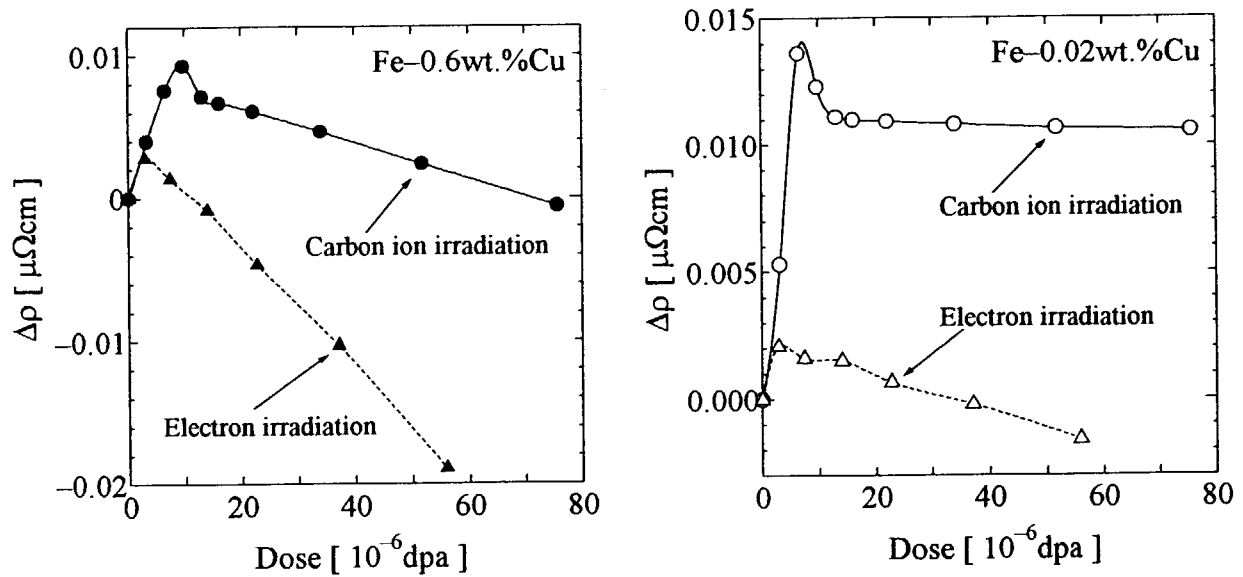


Fig.1. Dose dependence of resistivity change with 100MeV  $^{12}\text{C}$  ion as compared with 2MeV electrons.

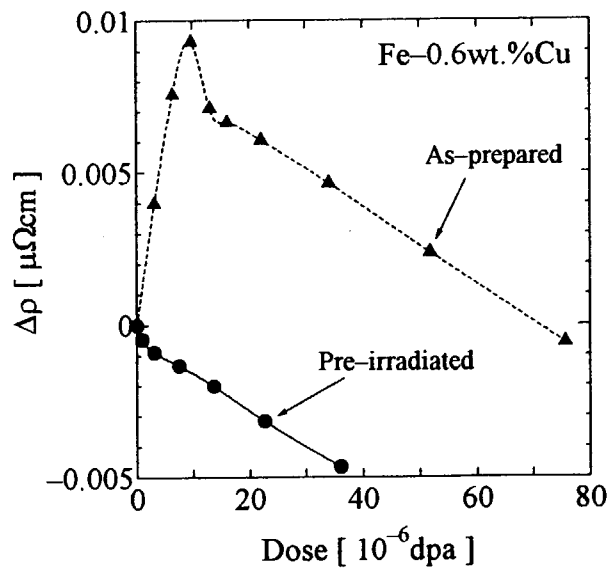


Fig.2. Effect of pre-irradiation.

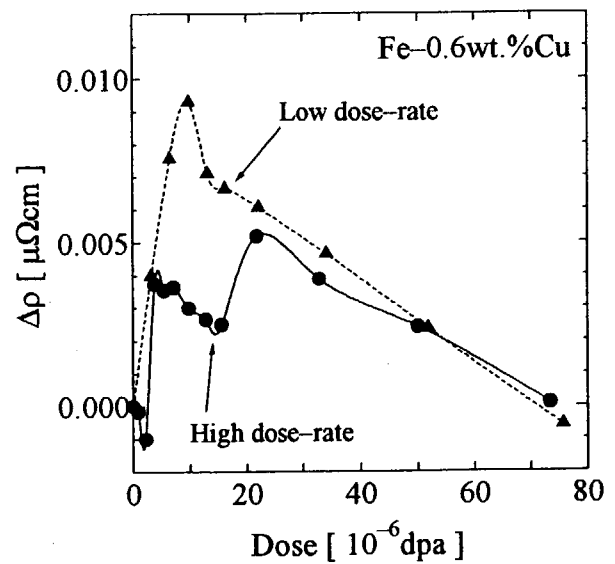


Fig.3. Effect of dose rate.

## 7.8 RADIATION EFFECTS OF HIGH ENERGY FISSION PRODUCTS IN LIGHT WATER REACTOR FUELS

T. SONODA<sup>1</sup>, M. KINOSHITA<sup>1</sup>, N. ISHIKAWA, Y. CHIMI, A. IWASE

High burnup extension of LWR fuel is progressing to reduce the amount of total process flow in the nuclear fuel cycle and eventually to reduce the fuel cycle costs. At the rim area of high burnup fuel pellets in LWRs, a crystallographic re-structuring is commonly observed, as named “rim structure” [1]. This structure may be formed by the accumulation and mutual interactions of radiation damage including point defects and dislocations a), fission products (FPs) including gas bubbles and metal particles b), and electronic excitations deposited partially by high energy fission products c) [2].

In order to separate each processes and understand the mutual interactions among them, 70 – 210 MeV FP ions (Xe, I) irradiation examination on CeO<sub>2</sub>, as a simulation fluorite ceramics of UO<sub>2</sub>, have been done at JAERI-Tandem facility. Microstructural evolutions in the specimen are observed in a 200 kV TEM, JEOL 200CX at CRIEPI. Moreover, in order to compare the microstructural changes under irradiation with ions and electrons, 200 keV electron irradiation examinations are also progressed in the TEM.

Figure 1 shows typical micrographs of CeO<sub>2</sub> under irradiations with 70 MeV I ion (a), 100 MeV Xe ion (b) and 210 MeV Xe ion (c) at room temperature. This figure indicates that the irradiations of high energy FPs at room temperature cause the typical radiation damage, “ion tracks”. Figure 2 summarizes that the average diameters of ion tracks of (a) - (c) are ~ 4.6 nm, ~ 7.9 nm and ~ 9.3 nm, respectively. These results suggest that the affected area of electronic excitation by fissions in CeO<sub>2</sub> seems to be around 6 ~ 7 nmφ. Figure 3 shows the microstructural evolution under 100 MeV Xe ions irradiation. In this figure, the elliptical deformation of diffraction spots and faint “halo-pattern” become clear as the fluence becomes higher, > 1 x 10<sup>12</sup> ions/cm<sup>2</sup>. These figures indicate that the inner structure of ion tracks under room temperature seems to be amorphous or grain-subdivided.

Figure 4 shows the sequential micrographs of CeO<sub>2</sub> under irradiation with a 200 keV electron at room temperature. In this figure, two types of defect contrasts are observed. One is small defect cluster whose average size is ~ 8 nm, and the other is big strain contrast whose average size is ~ 100 nm. The sizes of small clusters keep almost constant under electron irradiation. On the contrary, the big strain contrasts suddenly appear after electron irradiation and grow rapidly until the size becomes ~ 100 nm. After growth, some of the contrasts are slightly moved and disappeared. This kind of contrasts is also observed in another fluorite structure ceramics [3]. By the reason of almost no possibility to produce point defects through nuclear energy depositions by 200 keV electron irradiations, the formation of this big contrast might be caused by the effect of electronic energy depositions and radiation-enhanced diffusion through them.

### References

- [1] J. O. Barner, M. E. Cunningham, M. D. Freshley, and D. D. Lanning, HBEP-61, 1990, Battelle Pacific Northwest Laboratories.
- [2] T. Sonoda, M. Kinoshita, I.L.F. Ray, T. Wiss, H. Thiele, D. Pellottiero, V.V. Rondinella and H.J. Matzke, , Nucl. Instr. and Meth. B, 2001, in press..

<sup>1</sup> Nuclear Energy Systems Department, Komae Lab., Central Research Institute of Electric Power Industry (CRIEPI)

[3] K. Yasuda, C. Kinoshita, T. Inoue, S. Matsumura, H. Abe and K.E. Sickafus, JAERI Review 99-025, 1999, pp149-151.

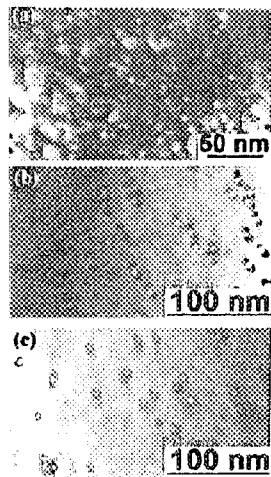


Fig. 1 Typical micrographs of  $\text{CeO}_2$  under irradiations with 70 MeV I (a), 100 MeV Xe (b) and 210 MeV Xe (c).

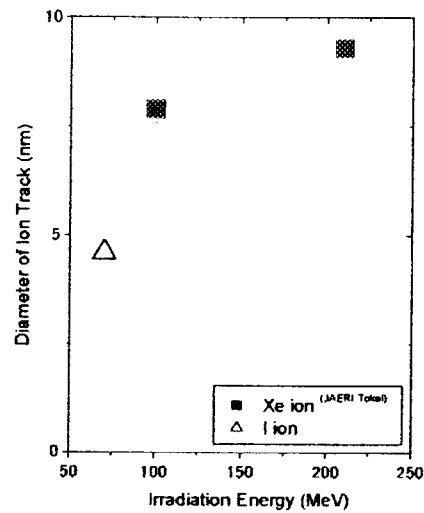


Fig. 2 Average diameter of ion tracks.

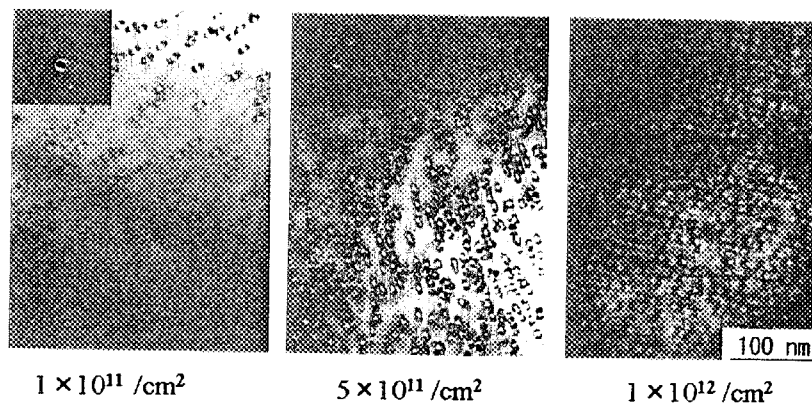


Fig. 3 Microstructural evolutions of  $\text{CeO}_2$  under irradiation with 100 MeV Xe ions.

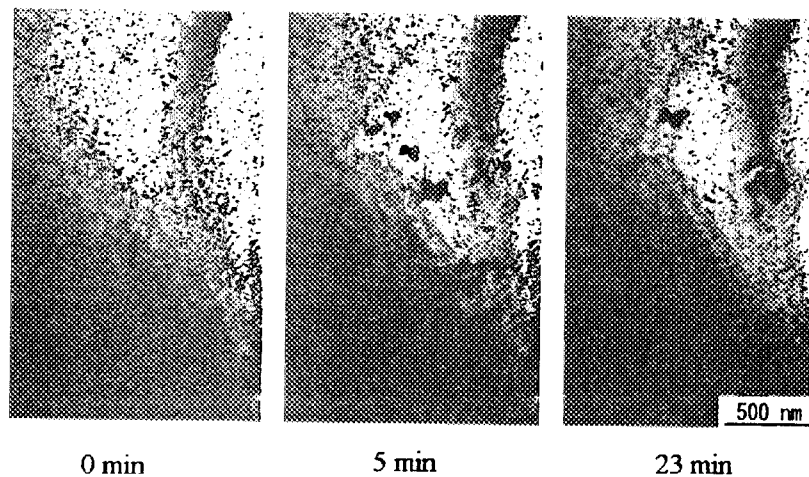


Fig. 4 Sequential micrographs of  $\text{CeO}_2$  under irradiation with 200 keV electrons.

## 7.9 STUDY ON DISORDERING IN $\text{Li}_2\text{TiO}_3$ IRRADIATED WITH HIGH ENERGY IONS

T. NAKAZAWA, T. ARUGA, V. GRISMANOV<sup>1</sup> and D. YAMAKI

The study of irradiation effects on the lithium metatitanate ( $\text{Li}_2\text{TiO}_3$ ) ceramics exposed to the high energy ions is reported here. The  $\text{Li}_2\text{TiO}_3$  ceramics are regarded as one of the most suitable candidates for solid breeder of D-T fusion reactors. It is common knowledge that the radiation damage in  $\text{Li}_2\text{TiO}_3$  will be produced in an operating fusion reactor. The damage caused by ionizing radiation may result in the microstructure changes and hence may have an impact on the tritium release behaviour, thermal and mechanical properties of  $\text{Li}_2\text{TiO}_3$ . Thus, the study of irradiation defects and damage microstructure in  $\text{Li}_2\text{TiO}_3$  is essential in order to evaluate its irradiation performance.

The  $\text{Li}_2\text{TiO}_3$  ceramic specimens (78% of theoretical density) were irradiated at ambient temperature with high energy oxygen ions (30 MeV) from a tandem accelerator at JAERI-Tokai. The accumulated ion fluences were  $2.6 \times 10^{18}$  and  $1.2 \times 10^{19}$  ions/m<sup>2</sup>. Then, the irradiated samples have been examined by using Raman spectroscopy, electron-spin resonance (ESR) spectroscopy, X-ray diffraction (XRD) and scanning electron microscopy (SEM).

Some small changes in the Raman spectra of  $\text{Li}_2\text{TiO}_3$  ceramics exposed to high energy oxygen ions were found but those gave no way for analysis. The ESR measurement showed that there were no paramagnetic radiation defects in  $\text{Li}_2\text{TiO}_3$  irradiated with oxygen ions. On the other hand, the XRD measurements and the SEM observations showed that significant changes due to the irradiation were caused in the  $\text{Li}_2\text{TiO}_3$ .

The influence of fluences on the intensities of XRD peaks, which were calculated as area of peaks, is shown in Fig. 1. The peak intensities were decreased with the fluences but without any peak broadening. In the XRD pattern of  $\text{Li}_2\text{TiO}_3$  irradiated with 30 MeV  $\text{O}^{4+}$  ions to  $2.6 \times 10^{18}$  ions/m<sup>2</sup>, the decrease in intensity of (002) supercell peak was less than that in intensities of other peaks. However, the increase in fluences from  $2.6 \times 10^{18}$  to  $1.2 \times 10^{19}$  ions/m<sup>2</sup> decreased the (002) peak intensity remarkably, compared with the decrease in other peak intensities. The decrease in intensity of (002) supercell peak means partial site mixing between Li and Ti sites in  $\text{Li}_2\text{TiO}_3$  [1]. The partial site mixing between Li and Ti atoms is considered to be drastically enhanced by the irradiation with the fluence up to  $1.2 \times 10^{19}$  ions/m<sup>2</sup>. The transition to such a disordering caused by the site mixing was observed also by the SEM examination. Fig. 2. shows the SEM image of the cross sections of  $\text{Li}_2\text{TiO}_3$  pellets irradiated with 30 MeV  $\text{O}^{4+}$  ions. The SEM observations disclosed beyond a doubt that grain structure was vanished in the surface layer of  $\text{Li}_2\text{TiO}_3$  ceramics irradiated. The width of the vanishing region is estimated at about 15-20  $\mu\text{m}$ , which is in a good agreement with the region of the electronic energy deposition calculated by using TRIM code [2]. Such a vanishing of the grain structure was not observed in the surface layer of  $\text{Li}_2\text{TiO}_3$  pellet before irradiation.

These results obtained by the XRD measurements and SEM observations indicate that the disorder transition was caused in the surface layer of  $\text{Li}_2\text{TiO}_3$  ceramics irradiated with 30 MeV  $\text{O}^{4+}$  ions. However, the disordered layer did not result in the entire amorphization because the disappearance of peaks in the XRD patterns and Raman spectra of  $\text{Li}_2\text{TiO}_3$  ceramics irradiated with 30 MeV  $\text{O}^{4+}$  ions to  $1.2 \times 10^{19}$  ions/m<sup>2</sup> was not complete. The disorder transition due to the irradiation is considered to occur through the mechanism of the electronic energy deposition [3].

---

<sup>1</sup>OECD Halden Reactor Project, P.O. Box 173, N-1751, Halden, Norway

## References

- [1] L. Baños, M.E. Villafuerte-Castrejón, R. Valenzuela and A.R. West, J. Chem. Soc. Faraday Trans. 86 (1990) 2979.  
 [2] J.F. Ziegler, J.P. Biersack and U. Littmark, The Stopping and Range of Ions in Solids, Pergamon, Oxford, 1985.  
 [3] T. Aruga, Y. Katano, T. Ohmichi, S. Okayasu and Y. Kazumata, Nucl. Instrum. Methods Phys. Res. B, 166-167 (2000) 913.

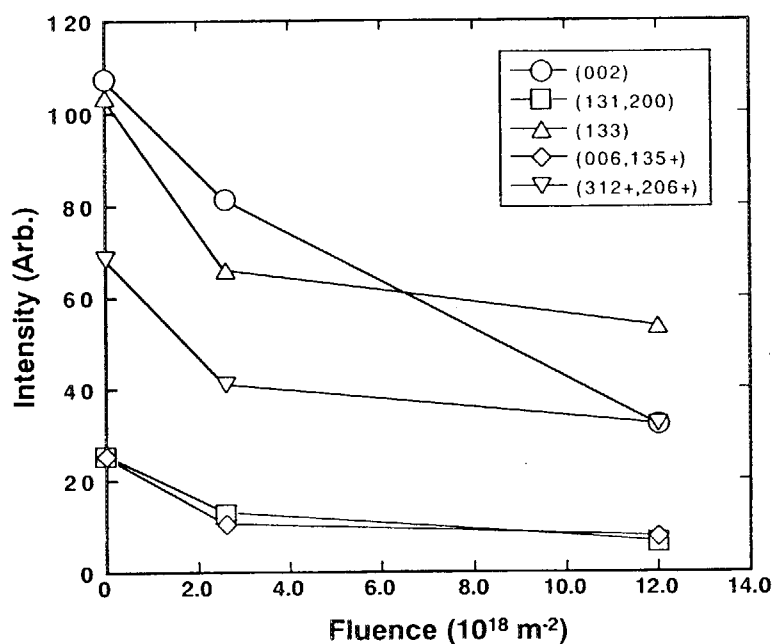


Fig. 1. Changes in Bragg peak intensities with the fluences for  $\text{Li}_2\text{TiO}_3$  irradiated with 30MeV  $\text{O}^{4+}$  ions

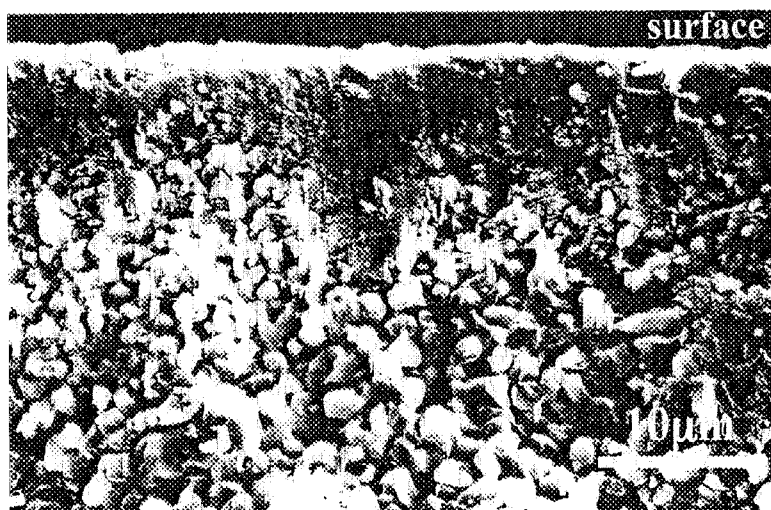


Fig. 2. Bulk micrographs of  $\text{Li}_2\text{TiO}_3$  irradiated with 30MeV  $\text{O}^{4+}$  ions to the fluence up to  $1.2 \times 10^{19}$  ions/ $\text{m}^2$ .



## 7.10 EFFECTS OF Zr ION IRRADIATION ON SOME PROPERTIES OF SUPERPLASTIC CERAMIC 3Y-TZP

Y. MOTOHASHI<sup>1</sup>, T. KOBAYASHI<sup>2</sup>, S. HARJO<sup>1</sup>, T. SAKUMA<sup>1</sup>,  
T. SHIBATA<sup>3</sup>, M. ISHIHARA<sup>3</sup>, S. BABA<sup>3</sup> and T. HOSHIYA<sup>3</sup>

Recently, it has become clear that some of structural ceramics show superplasticity, i. e., very high ductility[1]. Application of the superplastic phenomena found in the ceramics is very promising. That is to say, the structural ceramics, which usually possess more superior mechanical and thermal properties than metallic materials except for their brittle behavior, can be formed into complicated shapes by means of plastic working. The superplastic ceramics have potential ability for application to atomic energy fields. Up to date, however, as far as we know, there have been few studies concerning the effects of irradiation on the properties of the superplastic ceramics.

In this study, the effects of Zr ion irradiation on the mechanical properties and phase transformation characteristics of a typical superplastic ceramic 3mol% yttria containing tetragonal zirconia polycrystals (3Y-TZP) were examined and discussed. The effect of annealing on the variations of these properties was also investigated. Chemical composition of the 3Y-TZP is ;  $Y_2O_3=5.15$ ,  $Al_2O_3\leq 0.10$ ,  $SiO_2\leq 0.02$ ,  $Fe_2O_3\leq 0.01$ ,  $Na_2O\leq 0.04$  and  $ZrO_2 = \text{bal.}$ , in mass%. Some material constants are shown in Table 1.

Table 1 Material properties of 3Y-TZP

Density [g/cm <sup>3</sup> ]	Grain size [ $\mu\text{m}$ ]	Bending strength [MPa]	Fracture toughness $K_{IC}$ [MN/m <sup>3/2</sup> ]	Young's modulus [GPa]	Thermal expansion [10 <sup>-6</sup> /K]
6.05	0.3	1180	7.2	206	12

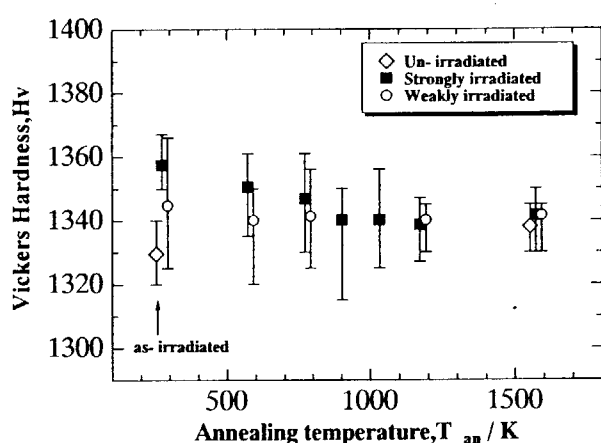


Fig.1 Variation in Vickers hardness measured on the irradiated plane with annealing temperature.

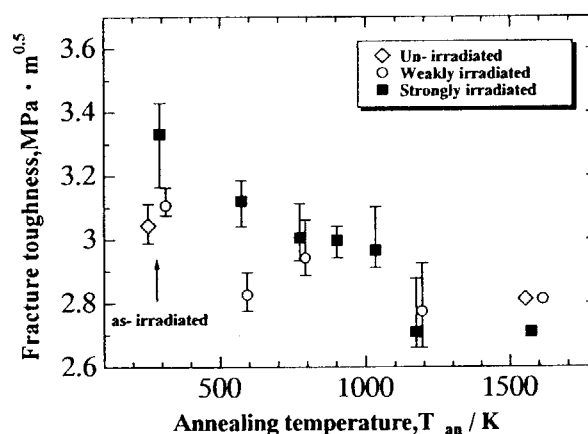


Fig.2 Variation in fracture toughness measured on the irradiated plane with annealing temperature.

<sup>1</sup>The Research Center for Superplasticity, Faculty of Engineering, Ibaraki University.

<sup>2</sup>Graduate Student, Ibaraki University.

<sup>3</sup>Oarai Research Establishment, Japan Atomic Energy Research Institute.

The 3Y-TZP specimens were irradiated using 130MeV  $Zr^{+11}$  ions from the TANDEM accelerator facility at JAERI, Tokai. Irradiation was performed with the fluence of  $3.5 \times 10^{12}$  and  $2.1 \times 10^{13}$  ions /  $cm^2$ . The shape of the specimen is a rectangular thin plate with the dimension of  $1 \times 2 \times 20 mm^3$ . One of the widest side surfaces ( $2 \times 20 mm^2$ ) of the specimen was polished to mirror-like plane. The  $Zr^{+11}$  ions were irradiated normal to this polished plane.

Figure 1 and 2 show variations in Vickers hardness and fracture toughness, measured on the irradiated planes of the specimens, with annealing temperature. The fracture toughness was evaluated by the Indentation Fracture (IF) method. It is seen in the as-irradiated data that the hardness and fracture toughness were increased with the amount of the irradiation. The hardness and fracture toughness values were decreased as the annealing temperature,  $T_{an}$ , was raised and their values returned to those of the un-irradiated state when  $T_{an} \geq 1173K$ .

As well known, the 3Y-TZP possesses high toughness because it has ability to absorb external energy, for example, work done by external force, through its own stress induced martensitic transformation from  $t$ - to  $m$ - phase. Since the irradiation might change the  $t$ -phase to other phases, which might deteriorate the toughening mechanism of 3Y-TZP, the phase transformation characteristics was studied by means of Rietvelt analysis on X-ray diffraction patterns. It was found that the irradiation caused no phase transformations within the present experimental range.

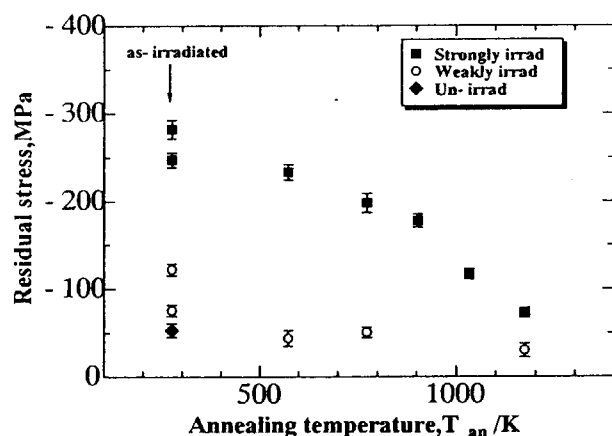


Fig.3 Variation in residual stress measured on irradiated plane with annealing temperature.

compressive residual stresses were decreased monotonously with raising the annealing temperature similar to those observed for the hardness and fracture toughness. We can conclude from these results that the influence of the  $Zr$ -ion irradiation disappeared at  $T_{an} \geq 1173K$ .

The increased hardness, fracture toughness and residual stress were gradually decreased with raising the annealing temperature, and returned to the values of un-irradiated state at around  $T_{an} \approx 1200K$ . A highly probable species that can well diffuse in the 3Y-TZP lattice at around 1200K and can relieve the residual stresses is  $O^{2-}$  ions. We can say, therefore, that one of main species which was knocked-on by the  $Zr^{+11}$  ion irradiation and subsequently was recovered through diffusion by the annealing is  $O^{2-}$  ions. A main cause of the increases in the hardness and fracture toughness after the irradiation may be the residual compressive stresses left in the irradiated surface region of the specimens.

#### References

- [1] For example, Y.Motohashi, Shinsozai, 4-6 (1993) 33.

## 7.11 RADIATION DEFECTS IN NANOCRYSTALLINE MATERIALS

H.OHTSUKA and H.SUGAI

The aim of this study is to realize radiation resistant materials advantage of intrinsic effects of the nanocrystalline. So far, we have observed a diffusion-limited reaction of defects in a single particle. With supports of a computer simulation, we have concluded that the nano-particles have the promising property against radiation damage [1]. For practical use of the nanocrystalline materials, which consist of nano-scaled particles, the next step of this study is to show that they still have the radiation resistant properties as base materials. To examine such property we have to first develop a method to sense defects in the nanocrystalline. As a diagnostic tool we use a X-ray diffractometer which tests samples at the real scale of the materials. Furthermore, the penetration depth of the X-ray agrees with the range of incident ions from the tandem accelerator. A question before the experiment was whether radiation defects within the nanocrystalline is detectable with X-ray or not. Preliminary experiments showed changes in the X-ray profile before and after the irradiation, as shown in Fig.1. Detailed analyses of the X-ray data are under study with a help of TEM (transmission electron microscopy) observations as shown in Fig.2, where one can see the defect clusters. We concluded that the defect clusters are detectable with XRD. This result encourages us to study further.

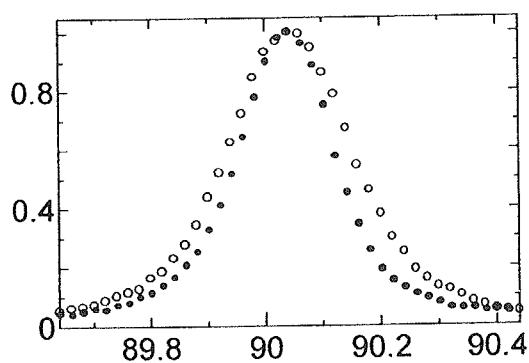


Fig.1 X-ray signals from  $2\theta$  scan around 311 reflection of Cu; close and open circles refer to before and after irradiation with 200MeV Ni, up to  $10^{15}$  ions/cm<sup>2</sup>, respectively.

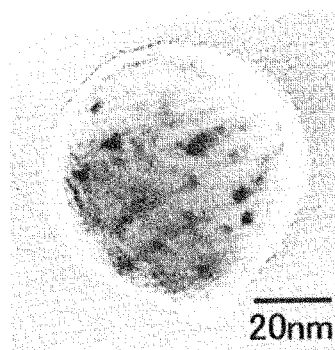


Fig.2 TEM observation of a single Cu particle under the same irradiation condition as of Fig.1. Clear black spots show defect clusters.

### Reference

- [1] H.Ohtsuka, K.Hojo, H.Maeta, H.Otsu, H.Sugai and H.Yamamoto, Eur. Phys. J.D. 16 (2001) 309.

## 7.12 ION IRRADIATION EFFECTS OF NEW CARBON COMPOSITE MATERIALS AND CARBON FIBERS HAVING HIGH THERMAL CONDUCTIVITY

A. KURUMADA<sup>1</sup>, Y. IMAMURA<sup>2</sup>, T. OKU<sup>3</sup>,  
M. ISHIHARA, Y. HOSHIYA, S. BABA and J. AIHARA

Carbon/Carbon composite materials have high thermal conductivity and excellent mechanical properties at high temperatures. They have been used as structural materials at high temperatures in fission and experimental fusion reactors. So, the changes in the microstructures and the mechanical properties due to irradiation damage must be measured for the safety design and the life assessment of the materials.

A purpose of this study is to obtain the basic knowledge of the development of new carbon composite materials having high thermal conductivity and excellent resistance to irradiation damage.

In this study, four kinds of carbon fibers were selected, which were a vapor growth carbon fiber (VGCF; K1100X), a polyacrylonitrile based fiber (PAN; M55JB by Toray Corp.), a mesophase pitch based fiber (YS-70-60S by Nippon Graphite Fiber Corp.) and a pitch based fiber (K13C2U by Mitsubishi Chemical Co.). They were irradiated by high-energy carbon and nickel ions. Carbon ions ( $^{12}\text{C}^{+6}$ ) of 100 MeV with 100 nA were irradiated to  $3 \times 10^{-5}$  dpa and nickel ions ( $^{58,7}\text{Ni}^{+13}$ ) of 200 MeV with 300 nA were irradiated from  $1 \times 10^{-5}$  dpa to  $5 \times 10^{-4}$  dpa using the TANDEM in JAERI Tokai. The ranges of carbon and nickel ions calculated by TRIM-98 code are 221  $\mu\text{m}$  and 35  $\mu\text{m}$ , respectively. Irradiation damages in the carbon fibers are expected to be uniform across the cross section, because the diameters of carbon fibers are about 20  $\mu\text{m}$  and are smaller enough than the ranges.

Figure 1 shows changes in cross sectional areas of carbon fibers after ion irradiation. The cross sectional areas increased due to ion irradiation except for the K1100X of VGCF. One of the reasons of the increases is the swelling of carbon basal planes due to lattice defects in the graphite interlayer. Effects of different irradiation particles and different irradiation energy couldn't be found clearly.

Figure 2 shows changes in tensile strengths of carbon fibers after ion irradiation. The tensile strengths decreased due to ion irradiation except for the K1100X of VGCF. The tendency of the decreases was the same as that of carbon fibers due to neutron irradiation.[1] One of the reasons of the decreases is thought that the microstructures of carbon fibers are damaged on the axial direction. Because ions were irradiated vertically to the longitudinal direction of carbon fibers. And the Young's modulus also tends to decrease with the irradiation like that of tensile strength.

About the VGCF fiber, it is thought that the cross sectional area didn't change and the tensile strength increased by ion irradiation because of the good crystallization and the random structure.

---

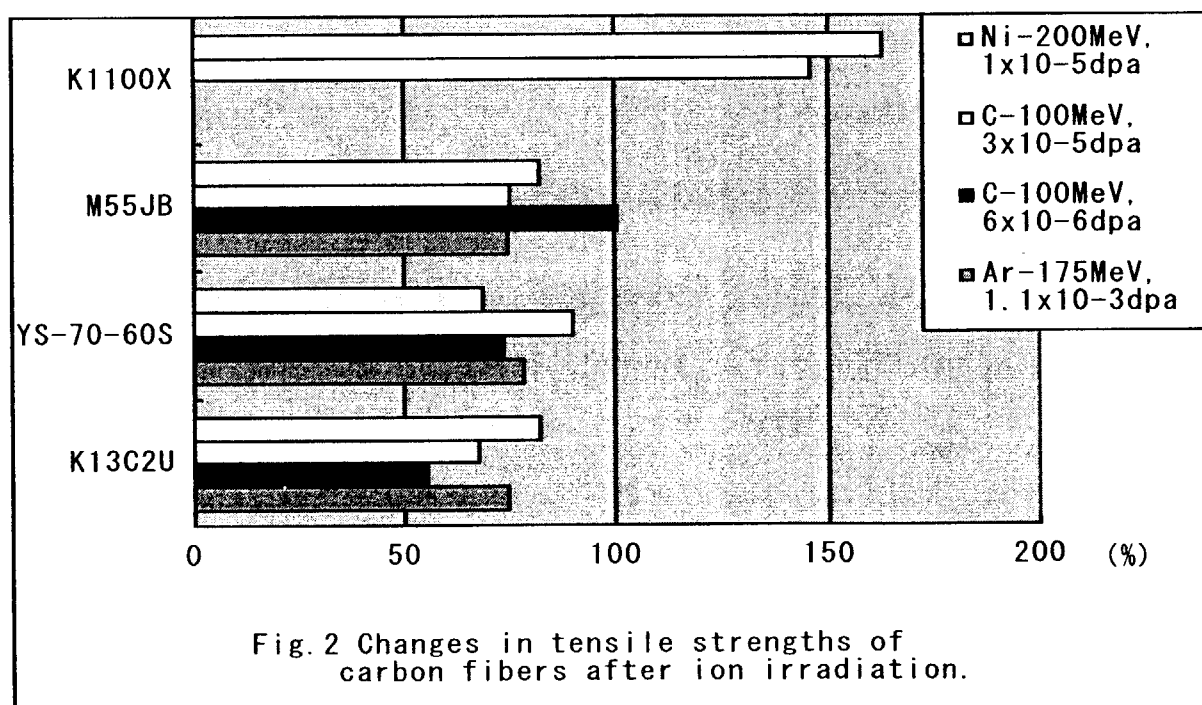
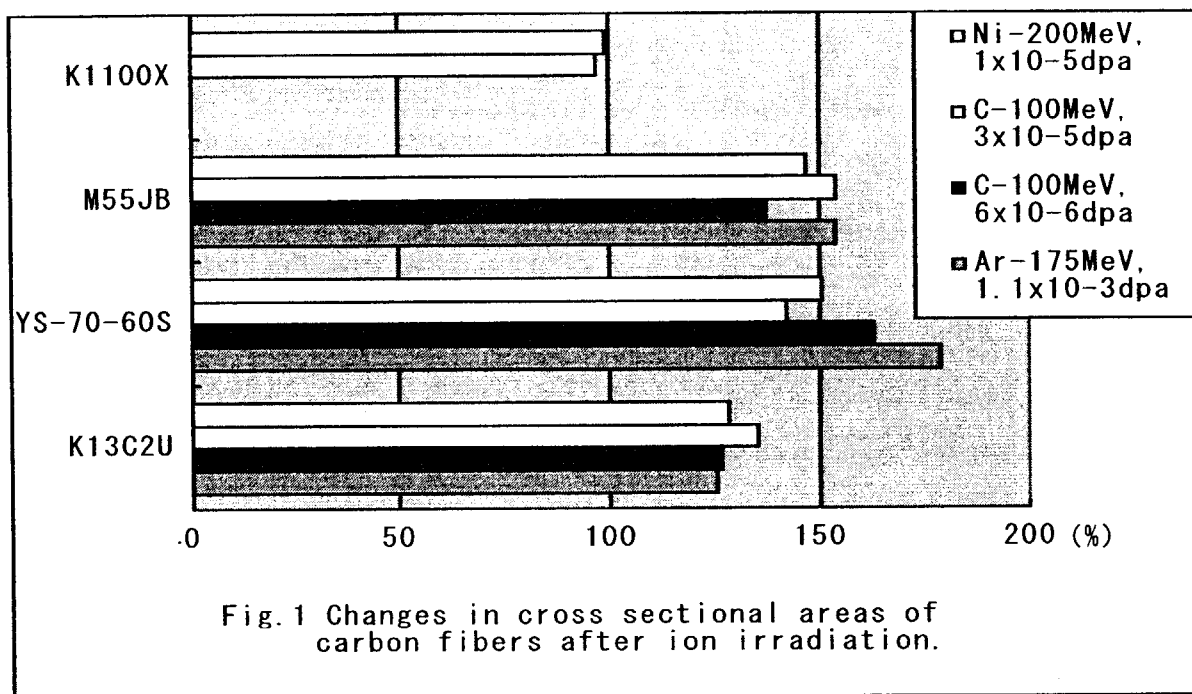
<sup>1</sup> Research Center for Superplasticity, Faculty of Engineering, Ibaraki University

<sup>2</sup> Department of Mechanical Engineering, Faculty of Engineering, Ibaraki University

<sup>3</sup> Ibaraki Study Center, The University of the Air

By the results of this study and results obtained in previous study, the VGCF and the mesophase pitch based carbon fibers are considered to be useful as a reinforcement fiber of new carbon composite materials having high thermal conductivity and excellent resistance to irradiation damage.

Reference: [1] T.Oku, Y.Imamura, A.Kurumada, M.Inagaki and K.Kawamata, TANSO 1999 [No.190] 262-266.



### 7.13 THE STUDY ABOUT THE STRUCTURE OF POWER MOSFETS WITH HIGH RADIATION TOLERANCE

H. SHINDO <sup>1</sup>, T. HIRAO, S. SOMEKAWA <sup>1</sup>, S. KUBOYAMA <sup>1</sup>  
H. ITO, H. OHIRA <sup>2</sup>, Y. NAGAI <sup>2</sup> and S. MATSUDA <sup>1</sup>

Single-event effects (SEE) are the most serious problem in applying highly sophisticated modern electronic devices in space environments. Single Event Burnout (SEB) was identified as a possible catastrophic failure mode for Power MOSFETs. It is known that SEB is triggered when a heavy ion passes through a power MOSFET biased in the OFF state. Transient current generated by a heavy ion turns on a parasitic bipolar transistor (BJT) inherent to the device structure, creates a short-circuit between the source and drain and destroys the device [1]. In our previous report, it has been clarified that SEB tolerance was improved by the change of the design parameter of Power MOSFETs. The thickness of the epitaxial layer (t-epi) is one of the most effective parameters to improve SEB tolerance. It was found that as the t-epi became thicker, the SEB threshold Voltage was increased. However, the increase of t-epi also leads the increase of the resistance of ON state ( $R_{ON}$ ) and degrades the electrical characteristics.

As the new way of improving SEB tolerance as it kept the resistance value of  $R_{ON}$  low, we adopted the device structure that has two epitaxial layers with different resistance value, and evaluated test samples by the high-energy heavy ion irradiation. The tests were performed by using Energetic Particle Induced Charge Spectroscopy (EPICS) system [2] (Figure 1). EPICS is a specially designed pulse-height analyzer (PHA) system to characterize the charge collection characteristics in semiconductor devices. Figure 2 show the typical EPICS spectrum. The 1st and 2nd peak correspond to the collected charge from an ion track that traverses the base-collector junction only and both of the emitter-base and base-collector junctions, respectively. The 2nd peak moves to the right as applied bias voltage is increased and SEB signals appear at certain voltage. It is said the movement of the 2nd peak plays a key role to trigger SEB. In the irradiation test, we used Ni ions ( $LET=28.0[\text{MeV}/(\text{mg}/\text{cm}^2)]$ ) from the TANDEM accelerator at JAERI. The beam current was about 1.0 nA. The primary ion beam was scattered by an Au foil to obtain uniform beam intensity over the surface of the samples.

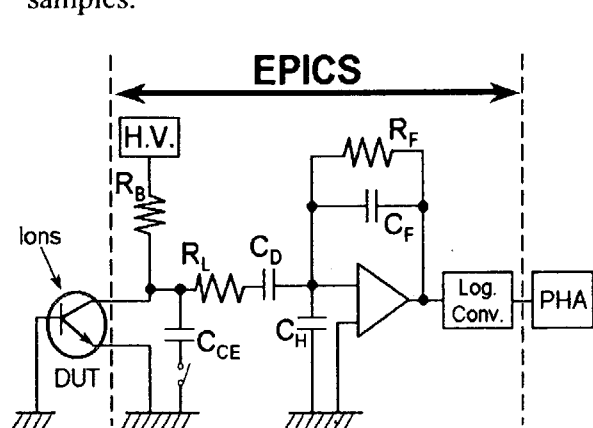


Fig.1 Block diagram of EPICS

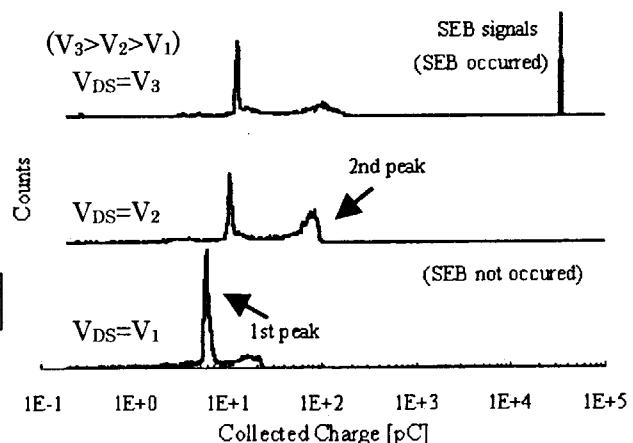


Fig.2 Typical EPICS Spectrum

<sup>1</sup>Technology Research Department, Office of Research and Development,  
National Space Development Agency of Japan.

<sup>2</sup>Components Engineering Section, Engineering Dept., RYOEI TECHNICA Corporation.

Figure 3 shows the cross section diagram of test and reference sample. We prepared two types of test samples that have two epitaxial layers with different resistance value. The resistance value of each layer is also shown in Figure 3. These were manufactured based on Power MOSFET (2SK3041) that NASDA had developed for space use. The reference sample has only one epitaxial layer which the specific resistance value is  $5.6 [\Omega \text{ cm}]$ . On the other hand, test samples was added another epitaxial layer which the specific resistance is relatively low ( $0.1$  or  $0.5 [\Omega \text{ cm}]$ ). This layer (we call "1<sup>st</sup> epitaxial layer") serve effectively to keep the resistance value of  $R_{\text{ON}}$  low.

The comparison of the EPICS spectrum between test and reference sample at the same bias voltage condition is shown in Figure 4. From the result, it is said that the 2nd peak position of the test sample is lower than that of the reference. SEB was not observed at the maximum rating voltage (250V) in both test sample 1 and 2. It is clearly said that the SEB tolerance is improved from the reference. We expect that this device structure is quite useful to develop high SEB tolerance Power MOSFETs for space application. Now we are planning to design and evaluate the prototype sample of Power MOSFET for space use based on this experimental result.

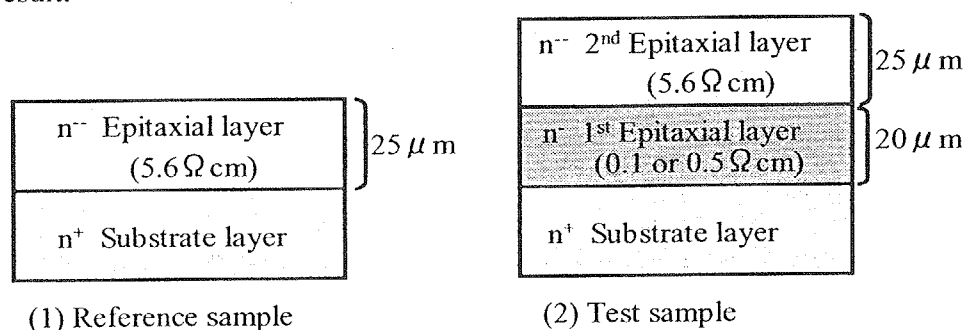


Fig. 3 Cross section diagram of the epitaxial layer of both reference and test sample

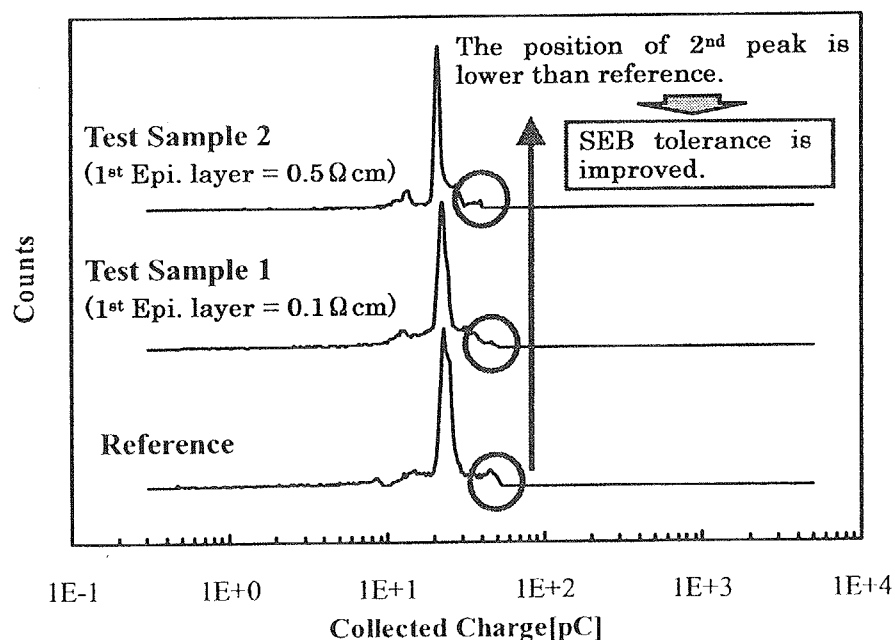


Fig.4 Comparison of the EPICS spectrum between test and reference sample ( $V_{\text{DS}}=200[\text{V}]$ )

#### References

- [1] M.Allenspach, et al, IEEE. Trans.Nucl.Sci., Vol.NS-43,No.6 (1996) 2927.
- [2] S.Kuboyama, et al, IEEE. Trans.Nucl.Sci. Vol.NS-39,No.6(1992) 1698.

This is a blank page.



**8. Publication in Journal and Proceedings, and Contribution to  
Scientific Meetings**

This is a blank page.

## ACCELERATOR OPERATION AND DEVELOPMENT

### Journal/Proceedings

Takeuchi, S.

*JAERI-KEK Secondary Beam Acceleration Project*

Proc. of the 14<sup>th</sup> Workshop of Tandem Accelerators and their associated Technologies,  
Gifu (Jun.28-29,2001) pp76-79.

Takeuchi, S., Matsuda, M., Ishizaki, N., Tayama, H., Iijima, A., Yoshida, T.

*Operational Status of Superconducting Resonators of the JAERI Tandem-Booster*

Proc. of The 10th Workshop on RF Superconductivity, Tsukuba (Sep. 6-11, 2001)  
PE001.

Tsukihashi, Y., Yoshida, T., Kanda, S., Takeuchi, S., Hanashima, S., Ohuchi, I.,

Horie, K., Abe, S., Ishizaki, N., Tayama, H., Matsuda, M.

*The Status of the JAERI Tandem Accelerator*

Proc. of the 14th Workshop of Tandem Accelerators and their associated Technologies,  
Gifu, (Jun. 28-29, 2001) pp35-38.

### Meetings

Matsuda, M., Fujii, Y., Tayama, H., Ishizaki, N., Abe, S., Hanashima, S., Tsukihashi, Y.,

Horie, K., Ohuchi, I., Kanda, S., Takauchi, S., Yoshida, T

*Status Report of in-Terminal ECR Ion Source*

The 14th Workshop on Tandem Accelerations and their associated Technologies, Gifu  
(Jun. 28-29, 2001)

Takeuchi, S.

*Status of Superconducting Heavy-ion Linac at JAERI*

The 4th Superconducting Linear Accelerator Meeting in Japan, Tsukuba (Mar. 12, 2002)

## NUCLEAR STRUCTURE

### Journal/Proceedings

Ichikawa, S., Tsukada, K., Asai, M., Haba, H., Sakama, M., Kojima, Y., Shibata, M., Nagame, Y., Oura, Y., Kawade, K.

*Performance of the Multiple Target He/PbI<sub>2</sub> Aerosol Jet System for Mass Separation of Neutron-deficient Actinide Isotopes*

Nucl. Instrum. Methods **B187** (2002) 548.

Iimura, H., Ishida, Y., Koizumi, M., Shinohara, N., Shibata, T., Horiguchi, T., Schuessler, H.A.

*Isotope Shift Measurements of La II by Collinear Laser Spectroscopy*

Proc. Second Sym. on Advanced Photon Research, JAERI-Conf **2001-011** (2001) 300.

Ishii, T., Asai, M., Matsuda, M., Ichikawa, S., Makishima, A., Hossain, I., Kleinheinz, P., Ogawa, M.

*Nano-Second Isomers in Neutron-Rich Ni Region Produced by Deep-Inelastic Collisions*

Acta. Phys. Polonica **B 32** (2001) 739.

Ishii, T.

*Nuclear Shell Structure of the Neutron-Rich Ni Region through Isomer  $\gamma$ -ray Spectroscopy*

Buturi **56** (2001) 684.

Kusakari, H., Morikawa, T., Oshima, M., Toh, Y., Hayakawa, T., Sugawara, M., Hatsukawa, Y., Katakura, J., Sugie, M., Sato, Y.

*Study of Electromagnetic Transitions of Nuclei with Multipole Deformations*

Proc. of Materials Science Symposium 'Heavy Ion Science in Tandem Energy Region', JAERI-Conf **2001-014** (2001) 92.

Liu, Z., Zhang, Y., Zhou, X., Liu, M., Luo, W., Pan, Q., Gan, Z., Hayakawa, T., Oshima, M., Toh, Y., Shizuma, T., Hatsukawa, Y., Osa, A., Ishi, T., Sugawara, M.

*New Yrast Excited States of the  $N=84$  Nucleus  $^{142}\text{Ce}$  Observed in Deep Inelastic Reactions*

Eur. Phys. J. **A13** (2002) 277.

Shibata, M., Iimura, H., Asai, M., Osa, A., Kawade, K., Ichikawa, S., Oshima, M., Sekine, T., Shinohara, N.

*Half-Life and Internal Conversion Electron Measurements in Low-Lying Levels of  $^{125,127}\text{Ba}$*

Phys. Rev. C **65** (2002) 024305.

Shizuma, T., Matsuura, K., Toh, Y., Hayakawa, T., Oshima, M., Hatsukawa, Y., Matsuda, M., Furuno, K., Sasaki, Y., Komatsubara, T., Shimizu, Y.R.

*Multi-Quasiparticle States and K-Forbidden Transitions in  $^{183}\text{Os}$*

Nucl. Phys. **A 696** (2001) 337.

Sugawara, M., Mitarai, S., Kusakari, H., Oshima, M., Hayakawa, T., Toh, Y., Hatsukawa, Y., Katakura, J., Iimura, H., Zhang, Y., Sugie, M., Sato, Y.

*Rotational Bands of  $^{159}\text{Dy}$*

Nucl. Phys. **A699** (2002) 450.

Toh, Y., Oshima, M., Hayakawa, T., Hatsukawa, Y., Katakura, J., Matsuda, M., Iimura, H., Kusakari, H., Nishimiya, D., Sugawara, M., Zhang, Y.H.

*A Position-Sensitive Particle Detector for Coulomb Excitation Experiment*

Rev. Sci. Instrum. **73** (2002) 47.

Zhang, Y.H., Oshima, M., Toh, Y., Koizumi, M., Osa, A., Shizuma, T., Hayakawa, T., Sugawara, M., Kusakari, H., Morikawa, T., Wen, S.X., Zhu, L.H.

*Rotational Bands and Signature Inversion Phenomena in  $\pi h_{9/2} \otimes \nu i_{13/2}$  and  $\pi i_{13/2} \otimes \nu i_{13/2}$  Structures in Odd-Odd  $^{176}\text{Ir}$*

Eur. Phys. J. **A13** (2002) 429.

Zhang, Y. H., Hayakawa, T., Oshima, M., Toh, Y., Katakura, J., Hatsukawa, Y., Matsuda, M., Shinohara, N., Ishii, Y., Kusakari, H., Sugawara, M., Komatsubara, T., Furuno, K.

*Search for Signature Inversion in  $\pi_{13/2} \otimes \nu_{13/2}$  Band in  $^{178}\text{I}$*

Chinese Physics Letter **18** (2001) 1323-1326.

Zhou, X., Zheng, Y., Zhang, Y., Liu, Z., Pan, Q., Gan, Z., Hayakawa, T., Oshima, M., Toh, Y., Shizuma, T., Katakura, J., Hatsukawa, Y., Matsuda, M., Kusakari, H., Sugawara, M., Furuno, K., Komatsubara, T.

*In-Beam Study of  $^{145}\text{Tb}$*

Eur. Phys. J. **A12** (2001) 253.

Zielinska, M., Czosnyka, T., Choinski, J., Iwanicki, J., Napiorkowski, P., Srebrny, J., Osa, A., Utsuno, Y., Toh, Y., Oshima, M., Hatsukawa, Y., Katakura, J., Koizumi, M., Matsuda, M., Shizuma, T., Sugawara, M., Morikawa, T., Kusakari, H.

*Shape coexistence in  $^{98}\text{Mo}$*

Acta. Phys. Polonica **B33** (2002) 515.

## Meetings

Asai, M., Sakama, M., Tsukada, K., Ichikawa, S., Haba, H., Nishinaka, I., Nagame, Y., Goto, S., Kojima, Y., Oura, Y., Nakahara, H., Shibata, M., Kawade, K.

*Measurements of EC and Weak  $\alpha$  Decays of Neutron-Deficient Transuranium Isotopes*

ND2001: International Conference on Nuclear Data for Science and Technology,

Tsukuba (Oct. 7-12, 2001)

Asai, M., Ishii, T., Matsuda, M., Makishima, A., Ogawa, M.

*Spin Assignment for Excited States in Neutron-Rich  $^{32,33}\text{Si}$  and  $^{34}\text{P}$*

First Joint Meeting of the Nuclear Physics Divisions of APS and JPS, Hawaii (Oct. 17-20, 2001)

Asai, M., Sakama, M., Tsukada, K., Ichikawa, S., Haba, H., Nishinaka, I., Nagame, Y., Goto, S., Akiyama, K., Toyoshima, A., Kojima, Y., Oura, Y., Nakahara, H., Shibata, M., Kawade, K.

*Decay Studies of Neutron-Deficient Am, Cm, and Bk Nuclei Using an On-line Isotope Separator*

The 2nd International Symposium on Advanced Science Research

--- Advances in Heavy Element Research ---, Tokai (Nov. 13-15, 2001)

Hayakawa, T., Shizuma, T., Kusakari, H.

*Neucleosynthesis and Destruction of  $^{180}\text{Ta}$  Nuclei.*

Experiments with Low Energy Gamma's WorkShop in JASRI, Nishi-Harima (Jun. 1, 2001)

Hayakawa, T., Toh, Y., Oshima, M., Hatsukawa, Y., Shinohara, N., Matsuda, J., Katakura, J., Iimura, H., Sugawara, M., Kusakari, H.

*Deformation Systematics of Se Isotopes - Complete Spectroscopy with Coulomb Excitation-*

The International Nuclear Physics Conference, INPC2001, Berkeley (Jul. 30, 2001)

Hayakawa, T., Toh, Y., Oshima, M., Hatsukawa, Y., Shinohara, N., Matsuda, J., Katakura, J., Iimura, H., Sugawara, M., Kusakari, H.

*Deformation Systematics of Se isotopes -Complete Spectroscopy with Coulomb Excitation-*

International Conference on Nuclear Data for Science and Technology, ND2001, Tsukuba (Oct. 9, 2001)

Ichikawa, S., Asai, M., Osa, A., Tsukada, K., Haba, H., Goto, S., Nagame, Y., Shibata, M., Kojima, Y., Sakama, M., Tachibana, T.

*Systematic Studies of  $\beta$ -decay Half-lives of New Neutron-Rich Lanthanide Isotopes*

ENAM2001: 3rd International Conference on Exotic Nuclei and Atomic Masses, Hämeenlinna (Jul. 2-7, 2001)

Ichikawa, S., Asai, M., Osa, A., Tsukada, K., Haba, H., Nagame, Y., Goto, S., Shibata, M., Kojima, Y., Sakama, M.

*Identification of  $^{159}\text{Pm}$ ,  $^{162}\text{Sm}$  and  $^{166}\text{Gd}$*

2001 Asia-Pacific Symposium on Radiochemistry, Fukuoka (Oct. 30-Nov. 1, 2001)

Iimura, H., Ishida, Y., Koizumi, M., Shibata, T., Shinohara, N., Horiguchi, T., Schuessler, H.A.

*Hyperfine Structure and Isotope Shift Measurements of Long-Lived La Isotopes by Collinear Laser Spectroscopy*

3rd Int. Conf. on Exotic Nuclei and Atomic Masses, Hameenlinna, Finland (Jul. 3, 2001)

Iimura, H., Ohba, H., Shibata, T., Miyatake, H.

*Velocity and Population Distributions of Nd Atoms in Laser Ablation Plume*

Fall Meeting of the Physical Society of Japan, Tokushima (Sep. 17, 2001)

Iimura, H., Ohba, H., Shibata, T., Miyatake, H.

*Velocity Distributions of Neodymium Atoms in Laser Ablation Plume*

The Third Symposium on Advanced Photon Research, Kyoto (Dec. 14, 2001)

Ishii, T., Asai, M., Kleinheinz, P., Matsuda, M., Makishima, M., Kohno, T., Ogawa, M.  
 *$\gamma$ -Ray Spectroscopy of  $^{68,70}\text{Cu}$  produced in Heavy-Ion Deep-Inelastic Collisions*

2002 Phys. Soc. of Japan Spring Meeting, Kusatsu (Mar. 25, 2002)

Ishii, T.

*Isomer  $\gamma$ -ray Spectroscopy of Neutron-Rich Nuclei Produced by Deep-inelastic Collisions*

Int. Workshop on developments of Ge detector array and frontiers of gamma-ray spectroscopy, Wako (Dec. 12, 2001)



Shizuma, T.

*K-Forbidden Transitions in  $^{183}\text{Os}$  and its Neighbors*

International Nuclear Physics Conference 2001, Berkley, USA (Aug. 2001)

Shizuma, T., Shimizu, Y.R., Toh, Y., Hayakawa, T., Oshima, M., Furuno, K.,  
Sasaki, Y., Komatsubara, T.

*M1 and E2 Transitions from High-K Isomers*

International Symposium on Electromagnetic Interactions in Nuclear  
and Hadron Physics, Osaka (Dec. 2001)

Shizuma, T.

*Photo-Induced Nuclear Reactions and in-Beam Gamma-Ray Spectroscopy*

The 57th Meeting of the Physical Society of Japan, Shiga (Mar. 2002)

Sugawara, M., Mitarai, S., Kusakari, H., Sugie, M., Sato, Y., Oshima, M., Hayakawa, T.,  
Toh, Y., Hatsukawa, Y., Katakura, J., Iimura, H., Zhang, Y.

*Low Energy E1 Transitions between  $\nu[642]5/2$  and  $\nu[521]3/2$  Bands in  $^{157}\text{Gd}$  and  $^{159}\text{Dy}$*

First Joint Meeting of the Nuclear Physics Divisions of APS and JPS in Hawaii (Oct. 19,  
2001)

Toh, Y., Zielinska, M., Czosnyka, T., Oshima, M., Osa, A., Koizumi, M., Utsuno, Y.,  
Hatsukawa, Y., Shinohara, N., Kusakari, H., Sugawara, M.

*Shape coexistence in  $^{98}\text{Mo}$*

The 57th Meeting of Physical Society of Japan, Shiga (Mar. 28, 2002)

Zielinska, M., Czosnyka, T., Choinski, J., Iwanicki, J., Napiorkowski, P., Srebrny, J.,  
Osa, A., Utsuno, Y., Toh, Y., Oshima, M., Hatsukawa, Y., Katakura, J., Koizumi, M.,  
Matsuda, M., Shizuma, T., Sugawara, M., Morikawa, T., Kusakari, H.

*Shape coexistence in  $^{98}\text{Mo}$*

XXVII Mazurian Lakes School of Physics, "Growth Point of Nuclear Physics A.D.  
2001", Krzyze, Poland (Sep.2, 2001)

## NUCLEAR REACTIONS

### Journal/Proceedings

Ikezoe, H., Mitsuoka, S., Nishio, K., Satou, K., Nishinaka, I.

Dependence of Heavy-Ion Fusion Reaction on Nuclear Deformation and Nuclear Shell Structure

J. Nucl. Radiochem Sci. **3** (2002) 39.

Ishiyama, H.

*Radioactive Beam Production at JAERI-TANDEM*

KEK Proceedings **2001-18** (2001) p.91.

Ishiyama, H.

*Nuclear Astrophysical Experiments Using Radioactive Nuclear Beams*

JAERI-Conf **2001-014** (2001) p.13.

Mitsuoka, S., Ikezoe, H., Nishio, K., Satou, K., Duan, L.

*The Present and the Future of JAERI Recoil Mass Separator*

J. Nucl. Radiochem Sci, **3** (2002) 209.

Mitsuoka, S., Ikezoe, H., Nishio, K., Satou, K., Lu, J.

*Effects of Neutron Number and Nuclear Deformation on Complete Fusion of  $^{60,64}\text{Ni} + ^{154}\text{Sm}$  near the Coulomb Barrier*

Phys. Rev. C **65** (2002) 054608.

Nishio, K., Ikezoe, H., Mitsuoka, S., Satou, K., Jeong, S. C.

*Effects of Nuclear Deformation on Fusion Probability in the Reactions of  $^{76}\text{Ge} + ^{150}\text{Nd}$  and  $^{82}\text{Se} + ^{\text{nat}}\text{Ce}$*

J. Nucl. Radiochem. Sci. **3** (2002) 89.

Nishio, K., Ikezoe, H., Mitsuoka, S., Lu, J., Satou, K.

*Effects of Nuclear Deformation on Fusion Probability in the Reactions of  $^{76}\text{Ge} + ^{150}\text{Nd}$  and  $^{82}\text{Se} + ^{140}\text{Ce}$*

JAERI-Conf **2001-014** (2001) p.70.

Satou, K., Ikezoe, H., Nishio, K., Mitsuoka, S., Jeong, S. C.

*Effect of Shell Structure in the Fusion Reactions  $^{82}\text{Se} + ^{134}\text{Ba}$  and  $^{82}\text{Se} + ^{138}\text{Ba}$*

Phys. Rev. C **65** (2002) 054602.

## Meetings

Goto, S., Kaji, D., Nishinaka, I., Nagame, Y., Ichikawa, S., Tsukada, K.,

Asai, M., Haba, H., Mitsuoka, S., Nishio, K., Sakama, M., Zhao, Y. L.,

Sueki, K., Tanikawa, M., Takamiya, K., Kudo, H., Nakahara, H.

*Characteristics of Asymmetric Mass Distributions in Proton-Induced Fission of Actinides*

2001 Asia-Pacific Symposium on Radiochemistry and the Annual Meeting of the Japan Society of Nuclear and Radiochemical Sciences, Fukuoka (Oct. 30, 2001)

Katoh, K., Miyahara, H., Marnada, N., Ueda, N., Ikeda, K., Fujiki, K., Haba, H.,

Nishinaka, I., Tsukada, K., Nagame, Y., Ichikawa, S.

*Production of  $^{147}\text{Eu}$  for Gamma-Ray Emission Probability Measurement*

International Symposium on Isotope Effects in Physics, Chemistry and Engineering, Nagoya (Aug. 22-24, 2001)

Katoh, K., Miyahara, H., Fujiki, K., Ichikawa, S., Nagame, Y., Haba, H., Nishinaka, I., Tsukada, K.

*The Measurement of Emission Probability for  $^{147}\text{Eu}$*

2001 Fall Meeting of the Atomic Energy Society of Japan, Sapporo (Sep. 19-21, 2001)

Katoh, K., Miyahara, H., Fujiki, K., Ichikawa, S., Nagame, Y., Haba, H., Nishinaka, I., Tsukada, K.

*The Measurement of Emission Probability for  $^{66}\text{Ga}$*

2002 Annual Meeting of the Atomic Energy Society of Japan, Kobe (Mar. 27-29, 2002)

Kawamura, T., Ishikawa, T., Hashimoto, T., Nakai, K., Furukawa, T., Ishiyama, H., Tanaka, M-H., Miyatake, H., Fuchi, Y., Yoshikawa, N., Matsuyama, Y., S. C. Jeong, Katayama, I., Nomura, T., Nishio, K., Mitsuoka, S., Ikezoe, H., Tasgihi, Y., Komatsubara, T., Fukuda, T., Mizoi, Y., Watanabe, Y.

*Pulse Height Defects of MSTPC under the High Rate Measurements*

Spring Meeting of the Physical Society of Japan, Shiga (Mar. 24, 2002)

Mitsuoka, S., Ikezoe, H., Nishio, K., Satou, K., Lu, J.

*Fusion Enhancement in the Sub-Barrier Fusion Reactions of  $^{60,64}\text{Ni}$  Projectiles with Deformed  $^{154}\text{Sm}$  Target*

First Joint meeting of the Nuclear Physics Divisions of APS and JPS ,Hawaii (Oct. 16-20, 2001)

Nishio, K.

*Fusion Probability in the Reactions of  $^{76}\text{Ge}+^{150}\text{Nd}$  and  $^{82}\text{Se}+^{nat}\text{Ce}$*

Specialists Meeting on Nuclear Chemistry of Heavy Element, Research Reactor Institute, Osaka (Oct. 23, 2001)

Nishio, K.

*Experimental Results on the Fission through the Resonance Tunneling in  $^{239}\text{Pu}(d,pf)$*

Specialists Meeting on Nuclear Fission, Research Reactor Institute, Osaka (Jan. 17, 2002)

Nishio, K.

*Resonance Fission induced by Photons*

Physics with Laser-electron Photon Beams at MeV, Kobe (Dec. 11, 2001)

Nishio, K.

*Resonance Fission using Monochromatic Photons*

Workshop on Application IFFEL and Nuclear Isomer, Tokai (Sep. 28, 2001)

Nishinaka, I., Nagame, Y., Ikezoe, H., Tanikawa, M., Zhao, Y. L., Goto, S.,

Tsukada, K., Ichikawa, S., Sueki, K., Nakahara, H.

*Different Scission Shapes in Two Mass Division Modes*

INPC2001, International Nuclear Physics Conference, Nuclear Physics in the 21st Century, Berkeley, USA (Jul. 30 - Aug. 3, 2001)

Nishinaka, I., Nagame, Y.

*Fragment Mass and Total Kinetic Energy Distributions in Fission of Light Actinides*

2001 Asia-Pacific Symposium on Radiochemistry and the Annual Meeting of the Japan Society of Nuclear and Radiochemical Sciences, Fukuoka (Oct. 30, 2001)

Satou, K., Ikezoe, H., Nishio, K., Mitsuoka, S., Jeong, S. C.

*Effect of Shell Structure in the Fusion Reactions  $^{82}\text{Se} + ^{134}\text{Ba}$  and  $^{82}\text{Se} + ^{138}\text{Ba}$*

The 57th Meeting of Physical Society of Japan, Shiga (Mar. 27, 2002)

Tsukada, K., Asai, M., Haba, H., Nishinaka, I., Nishio, K., Goto, S., Sakama, M.,

Ichikawa, S., Nagame, Y., Nakahara, H., Gaggeler, H.W., Türler, A., Schädel, M.

*Production cross sections of  $^{262}\text{Db}$ ,  $^{261}\text{Rf}$  and  $^{255}\text{No}$  in the  $^{248}\text{Cm} + \text{HI}$  reaction systems*

International Conference of ACTINIDES-2001, Hayama (Nov. 4, 2001)

Zhao, Y. L., Nishinaka, I., Nagame, Y., Tsukada, K., Sueki, K., Goto, S.,

Tanikawa, M., Nakahara, H.

*Primary Fragment Mass-Yield Distributions for Mass-Asymmetric Fission Path of Heavy Nuclei*

2001 Asia-Pacific Symposium on Radiochemistry and the Annual Meeting of the Japan Society of Nuclear and Radiochemical Sciences, Fukuoka (Oct. 30, 2001)

## NUCLEAR CHEMISTRY

### Journal/Proceedings

Akiyama, K., Sueki, K., Tsukada, K., Yaita, T., Miyake, Y., Haba, H., Asai, M., Kodama, T., Kikuchi, K., Ohtsuki, T., Nagame, Y., Katada, M., Nakahara, H.

*Study of Metallofullerenes Encapsulating Actinides.*

J. Nucl. Radiochem. Sci. **3** (2002) 151.

Haba, H., Tsukada, K., Asai, M., Nishinaka, I., Sakama, M., Goto, S., Hirata, M., Ichikawa, S., Nagame, Y., Kaneko, T., Kudo, H., Toyoshima, A., Shoji, Y., Yokoyama, A., Shinohara, A., Oura, Y., Sueki, K., Nakahara, H., Schädel, M., Kratz, J. V., Türlér, A., Gäggeler, H. W.

*Startup of Transactinide Chemistry in JAERI*

Radiochim. Acta **89** (2001) 733.

Hatsukawa, Y., Oshima, M., Hayakawa, T., Toh, Y., Shinohara, N.

*Application of Multidimensional Spectrum Analysis for Neutron Activation Analysis*

J. Radioanal. Nucl. Chem. **248** (2001) 121.

Hatsukawa Y., Oshima, M., Hayakawa, T., Toh, Y., Shinohara, N.

*Application of the Multiparameter Coincidence Method to Neutron Activation Analysis*

Nucl. Instrum. Methods **A482** (2002) 301.

Hatsukawa, Y., Toh, Y., Oshima, M., Hayakawa, T., Shinohara, N., Kushita, K., Ueno, T.

*Measurements of Long-lived Radioisotopes using Multiparameter Coincidence Method*

Proceedings of the Second Workshop on Environmental Radioactivity, KEK, Tsukuba (Mar. 15-16, 2001) pp 193-196.

Kato, K., Miyahara, H., Marnada, N., Ueda, N., Ikeda, K., Fujiki, K., Haba, H., Nishinaka, I., Tsukada, K. Nagame, Y., Asai, M., Ichikawa, S.

*Production of  $^{147}\text{Eu}$  for Gamma-Ray Emission Probability Measurement*

J. Nucl. Sci. Technol. (Tokyo) **39** (2002) 329.

Shibata, M., Kojima, Y., Uno, H., Kawade, K., Taniguchi, A., Kawase, Y., Ichikawa, S., Mackawa, F., Ikeda, Y.

*Application of a Total Absorption Detector to  $Q_\beta$  Determination without the Knowledge of the Decay Scheme*

Nucl. Instrum. Methods **A 459** (2001) 581.

Shibata, M., Iimura, H., Asai, M., Osa, A., Ichikawa, S., Oshima, M., Sekine, T., Shinohara, N.

*Half-Life and Internal Conversion Electron Measurements in Low-Lying Levels of  $^{125,127}\text{Ba}$*

Phys. Rev. C **65** (2002) 024305.

## Meetings

Akiyama, K., Sueki, K., Haba, H., Tsukada, K., Asai, M., Yaita, T., Nagame, Y., Kikuchi, K., Katada, M., Nakahara, H.

*Production and Characterization of Actinide Metallofullerenes*

2001 Asia-Pacific Symposium on Radiochemistry, Hakata (Oct. 31, 2001)

Akiyama, K., Sueki, K., Tsukada, K., Haba, H., Yaita, T., Kodama, T., Nagame, Y., Kikuchi, K., Katada, M., Nakahara, H.

*Properties of Light Actinides in Fullerene*

Actinides-2001 International Conference, Hayama (Nov. 4, 2001)

Haba, H.

*Anion Exchange Studies of Rf in HCl and HNO<sub>3</sub> Solutions*

5<sup>th</sup> Workshop on the Chemistry of the Heaviest Elements, Hasliberg (Aug. 28, 2001)

Haba, H., Tsukada, K., Asai, M., Toyoshima, A., Akiyama, K., Goto, S., Nishinaka, I., Hirata, M., Ichikawa, S., Nagame, Y., Kratz, J. V., Schädel, M.

*Adsorption of Zr, Hf, and Th from HCl and HNO<sub>3</sub> Solutions by Anion and Cation Exchanges: Model Experiments for the Chemical Characterization of Rutherfordium (Element 104)*

2001 Asia-Pacific Symposium on Radiochemistry, Fukuoka (Nov. 1, 2001)

Haba, H., Tsukada, K., Asai, M., Akiyama, K., Toyoshima, A., Goto, S., Nishinaka, I., Ichikawa, S., Nagame, Y., Hirata, M., Yaita, T., Narita, H., Kratz, J. V., Schädel, M.

*Ion exchange experiments with rutherfordium homologues in HNO<sub>3</sub> and HCl*

Actinides-2001 International Conference, Hayama (Nov. 8, 2001)

Haba, H., Tsukada, K., Asai, M., Nishinaka, I., Goto, S., Toyoshima, A., Akiyama, K., Hirata, M., Ichikawa, S., Nagame, Y., Shoji, Y., Shigekawa, M., Koike, T., Iwasaki, M., Shinohara, A., Kaneko, T., Maruyama, T., Ono, S., Kudo, H., Oura, Y., Sueki, K., Nakahara, H., Sakama, M., Yokoyama, A., Kratz, J. V., Schädel, M.

*Anion Exchange Behavior of Rf in HCl and HNO<sub>3</sub> Solutions*

The 2nd International Symposium on Advanced Science Research, Advances in Heavy Element Research, Tokai (Nov. 14, 2001)

Hatsukawa, Y., Toh, Y., Oshima, M., Hayakawa, T., Shinohara, N., Kushita, K., Ueno, T., Toyoda, K.

*New Technique for Determination of Trace-Elements Using Multiparameter Coincidence Spectrometry*

2001 Asia-Pacific Symposium on Radiochemistry, Fukuoka (October, 2001)

Tsukada, K., Haba, H., Asai, M., Nishinaka, I., Ichikawa, S., Nagame, Y., Hirata, M., Yaita, T., Goto, S., Kaneko, T., Maruyama, T., Akiyama, K., Kudo, H., Shinohara, A., Shoji, Y., Shigekawa, M., Toyoshima, A., Yokoyama, A., Nakahara, H., Oura, Y., Sueki, K., Sakama, M., Schädel, M., Kratz, J.V.

*Anion-Exchange Behavior of Rutherfordium (Element 104) in Nitric and Hydrochloric Acid Media*



2001 Asia-Pacific Symposium on Radiochemistry (APSORC2001) and the Annual Meeting of the Japan Society of Nuclear and Radiochemical Sciences, Fukuoka (Oct. 29, 2001)

Tsukada, K., Nishinaka, I., Asai, M., Goto, S., Sakama, M., Haba, H., Ichikawa, S., Nagame, Y., Schädel, M.

*Automated Liquid Chromatography Apparatus Coupled with an On-line Alpha-Particle Detection System*

The 2nd International Symposium on Advanced Science Research, ASR2001, Tokai (Nov. 13, 2001)

## NUCLEAR THEORY

### Journal/Proceedings

Brentano, P.von, Lisetskiy, A.F., Friessner, C., Pietralla, N., Schmidt, A., Schneider, I., Jolos, R.V., Otsuka, T., Sebe, T., Utsuno, Y.

*Approaching Rotational Collectivity in odd-odd  $N=Z$  nuclei in  $pf$ -shell*

Prog. Part. Nucl. Phys. **46** (2001) 197.

Chikazumi, S., Iwamoto, A.

*First Order Phase Transition of Expanding Matter and its Fragmentation,*

Phys. Rev. C**65** (2002) 067601.

Fukushima, M., Suganuma, H., Chiba, S.

*Instanton and Monopole in External Chromomagnetic Fields*

Prog. Theor. Phys. **107** (2002) 1147.

Otsuka, T., Fujimoto, R., Utsuno, Y., Brown, B.A., Honma, M., Mizusaki, T.

*Magic Numbers in Exotic Nuclei and Spin-Isospin Properties of the NN Interaction,*

Phys. Rev. Lett. **87** (2001) 082502.

Otsuka, T., Honma, M., Mizusaki, T., Shimizu, N., Utsuno, Y.

*Monte Carlo Shell Model for Atomic Nuclei*

Prog. Part. Nucl. Phys. **47** (2001) 319.

Otsuka, T., Utsuno, Y., Mizusaki, T., Honma, M.

*Exotic Nuclei in the Monte Carlo Shell Model Calculations*

Nucl. Phys. **A685** (2001) 100c.

Otsuka, T., Utsuno, Y., Honma, M., Mizusaki, T.

*Structure of Unstable Nuclei*

Prog. Part. Nucl. Phys. **46** (2001) 155.

Papa, M., Maruyama, T., Bonasera, A.

*Constrained Molecular Dynamics Approach to Fermionic Systems*

Phys. Rev. C **64**, (2001) 024612.

Tanigawa, T.

*Study of Superfluidity in Nuclear Matter with Quantum Hadrodynamics*

Genshikaku Kenkyu **46-3** (2001) 97.

Utsuno, Y., Otsuka, T., Mizusaki, T., Honma, M.

*Extreme Location of F Drip Line and Disappearance of the N=20 Magic Number*

Phys. Rev. C **64** (2001) 011301(R).

## Meetings

S. Chikazumi, S., Iwamoto, A.

*Molecular Dynamics Simulation of Expanding Matter*

First Joint Meeting of the Nuclear Physics Divisions of APS and JPS , Hawai (Oct. 19, 2001)

Chikazumi, S., Iwamoto, A.

*First Order Phase Transition of Expanding Matter and its Fragmentation*

The 4th Symposium of Science of Hadrons under Extreme Conditions, JAERI, Tokai, (Mar. 4, 2002)

Chikazumi, S., Iwamoto, A.

*First Order Phase Transition of Expanding Matter*

The 57th Meeting of Japan Physical Society , Shiga (Mar. 24, 2002)

Hayakawa, T., Shizuma, T., Yamauchi, T., Arisawa, T.

*Nucleosynthesis of Heavy Element*

Yukawa International Seminar 2001, Kyoto (Nov. 9, 2001)

Hayakawa, T., Shizuma, T., Yamauchi, T. Minehara, E., Arisawa, T.

*The Nuclear Isomer and Photoreaction on the p/s Process*

Workshop of the Photoreaction and p/s Process, Tokyo (Nov. 28, 2001)

Maruyama, T., Bonasera, A., Chiba, S.

*Nuclear Fragmentation by Tunneling*

Quantum Tunneling in Nuclear Systems, Kyoto (Jul. 2-4, 2001)

Maruyama, T., Bonasera, A., Chiba, S.

*Nuclear Fragmentation by Tunneling*

International Nuclear Physics Conference 2001, Berkley, USA (Jul.30 - Aug.3, 2001)

Maruyama, T., Bonasera, A., Papa, M., Chiba, S.

*Formation and Decay of Super Heavy Systems*

Yukawa International Seminar 2001, Kyoto (Nov. 5-10, 2001)

Maruyama, T., Bonasera, A., Papa, M., Chiba, S.

*Formation and Decay of Super Heavy Systems*

The 2nd International Symposium on Advanced Science Research, Advances in Heavy Element Research, Tokai (Nov. 14-16, 2001)

Maruyama, T., Bonasera, A., Papa, M. and Chiba, S.

*Constrained Molecular Dynamics and its Application to Nuclear Reactions*

The 57th Meeting of Japan Physical Society, Shiga (Mar. 24-27, 2002)

Tanigawa, T., Matsuzaki, M.

*Relativistic Study of Dinucleon Condensate in Nuclear Matter*

RIKEN Workshop on Alpha Particle and Two-Neutron Condensation in Neutron-Rich Nuclei, Wako (May 1-2, 2001)

Tanigawa, T., Matsuzaki, M., Chiba S.

*$\Lambda\Lambda$  Pairing in  $NA$  Composite Matter*

The 4th Symposium on Science of Hadrons under Extreme Conditions, Tokai, (Mar. 4-6, 2002)

Tanigawa, T., Matsuzaki, M., Chiba S.

*$\Lambda\Lambda$  Pairing in  $NA$  Composite Matter*

Recent Development in Strangeness Nuclear Physics, KEK, Tsukuba (Mar. 15-17, 2002)

Utsuno, Y., Otsuka, T., Mizusaki, T., Honma, M., Fujimoto, R.

*Shell Formation and Disappearance in Exotic Nuclei,*

The Fourth Italy-Japan Symposium on Heavy Ion Physics, Tokyo (Sept. 26-29, 2001)

Utsuno, Y., Otsuka, T., Mizusaki, T., Honma, M.

*Vanishing of the  $N=20$  Magic Number studied by the Monte Carlo Shell Model,*

Inter. Conf. on Nuclear Data for Science and Technology (ND2001), Tsukuba (Oct. 7-12, 2001).

Utsuno, Y., Otsuka, T., Mizusaki, T., Honma, M.

*Yrast and Yrare Structure of Exotic Nuclei with  $N\sim 20$ ,*

First Joint Meeting of the Nuclear Physics Divisions of APS and JPS, Hawaii (Oct. 17-20, 2001)

Utsuno, Y., Otsuka, T., Mizusaki, T., Honma, M.

*Electromagnetic Moments of Exotic Na Isotopes and their Relation to the  $N=20$  Magic Number*

Yukawa International Seminar 2001 (YKIS01) on Physics of Unstable Nuclei, Kyoto (Nov. 5-10, 2001)

Utsuno, Y., Otsuka, T., Mizusaki, T., Honma, M.

*Disappearance of the Magic Number and Deformation in Unstable Nuclei around  $N=20$*

Workshop on Microscopic Description of Nuclear Collective Motion, Fukuoka (Dec. 13-15, 2001)

## ATOMIC PHYSICS AND SOLID STATE PHYSICS

### Journal/Proceedings

Ishikawa, N., Iwase, A., Chimi, Y., Michikami, O., Wakana, H., Kambara, T.  
*Electronic Excitation Effects in High-Energy Ion Irradiated Oxide Superconductors*  
Particle Beam Science using Tandem Accelerators Symposium Proceedings, UTTAC  
-J-9 2001(2001)88.

Sataka, M., Imai, M., Kawatsura, K., Komaki, K., Tawara, H., Vasilyev, A.,  
Safronova, U.I.  
*Coster-Kronig Electrons from the autoionizing Rydberg States of 2 MeV/u  $\text{Si}^{5+}$  Ions  
excited through a Thin C-Foil Target*  
J. Phys. **B35** (2002) 267.

### Meetings

Imai, M., Sataka, M., Kitazawa, S., Kawatsura K., Komaki, K., Shibata, H. Tawara, H.,  
Azuma, T., Kanai, Y., Yamazaki, Y.  
*Angular Momentum Distribution of Sulfur Rydberg States produced through Foil  
Penetration*  
19th. Int. Conf. on the Atomic Collision in Solids , Paris ( Jul. 2001)

Imai, M., Sataka, M., Kitazawa, S., Kawatsura K., Komaki, K., Shibata, H. Tawara, H.,  
Azuma, T., Kanai, Y., Yamazaki, Y.  
*Angular Momentum Distribution of Sulfur Rydberg States produced through Foil  
Penetration (III)*  
2001 Fall Meeting of the Physical Society of Japan, Tokushima (Sep. 27, 2001)

Sekioka, T., Terasawa, M., Sataka, M., Kitazawa, S., Niibe, M.

*Electronic Excitation Effects on Secondary Ion Emission from a Foil of Conducting Material Bombarded by High Energy Heavy Ions*

19th Int.Conf. on the Atomic Collision in Solids, Paris (Aug. 2001)



## RADIATION EFFECTS IN MATERIALS

### Journal/Proceedings

Chimi, Y., Iwase, A., Ishikawa, N., Kobiyama, M., Inami, T., Okuda, S.

*Accumulation and Recovery of Defects in Ion-irradiated Nanocrystalline Gold*

J. Nucl. Mater. **297** (2001) 355.

Chimi, Y., Adachi, K., Iwase, A., Ishikawa, N., Yamakawa, K.

*Thermal Relaxation of Hydrogen Disordering in Pd-II System Irradiated with High-energy Particles*

J. Alloys and Compounds **330-332** (2002) 187.

Ishikawa, N., Sueyoshi, T., Iwase, A., Chimi, Y., Fujiyoshi, T.,

Miyahara, K., Kiss, T.

*Critical Current Density of  $YBa_2Cu_3O_y$  Containing Inclined Columnar Defects*

Physica **C357-360** (2001) 505.

Ishino, S.

*Historical Survey of the Study of Radiation Damage Mechanisms of Reactor Pressure Vessel Steels*

Kinzoku (Metals & Technologies) **71** (2001) 719 (in Japanese).

Kurumada, A., Imamura, Y

*Irradiation Effect on Mechanical and Thermal Properties of Carbon Composite and Ceramics Materials*

Ooarai Research Meeting Report, Institute for Materials Research, Tohoku University, (Sep. 6-7, 2001) pp 205-213.

Matsunami, N., Sataka, M., Iwase, A.

*Sputtering of High  $T_c$  Superconductor  $YBa_2Cu_3O_{7-\delta}$  by High Energy Heavy Ions,*

Nucl. Instrum. Methods. **B175-177** (2001) 56.

Matsunami, N., Sataka, M, Iwase, A., Inami, T., Kobiyama, M.  
*Sputtering of Nano-Crystalline Gold by High Energy Heavy Ions*  
 J. Nucl. Mater. **302** (2002) 206.

Ohtsuka, H., Hojo, K., Maeta, H., Otsu, H., Sugai, H., Yamamoto, H.  
*Radiation Defects in Nano-structured Materials*  
 Eur. Phys. J. **D. 16** (2001) 309.

Sasase, M., Okayasu, S., Kurata, H., Hojou, K.  
*Irradiated Damage of High-Tc Superconductor.*  
 Physica **C 357-360** (2001) 497.

Sasase, M., Okayasu, S., Kurata, H., Hojou, K.  
*Defect Structure of High-Tc Superconductor by High-Energy Heavy Ion Irradiation.*  
 J. Electron Microscopy **51** (2001) 235.

Sasase, M.  
*Formation of Irradiation Defects and Improvement of Critical Current Density  $J_c$  Induced by High-Energy Heavy Ion Irradiation in High-Tc Superconductor*  
 Radiat. Chemi. **72** (2001) 41.

Soneda, N. Ishino, S., Diaz de la Rubia, T.  
*Vacancy Loop Formation by 'Cascade Collapse' in  $\alpha$ -Fe: A Molecular Dynamics Study of 50 keV Cascades*  
 Philos. Mag. Lett. **81** (2001) 649.

## Meetings

Aruga, T., Katano, Y., Ohmichi, T., Okayasu, S., Kazumata, Y., Jitsukawa, S.  
*Depth-Dependent and Surface Damages in  $MgAl_2O_4$  and MgO irradiated with Energetic Iodine Ions*  
 11-th Int.. Conf. on Radiation Effects in Insulators(REI-11), Lisbon (Sep. 3-7, 2001)

Aruga, T., Katano, Y., Ohmichi, T., Jitsukawa, S..

*The Interpretation of Surface Damages in  $Al_2O_3$ ,  $MgAl_2O_4$  and  $MgO$  irradiated with Energetic Iodine Ions*

12-th International Conf. on Surface Modification of Materials by Ion Beam, (SMMIB-12), Marburg (Sept. 9-14, 2001)

Aruga, T., Katano, Y., Ohmichi, T.

*Electronic Excitation Effects observed in Damage Structures in Al-Mg Oxides irradiated with Energetic I-Ions*

Fall meeting of Japan Institute of Metals, Fukuoka (Sept. 22, 2001)

Chimi, Y., Iwase, A., Ishikawa, N., Kambara, T.

*Defect Production Induced by Electronic Excitation in Iron*

19th International Conference on Atomic Collisions in Solids, Paris (Jul. 30, 2001)

Chimi, Y., Iwase, A., Adachi, K., Ishikawa, N., Yamakawa, K.

*Thermal Relaxation of Hydrogen Atoms in Pd-H System Irradiated with Energetic Ions*

Fall Meeting of the Physical Society of Japan, Tokushima (Sep. 19, 2001)

Chimi, Y., Iwase, A., Ishikawa, N., Kambara, T.

*Defect Production and Annihilation Process through High Density Electronic Excitation in Iron*

57th Annual Meeting of the Physical Society of Japan, Shiga (Mar. 25, 2002)

Ishino, S., Hasegawa, T., Chimi, Y., Ishikawa, N., Iwase, A., Tobita, T., Suzuki, M.

*Electrical Resistivity Measurements in Fe-Cu Alloys irradiated with Energetic Heavy Ions and Electrons*

The (129<sup>th</sup>) 2001-Fall Meeting of the Japan Institute of Metals, Fukuoka (Sep. 21-24, 2001)

Ishino, S.

*Studies of Dose Rate Effects by Means of Ion Irradiation*

EPRI/CRIEPI Workshop on Dose Rate Effects in Reactor Pressure Vessel Materials,  
Olympic Valley, U.S.A., (Nov. 12-14, 2001)

Ishino, S., Hasegawa, T., Chimi, Y., Ishikawa, N., Iwase, A., Tobita, T.,

Suzuki, M.

*In-situ Measurements of Electrical Resistivity in Fe-Cu Alloys using Heavy Ion and  
Electron Accelerators*

Symposium on 'The Mechanism of Irradiation Embrittlement in Pressure Vessel  
Materials', Sendai, (Nov. 22-24, 2001)

Hamatani, Y., Iwase, A., Ishikawa, N., Chimi, Y., Kambara, T., Neumann, R., Mueller,  
C., Mukumoto, Y., Motoshimizu, Y., Ono, F.

*Electronic Excitation Effects in FeNi Invar Alloys Irradiated with High Energy Ions*

57th Annual Meeting of the Physical Society of Japan, Shiga (Mar. 25, 2002)

Matsunami, N., Sataka, M., Iwase, A.

*Electronic Sputtering of Insulating and Semiconducting Oxides by High Energy Ion  
Impact*

Int. Conf. on Atomic Collisions in Solids, Paris (Aug. 2001)

Nakazawa, T., Grismanovs, V., Katano, Y., Aruga, T., Yamaki, D., Iwamoto, A.,  
Jitsukawa, S.

*Study of Ion-induced Damage in  $\text{Li}_2\text{TiO}_3$  Ceramics*

2001 Annual Meeting of the Atomic Energy Society of Japan, Tokyo (Mar. 27-29, 2001)

Oku, T., Kurumada, A., Imamura, Y., Ishihara, M.

*Ion Irradiation Effects on the Mechanical Properties of Carbon Materials,*

2nd International Specialist Graphite Meeting, Rain, Germany (Sep. 24-25, 2001).

Ono, F., Takahashi, A., Inoue, H., Wei, S., Iwase, A., Ishikawa, N., Chimi, Y.,  
Kuroda, N., Kambara, T.

*Effect of GeV-Ion Irradiations on Magnetic Properties in Fe-Ni Invar Alloys*

19th International Conference on Atomic Collisions in Solids, Paris (Jul. 30, 2001)

Sasase, M., Okayasu, S., Yamamoto, H., Kurata, H., Hojou, K.

*Effect of High-Energy Heavy Ion Irradiation in Bi-2212.*

Spring Meeting of the Japan Society of Applied Physics, Tokyo (Mar. 31, 2001)

Sato, H., Ishikawa, N., Iwase, A., Chimi, Y., Michikami, O., Hashimoto, T.

*Electronic Excitation Effects in Oxygen-Controlled  $\text{EuBa}_2\text{Cu}_3\text{O}_{7.6}$  irradiated  
with High Energy Ions*

Fall Meeting of the Physical Society of Japan, Tokushima (Sep.17, 2001)

Sato, H., Ishikawa, N., Iwase, A., Chimi, Y., Michikami, O., Hashimoto, T.

*Structural Change by High-Energy Irradiation and Post-Annealing in  $\text{EuBa}_2\text{Cu}_3\text{O}_y$*

International Symposium on Superconductivity (ISS 2001), Kobe (Sep. 26, 2001)

Sonoda, T., Kinoshita, M., Ray, I.L.F., Wiss, T., Thiele, H., Pellottiero, D.,

Rondinella, V.V., Matzke, H.

*TEM Observation on Irradiation - Induced Microstructural Evolution in High Burn-up  
 $\text{UO}_2$  Disk Fuel,*

11<sup>th</sup> Int. Conf. on Radiation Effects in Insulators (REI-11) Lisbon (Sep. 03-07,  
2001)

Sonoda, T., Kinoshita, M.,

*Mechanism of Rim Structure Formation in High Burn-up LWR Fuels-Effects  
of Electron Excitation on the Rim Structure Formation*

Symposium on high density electronic excitation in solids and its application to  
materials processing, Tokai (Nov. 5-6, 2001)

Sonoda, T., Kitajima, S., Sasahara, A., Kameyama, T., Kinoshita, M., Hiernaut,  
Rondinella, V.V., Matzke, Hj.

*High Burnup Rim Project (HBRP) (2) -Threshold of Rim Structure Formation, Density  
Change, Retrained Gas-*

2002 Annual Meeting of the Atomic Energy Society of Japan, Kobe (Mar. 27-29, 2002)

## **9. Personnel and Committees**

This is a blank page.



**(1) Personnel (FY 2001)****Department of Materials Science**

Akira	Iwamoto	Director
Katsuichi	Tachimori	Deputy Director
Tohor	Ogawa	Deputy Director (till Jan. 2002)
Sigeru	Mori	Administrative Manager (till Sep. 2001)
Yasutoshi	Komatsubara	Administrative Manager (from Oct. 2001)

***Tandem Accelerator Group*****Scientific Staff**

Tadashi	Yoshida*
Suehiro	Takeuchi
Susumu	Hanashima
Makoto	Matsuda
Takamitsu	Nakanoya

**Technical Staff**

Susumu	Kanda
Isao	Ohuchi
Katsuzo	Horie
Yoshihiro	Tsukihashi
Shinichi	Abe
Nobuhiro	Ishizaki
Hidekazu	Tayama

***Research Group for Innovative Nuclear Science***

Masumi	Oshima*
Akihiro	Iwase**
Nobuo	Shinohara
Hideki	Iimura
Youichi	Hatsukawa
Norito	Ishikawa**
Yasuhiro	Chimi**
Akihiko	Osa
Yutaka	Utsuno
Yosuke	Toh
Tetsuya	Hirade
Mitsuo	Koizumi

Yutaro	Hamatani**	(Student)
--------	------------	-----------

Hiroyuki	Sato**	(Student)
----------	--------	-----------

*Research Group for Solid State Physics under Extreme Conditions*

Kiichi	Hojou*
--------	--------

Masao	Sataka
-------	--------

Hideo	Ohtsuka
-------	---------

Satoru	Okayasu
--------	---------

*Research Group for Radiation Effects and Analyses*

Shiro	Jitsukawa*
-------	------------

Takeo	Aruga
-------	-------

Tetsuya	Nakazawa
---------	----------

Daijyu	Yamaki
--------	--------

Akira	Naito
-------	-------

**Advanced Science Research Center**

*Research Group for Fusion of Heavy Deformed Nuclei*

Hiroshi	Ikezoe*
---------	---------

Tetsuro	Ishii
---------	-------

Shin-ichi	Mitsuoka
-----------	----------

Katsuhisa	Nishio
-----------	--------

Kenichirou	Satou	(Student)
------------	-------	-----------

*Research Group for Hadron Science*

Satoshi	Chiba*
---------	--------

Toshiki	Maruyama
---------	----------

Hiroki	Takemoto
--------	----------

Masahiro	Fukushima
----------	-----------

V. N. Kondratyev	(Research Fellow)
------------------	-------------------

Tomonori	Tanigawa	(JSPS Domestic Research Fellow)
----------	----------	---------------------------------

Shinpei	Chikazumi	(Student)
---------	-----------	-----------

*Research Group for Nuclear Chemistry of Heavy Elements*

Yuichiro	Nagame*
----------	---------

Shin-ichi	Ichikawa
-----------	----------

Kazuaki	Tsukada
---------	---------

Ichiro	Nishinaka
--------	-----------

Masato	Asai
--------	------

Hiromitsu	Haba
-----------	------

Kazuhiko	Akiyama	(Post Doc.)
----------	---------	-------------

Atsushi Toyoshima (Student)

**Department of Health Physics**

*Radiation Control Division*

Yukihiro Miyamoto

Hitoshi Ogose

Kouichi Sato

**Advanced Photon Research Center**

*Free Electron Laser Research Group*

Takehito Hayakawa

Toshiyuki Shizuma

**Takasaki Radiation Chemistry Research Establishment**

*Radiation Engineering Division*

Toshio Hirao

**Oarai Research Establishment**

*High Temperature Irradiation Laboratory*

Taiji Hoshiya\*

Masahiro Ishihara

Shinchi Baba

Jun Aihara

\* Head

\*\* Research Group for Radiation Effects and Analyses from Oct. 2001

**(2) Tandem Consultative Committee**

(Chairman)	Toru	Nomura	(Professor, Prime Scientist, High Energy Accelerator Research Organization (KEK))
(Vice Chairman)	Akira	Iwamoto	(Director, Department of Materials Science)
	Hiroyasu	Ejiri	(Professor Emeritus of Osaka University)
	Kohei	Furuno	(Professor, Tsukuba University)
	Jun	Imasato	(Professor, High Energy Accelerator Research Organization (KEK))
	Kenji	Katori	(RI Beam Science Laboratory, RIKEN)
	Ken-ichiro	Komaki	(Professor, The University of Tokyo)
	Shigeru	Kubono	(Associate professor, The University of Tokyo)
	Hisaaki	Kudo	(Associate professor, Niigata University)
	Hiroshi	Kudo	(Professor, Tsukuba University)
	Shunpei	Morinobu	(Professor, Kyushu University)
	Kenji	Morita	(Professor, Nagoya University)
	Seiichi	Shibata	(Professor, Kyoto University)
	Hiromi	Shibata	(Associate professor, The University of Tokyo)
(Secretary)	Masao	Sataka	(Research Group for Solid State Physics under Extreme Conditions)
(Secretary)	Suchiro	Takeuchi	(Tandem Accelerator Group)
(Secretary)	Tadashi	Yoshida	(Head, Tandem Accelerator Group)
(Secretary)	Yasutoshi	Komatsubara	(Administrative Manager, Department of Materials Science)

**(3) Research Planning and Assessment Committee***(a) Sub-committee for Nuclear Physics and Nuclear Chemistry*

(Head)	Shunpei	Morinobu	(Professor, Kyushu University)
	Shigeru	Kubono	(Professor, The University of Tokyo)
	Seiichi	Shibata	(Professor, Kyoto University)
	Kouhei	Furuno	(Professor, Tsukuba University)
	Eisuke	Minehara	(Head, Free Electron Laser Research Group)

	Toshiaki	Sekine	(Deputy Director, Department of Radiation Research for Environment and Resources)
	Suehiro	Takeuchi	(Tandem Accelerator Group)
(Secretary)	Susumu	Hanashima	(Tandem Accelerator Group)
(Secretary)	Tadashi	Yoshida	(Head, Tandem Accelerator Group)

*(b) Sub-committee for Materials and Radiation Damage*

(Head)	Kenji	Morita	(Professor, Nagoya University)
	Ken-ichiro	Komaki	(Professor, The University of Tokyo)
	Hiromi	Shibata	(Associate professor, The University of Tokyo)
	Hiroshi	Kudo	(Professor, Tsukuba University)
	Kiichi	Hojou	(Head, Research Group for Solid State Physics under Extreme Conditions)
	Akihiro	Iwase	(Research Group for Innovative Nuclear Science)
	Suehiro	Takeuchi	(Tandem Accelerator Group)
(Secretary)	Susumu	Hanashima	(Tandem Accelerator Group)
(Secretary)	Tadashi	Yoshida	(Head, Tandem Accelerator Group)

This is a blank page.

## **10. Cooperative Researches**

This is a blank page.



<b>Title</b>	<b>Contact person</b> <b>Organization</b>
1. Precise Measurement of Gamma-Ray Emission Probability for Proton-Rich Nuclides	Hiroshi MIYAHARA Department of Radiological Technology, School of Health Science, Nagoya University
2. Direct Measurement of the Astro-Physical Reaction Rate with Radioactive Nuclear Beams	Hiroari MIYATAKE Institute of Particle and Nuclear Studies, High Energy Accelerator Research Organization
3. Nuclear Structure of the Neutron-Rich Ni Region by Deep-Inelastic Collisions	Masao OGAWA Department of Energy Sciences, Tokyo Institute of Technology
4. Synthesis of Actinide Metallo Fullerene	Motomi KATADA Department of Chemistry, Tokyo Metropolitan University
5. Development of Target/Ion-Source system for the JAERI-KEK Joint RNB Project	Sun Chan JEONG Institute of Particle and Nuclear Studies, High Energy Accelerator Research Organization
6. Study of Isomers and their Decay Mechanisms in Deformed or Spherical Nuclei	Masahiko SUGAWARA Department of Natural Science, Chiba Institute of Technology
7. Physics in Collective States of Deformed Rare Earth Nuclei - On Signatur Inversion and Shape Coexistence -	Hideshige KUSAKARI Faculty of Education, Chiba University

- |  |   |
|--|---|
| 8. Aqueous Chemistry of the Transactinide Elements, Rutherfordium and Dubnium.               | Atsushi SHINOHARA<br>Department of Chemistry,<br>Osaka University   |
| 9. Excitation Energy Dependence on the Asymmetric Mass Division Mode in Actinide Fission     | Hisaaki KUDO<br>Department of Chemistry,<br>Niigata University  |
| 10. Nuclear Structure Study by Coulomb Excitation  | Hideshige KUSAKARI<br>Faculty of Education,<br>Chiba University   |
| 11. M1 Band and Rotational Motion of the Nuclear Structure                                   | Kohei FURUNO<br>Tandem Accelerator Center,<br>Tsukuba University  |
| 12. Laser Spectroscopy of Radioactive Isotopes in the Light Rare Earth Elements              | Takayoshi HORIGUCHI<br>Hiroshima International University   |
| 13. Study on Interaction between Columnar Defects and Vortices in Oxide Superconductors      | Takanobu KISU<br>Department of Electrical and Electronic<br>Systems Engineering,<br>Kyushu University             |
| 14. Study on the Diffusion Processes in Solid Materials by Radioactive Nuclear Beams         | Ichiro KATAYAMA<br>Institute of Particle and Nuclear Studies,<br>High Energy Accelerator Research<br>Organization |
| 15. Study on Damage Production Mechanism in Steel Materials irradiated with High Energy Ions | Shiori ISHINO<br>Faculty of Engineering,<br>Tokai University  |

- |   |  |
|---|--|
| 16. Effects of Ion Irradiation to<br>Superplastic Ceramic Materials   | Yosinobu MOTOHASHI<br>Faculty of Engineering,<br>Ibaraki University  |
| 17. Effect of Ion Irradiation for New<br>Carbon Composite Materials and<br>Fibers with High Thermal<br>Conductivity | Akira KURUMADA<br>Faculty of Engineering,<br>Ibaraki University  |
| 18. Electron Spectra induced by the<br>Collision of highly charged Ions with<br>Matter                              | Ken-ichiro KOMAKI<br>Graduate School of Arts and Science,<br>The University of Tokyo                                 |
| 19. Electronic Excitation Effects in<br>Oxides by High Energy Heavy Ion   | Noriaki MATSUNAMI<br>School of Engineering,<br>Nagoya University   |
| 20. Development of Radiation Sensors<br>using High-Tc Superconductors   | Osamu MICHIKAMI<br>Faculty of Engineering,<br>Iwate University   |
| 21. High-Energy Ion Beam Irradiation of<br>Functional Electronic Materials  | Takayuki TERAII<br>Engineering Research Institute,<br>School of Engineering,<br>The University of Tokyo              |
| 22. Radiation Effects of High Energy<br>Fission Products in Light Water<br>Reactor Fuels                            | Motoyasu KINOSHITA<br>Nuclear Energy Systems Department,<br>Central Research Institute of Electric<br>Power Industry |
| 23. Study of Single-Events induced by<br>High Energy Ions   | Sumio MATSUDA<br>Technology Research Department,<br>National Space Development Agency of<br>Japan                    |

- |   |  |
|---|--|
| 24. Electron Excitation Effect on Sputtering induced by Heavy Ion Bombardment | Mititaka TERASAWA<br>Faculty of Engineering,<br>Himeji Institute of Technology |
| 25. Ion Irradiation Effect on a New Superconducting Material $\text{MgB}_2$   | Hiroshi IKEDA<br>Institute of Materials Science,<br>Tsukuba University         |

# 国際単位系 (SI) と換算表

表1 SI基本単位および補助単位

量	名称	記号
長さ	メートル	m
質量	キログラム	kg
時間	秒	s
電流	アンペア	A
熱力学温度	ケルビン	K
物質質量	モル	mol
光度	カンデラ	cd
平面角	ラジアン	rad
立体角	ステラジアン	sr

表3 固有の名称をもつSI組立単位

量	名称	記号	他のSI単位 による表現
周波数	ヘルツ	Hz	s <sup>-1</sup>
力	ニュートン	N	m·kg/s <sup>2</sup>
圧力, 応力	パスカル	Pa	N/m <sup>2</sup>
エネルギー, 仕事, 熱量	ジュール	J	N·m
工率, 放射束	ワット	W	J/s
電気量, 電荷	クーロン	C	A·s
電位, 電圧, 起電力	ボルト	V	W/A
静電容量	ファラド	F	C/V
電気抵抗	オーム	Ω	V/A
コンダクタンス	ジーメンズ	S	A/V
磁束	ウェーバ	Wb	V·s
磁束密度	テスラ	T	Wb/m <sup>2</sup>
インダクタンス	ヘンリー	H	Wb/A
セルシウス温度	セルシウス度	°C	
光束度	ルーメン	lm	cd·sr
照射度	ルクス	lx	lm/m <sup>2</sup>
放射能	ベクレル	Bq	s <sup>-1</sup>
吸収線量	グレイ	Gy	J/kg
線量当量	シーベルト	Sv	J/kg

表2 SIと併用される単位

名称	記号
分, 時, 日	min, h, d
度, 分, 秒	°, ', "
リットル	l, L
トン	t
電子ボルト	eV
原子質量単位	u

$$1 \text{ eV} = 1.60218 \times 10^{-19} \text{ J}$$

$$1 \text{ u} = 1.66054 \times 10^{-27} \text{ kg}$$

表4 SIと共に暫定的に維持される単位

名称	記号
オングストローム	Å
バ	b
バ	bar
ガ	Gal
キュリー	Ci
レントゲン	R
ラ	rad
レ	rem

$$1 \text{ Å} = 0.1 \text{ nm} = 10^{-10} \text{ m}$$

$$1 \text{ b} = 100 \text{ fm} = 10^{-28} \text{ m}^2$$

$$1 \text{ bar} = 0.1 \text{ MPa} = 10^5 \text{ Pa}$$

$$1 \text{ Gal} = 1 \text{ cm/s}^2 = 10^{-2} \text{ m/s}^2$$

$$1 \text{ Ci} = 3.7 \times 10^{10} \text{ Bq}$$

$$1 \text{ R} = 2.58 \times 10^{-4} \text{ C/kg}$$

$$1 \text{ rad} = 1 \text{ cGy} = 10^{-2} \text{ Gy}$$

$$1 \text{ rem} = 1 \text{ cSv} = 10^{-2} \text{ Sv}$$

表5 SI接頭語

倍数	接頭語	記号
10 <sup>18</sup>	エクサ	E
10 <sup>15</sup>	ペタ	P
10 <sup>12</sup>	テラ	T
10 <sup>9</sup>	ギガ	G
10 <sup>6</sup>	メガ	M
10 <sup>3</sup>	キロ	k
10 <sup>2</sup>	ヘクト	h
10 <sup>1</sup>	デカ	da
10 <sup>-1</sup>	デシ	d
10 <sup>-2</sup>	センチ	c
10 <sup>-3</sup>	ミリ	m
10 <sup>-6</sup>	マイクロ	μ
10 <sup>-9</sup>	ナノ	n
10 <sup>-12</sup>	ピコ	p
10 <sup>-15</sup>	フェムト	f
10 <sup>-18</sup>	アト	a

(注)

- 表1-5は「国際単位系」第5版, 国際度量衡局 1985年刊行による。ただし, 1 eV および 1 uの値は CODATA の1986年推奨値によった。
- 表4には海里, ノット, アール, ヘクトールも含まれているが日常の単位なのでここでは省略した。
- bar は, JISでは流体の圧力を表わす場合に限り表2のカテゴリーに分類されている。
- EC閣僚理事会指令では bar, barn および「血圧の単位」mmHgを表2のカテゴリーに入れている。

換算表

力	N (=10 <sup>5</sup> dyn)	kgf	lbf
	1	0.101972	0.224809
	9.80665	1	2.20462
	4.44822	0.453592	1

$$\text{粘度 } 1 \text{ Pa} \cdot \text{s} (\text{N} \cdot \text{s} / \text{m}^2) = 10 \text{ P (ポアズ)} (\text{g} / (\text{cm} \cdot \text{s}))$$

$$\text{動粘度 } 1 \text{ m}^2 / \text{s} = 10^4 \text{ St (ストークス)} (\text{cm}^2 / \text{s})$$

圧	MPa (=10 bar)	kgf/cm <sup>2</sup>	atm	mmHg (Torr)	lbf/in <sup>2</sup> (psi)
	1	10.1972	9.86923	7.50062 × 10 <sup>3</sup>	145.038
力	0.0980665	1	0.967841	735.559	14.2233
	0.101325	1.03323	1	760	14.6959
	1.33322 × 10 <sup>-4</sup>	1.35951 × 10 <sup>-3</sup>	1.31579 × 10 <sup>-3</sup>	1	1.93368 × 10 <sup>-2</sup>
	6.89476 × 10 <sup>-3</sup>	7.03070 × 10 <sup>-2</sup>	6.80460 × 10 <sup>-2</sup>	51.7149	1

	J (=10 <sup>7</sup> erg)	kgf·m	kW·h	cal (計量法)	Btu	ft·lbf	eV
エネルギー・仕事・熱量	1	0.101972	2.77778 × 10 <sup>-7</sup>	0.238889	9.47813 × 10 <sup>-4</sup>	0.737562	6.24150 × 10 <sup>18</sup>
	9.80665	1	2.72407 × 10 <sup>-6</sup>	2.34270	9.29487 × 10 <sup>-3</sup>	7.23301	6.12082 × 10 <sup>19</sup>
	3.6 × 10 <sup>6</sup>	3.67098 × 10 <sup>5</sup>	1	8.59999 × 10 <sup>5</sup>	3412.13	2.65522 × 10 <sup>6</sup>	2.24694 × 10 <sup>25</sup>
	4.18605	0.426858	1.16279 × 10 <sup>-6</sup>	1	3.96759 × 10 <sup>-3</sup>	3.08747	2.61272 × 10 <sup>19</sup>
	1055.06	107.586	2.93072 × 10 <sup>-4</sup>	252.042	1	778.172	6.58515 × 10 <sup>21</sup>
	1.35582	0.138255	3.76616 × 10 <sup>-7</sup>	0.323890	1.28506 × 10 <sup>-3</sup>	1	8.46233 × 10 <sup>18</sup>
	1.60218 × 10 <sup>-19</sup>	1.63377 × 10 <sup>-20</sup>	4.45050 × 10 <sup>-26</sup>	3.82743 × 10 <sup>-20</sup>	1.51857 × 10 <sup>-22</sup>	1.18171 × 10 <sup>-19</sup>	1

$$1 \text{ cal} = 4.18605 \text{ J (計量法)}$$

$$= 4.184 \text{ J (熱化学)}$$

$$= 4.1855 \text{ J (15 °C)}$$

$$= 4.1868 \text{ J (国際蒸気表)}$$

$$\text{仕事率 } 1 \text{ PS (仏馬力)}$$

$$= 75 \text{ kgf} \cdot \text{m/s}$$

$$= 735.499 \text{ W}$$

放射能	Bq	Ci
	1	2.70270 × 10 <sup>-11</sup>
	3.7 × 10 <sup>10</sup>	1

吸収線量	Gy	rad
	1	100
	0.01	1

照射線量	C/kg	R
	1	3876
	2.58 × 10 <sup>-4</sup>	1

線量当量	Sv	rem
	1	100
	0.01	1



古紙配合率100%  
白色度70%再生紙を使用しています